UNCLASSIFIED

AD NUMBER
ADC012517
CLASSIFICATION CHANGES
TO: **UNCLASSIFIED**
FROM: **CONFIDENTIAL**
LIMITATION CHANGES
TO: **Approved for public release; distribution is unlimited.**
FROM: **Distribution authorized to U.S. Gov't. agencies only; Test and Evaluation; NOV 1972. Other requests shall be referred to Army Air Mobility Research and Development Lab., Fort Eustis, VA.**
AUTHORITY
31 Dec 1987 per doc markings ; DOA/AATD ltr 22 Oct 1990

THIS PAGE IS UNCLASSIFIED

Best
Available
Copy

UNCLASSIFIED

AD NUMBER

C012517

CLASSIFICATION CHANGES

TO

UNCLASSIFIED

FROM

CONFIDENTIAL

AUTHORITY

OCA 31 Dec 1987

THIS PAGE IS UNCLASSIFIED

(UNCLASSIFIED)

AD NUMBER

C012 517

LIMITATION CHANGES

TO: Approved for Public Release; Distribution Unlimited.. — Code: A/1

FROM: Distribution Authorized to U.S. Gov't Agencies Only... — Code: B/3

AUTHORITY

DOA/AATD, 22 Oct 1990

(THIS PAGE IS UNCLASSIFIED)

AD C012517

UNCLASSIFIED

USAAMRDL-(S)-336-72

AD

USAAMRDL TECHNICAL REPORT 72-50

RESEARCH PROGRAM TO OPTIMIZE THE ST9 DEMONSTRATOR ENGINE IR SUPPRESSOR (U)

Downgrade to GDSNSF
on
CONFIDENTIAL
on 31 Dec 1977
Declassify on 31 Dec 1987
Classified by [illegible]

Classified by Director, Eustis Directorate, USAAMRDL. Exempt From General Declassification Schedule of EO 11652 Exemption Category 3. Declassify on: NLT 31 Dec 1987

By

D. E. Booz, Jr.
E. B. Thayer
C. M. Willard

November 1972

EUSTIS DIRECTORATE
U. S. ARMY AIR MOBILITY RESEARCH AND DEVELOPMENT LABORATORY
FORT EUSTIS, VIRGINIA

CONTRACT DAAJ02-71-C-0043
PRATT & WHITNEY AIRCRAFT DIVISION
UNITED AIRCRAFT CORPORATION
FLORIDA RESEARCH AND DEVELOPMENT CENTER
WEST PALM BEACH, FLORIDA

DDC
DEC 28 1977
D

Distribution limited to U.S. Government agencies only; test and evaluation; November 1972. Other requests for this document must be referred to the Eustis Directorate, U.S. Army Air Mobility Research and Development Laboratory, Fort Eustis, Virginia 23604.

Army Research and Technology Labs
*NATIONAL SECURITY INFORMATION

Copy 25 of 30 Copies

UNCLASSIFIED

DISCLAIMERS

The findings in this report are not to be construed as an official Department of the Army position unless so designated by other authorized documents.

When Government drawings, specifications, or other data are used for any purpose other than in connection with a definitely related Government procurement operation, the U.S. Government thereby incurs no responsibility nor any obligation whatsoever; and the fact that the Government may have formulated, furnished, or in any way supplied the said drawings, specifications, or other data is not to be regarded by implication or otherwise as in any manner licensing the holder or any other person or corporation, or conveying any rights or permission, to manufacture, use, or sell any patented invention that may in any way be related thereto.

Trade names cited in this report do not constitute an official endorsement or approval of the use of such commercial hardware or software.

DISPOSITION INSTRUCTIONS

When this report is no longer needed, Department of the Army organizations will destroy it in accordance with the procedures given in AR 380-5.

UNCLASSIFIED
SECRET

DEPARTMENT OF THE ARMY
U. S. ARMY AIR MOBILITY RESEARCH & DEVELOPMENT LABORATORY
EUSTIS DIRECTORATE
FORT EUSTIS, VIRGINIA 23604

(U) This report was prepared by Pratt and Whitney Aircraft, a Division of United Aircraft Corporation, West Palm Beach, Florida, under the terms of Contract DAAJ02-71-C-0043. The STD Demonstrator Engine IR Suppressor was optimized through analyses conducted with the aid of Government-furnished IR suppressor optimization computer programs and emissivity control coating information. A significant IR signature reduction over previous measurements was predicted and verified by tests.

(U) The summary findings stated herein are concurred in by this Directorate.

(U) The technical monitor for this contract was Mr. Wallace R. Conway, Military Operations Technology Division.

DDC
D

UNCLASSIFIED
SECRET

Preceding Page BLANK - NOT FILMED

ACCESSION IN
NTIS
DDC
UNANNOUNCED
JUSTIFICATION
BY
DISTRIBUTION/AVAILABILITY CODES
Dist. AVAIL and/or SPECIAL
B

UNCLASSIFIED
~~SECRET~~

Task 1F162205AA5203
Contract DAAJ02-71-C-0043
USAAMRDL Technical Report 72 - 50
November 1972

RESEARCH PROGRAM TO OPTIMIZE THE ST9 DEMONSTRATOR ENGINE IR SUPPRESSOR (U)

Final Report

[redacted]

By

D. E. Booz, Jr.
E. B. Thayer
C. M. Willard

[redacted]

Prepared By

Pratt & Whitney Aircraft Division
United Aircraft Corporation
Florida Research and Development Center
West Palm Beach, Florida

Classified by Eustis Directorate
exempt from GDS of DoD Dir 5200.10
Exempt Category 3
Declassify on 31 Dec 1987

for

EUSTIS DIRECTORATE
U. S. ARMY AIR MOBILITY RESEARCH AND DEVELOPMENT LABORATORY
FORT EUSTIS, VIRGINIA

This document contains information affecting the national defense of the United States within the meaning of the Espionage Laws, Title 18 U.S.C. Sections 793 and 794. The transmission or revelation of its contents in any manner to an unauthorized person is prohibited by law.

Distribution limited to U.S. Government agencies only; test and evaluation. November 1972. Other requests for this document must be referred to the Eustis Directorate, U.S. Army Air Mobility Research and Development Laboratory, Fort Eustis, Virginia 23604.

~~SECRET~~
UNCLASSIFIED

"NATIONAL SECURITY INFORMATION"

"Unauthorized Disclosure Subject to Criminal Sanctions"

(AD- 1472)

Preceding Page BLANK - NOT FILMED

(U) ABSTRACT

The purpose of this program was to optimize the surface temperature/emissivity of the ST9 Demonstrator Engine infrared (IR) suppressor to yield the lowest IR signature possible without additional cooling flow requirements. New IR-signature analysis computer programs developed by General Dynamics - Pomona under U. S. Army Air Mobility Research and Development Laboratory (USAAMRDL) Contract DAAJ02-69-C-0077 were used to conduct an analytical optimization study. A parametric variation of the temperature and emissivity of the suppressor wall surfaces, divided into many segments, permitted the optimum combination to be chosen. Emissivity-control coatings were then applied to the suppressor surfaces, and the coated suppressor was tested under simulated engine operating conditions. The test results showed that a 22% reduction in the IR signature was achieved, and that the measured signature compared favorably with that predicted by the computer programs.

Preceding Page BLANK - NOT FILMed

(U) TABLE OF CONTENTS

(U) TABLE OF CONTENTS (Continued)

(U) LIST OF ILLUSTRATIONS

(U) LIST OF ILLUSTRATIONS (Continued)

(U) LIST OF ILLUSTRATIONS (Continued)

(U) LIST OF ILLUSTRATIONS (Continued)

(U) LIST OF TABLES

(U) LIST OF TABLES (Continued)

(U) LIST OF SYMBOLS

A	Area, $in.^2$ or ft^2
Cp	Pressure recovery coefficient
F	Shape, or configuration factor, of radiation heat transfer
I	Radiant flux intensity, $w/ft^2/sr$
J	Source radiant intensity, w/sr
J_λ	Spectral source radiant intensity, $w/sr/\mu$
M	Mach number
P	Pressure, $lb_f/in.^2$
Q	Heat transfer rate, w
q	Dynamic pressure, $lb_f/in.^2$
r	Separation distance, in. or ft
sr	Solid angle unit of measure, steradian
V	Velocity, ft/sec or in./sec
W	Emissive power, w/ft^2
$\dot{w}$	Mass flow rate, lb_m/sec
α	Angle of swirling flow relative to axial direction, deg
ϵ	Surface emissivity
η	Normal direction to an incremental surface area
λ	Wavelength, μ
ρ	Density, lb_m/ft^3
ϕ	Angle, deg

SUBSCRIPTS

i	Denotes emitting surface when used with respect to shape factors
j	Denotes receiving surface when used with respect to shape factors
t	Denotes total, or stagnation conditions
1	Denotes suppressor inlet conditions
2	Denotes suppressor exit conditions
λ	Denotes spectral values when used with IR-related terminology

(U) INTRODUCTION

An infrared-suppressing exhaust diffuser was designed for the ST9 engine under the ST9 1500-shp Demonstrator Engine Program. A full-scale, hot-flow suppressor test rig was then built and tested, with the results presented in Reference 1. With the ST9 suppressor, IR suppression is achieved by blocking line-of-sight viewing of the turbine, and then cooling all of the surfaces that are visible. Thus, no hot metal surfaces are visible at any aspect angle. However, reflected radiation is also important; i. e., radiation that originates from the turbine and the nonvisible, uncooled upstream walls of the suppressor that is reflected into the environs by the visible surfaces, thereby contributing substantially to the IR signature. The level of reflected radiation is primarily a function of the reflectivity (or emissivity) of the surfaces of the suppressor. To minimize reflections, emissivity-control coatings must be applied to the suppressor surfaces. Thus, the design of an IR suppressor involves the calculation of not only the direct emission, which is a relatively straightforward process, but also the reflected radiation, which is considerably more difficult because of the complex geometry, and thus re-reflections, of curved-wall suppressors. Further, it is desirable to optimize the distribution of cooling air, in conjunction with emissivity-control coatings, to minimize cooling air requirements.

New IR-signature analysis computer programs, developed by General Dynamics-Pomona under USAAMRDL contract (Reference 2), enable more accurate calculations of reflected radiation, and thus total emission, than has heretofore been possible. Thus, the primary objective of this program was to use these new computer programs to optimize the surface temperature/emissivity of the ST9 IR suppressor. The goal was to attain the lowest possible IR signature without increasing the cooling flow, so as not to degrade engine performance.

The 7-month program was divided into three tasks as follows:

I. Analytical Optimization Study

II. Design of Suppressor Modifications

III. Modification and Test of Suppressor

(U) DESCRIPTION OF DEMONSTRATOR SUPPRESSOR

The ST9 Demonstrator IR suppressor is shown in Figure 1. It is designed to achieve IR suppression by blocking line of sight to the power turbine with a curved-wall annular flow path, then cooling all of the visible surfaces. Cooling louvers made of FINWALL^{TM} material, shown in Figure 2, are used to form the cooled structure for the visible inner (centerbody) and outer walls of the suppressor. An internal blower mounted on the power turbine shaft pumps the cooling air from the atmosphere. The front half of the six partitioned struts serves as the coolant inlets.

The suppressor test rig shown in Figures 3 and 4 was built and tested in the Demonstrator Program, with the results presented in Reference 1. This same rig was tested under this contract. The test rig is of flightweight construction where practical, including the FINWALL cooling louvers. The cooling air is supplied by an auxiliary test stand supply system to plenums for each of three cooled regions: the inner wall, outer wall, and base. The individual louvers are then fed from the three plenums. In this manner, the coolant flow rate to the three cooled regions is individually controllable.

The Demonstrator suppressor test rig also included a high-emissivity coating on both the visible inner and outer walls to reduce the reflected radiation from the turbine and the uncooled, nonvisible walls of the suppressor. A high-temperature, flat-black paint, PTI-404A, was used as the coating. However, problems with the coating coming off were experienced, primarily when testing uncooled, where the wall temperatures were over 1000°F.

To accomplish the objectives of this program, the following ground rules were established:

1. The Demonstrator IR-suppressor geometry, i.e., the aerodynamic flow path and cooling louver configurations, was not to be changed.

2. The total coolant flow rate was not to be increased from the 0.778 lb/sec design value of the Demonstrator configuration. However, the distribution, or split, of the total cooling flow to the three independently supplied regions could be varied to obtain maximum suppression, as long as the variations are accomplished without hardware changes.

3. The optimization study was to be conducted for the normal-rated-power (NRP) setting of the ST9 Demonstrator Engine, which is 83% maximum rated power (MRP).

(U) DESCRIPTION OF IR SUPPRESSOR OPTIMIZATION COMPUTER PROGRAMS

The development of new, rigorous computer programs by General Dynamics-Pomona for USAAMRDL has made the optimization of suppressor surface temperature and emissivity combinations by computer methods feasible. The Configuration Factors Program (CFP) deck of the computer program provides the capability of exact geometric simulation of suppressor geometry. The radiation calculations included in the Infrared Radiation Analysis Program (IRAP) portion of the computer program account for the effects of multiple reflections through the use of the shape factors, which are input to the IRAP deck after their determination from the CFP deck.

CONFIGURATION FACTORS PROGRAM

The basic meaning of shape factors is explained in Figure 5. This sketch shows an elemental area dA_i of total emissive power W radiating equally in all directions (diffuse or Lambertian) from one side, with some of its radiation being intercepted by another elemental area dA_j at a distance r from dA_i. A line connecting the two elemental areas forms the angles ϕ_i and ϕ_j with the normals η_i and η_j to the elemental areas, respectively. The heat transfer rate from dA_i to dA_j, $dQ_{i \rightarrow j}$ is directly proportional to the product of the apparent area of dA_i as seen from dA_j ($dA_i \cos\phi_i$) and the apparent area of dA_j as seen from dA_i ($dA_j \cos\phi_j$). It is also inversely proportional to the square of the separation distance r. A proportionality term I_i, representing the emitted intensity at the surface of dA_i, must be introduced. Thus, $dQ_{i \rightarrow j}$ is

$$dQ_{i \rightarrow j} = \frac{I_i \, dA_i \cos\phi_i \, dA_j \cos\phi_j}{r^2} \tag{1}$$

Since W has been defined as the total emissive power of dA_i, $dQ_{i \rightarrow j}$ may also be expressed as

$$dQ_{i \rightarrow j} = W dA_i \, F_{dA_i - dA_j} \tag{2}$$

where $F_{dA_i - dA_j}$ is defined as the shape factor between the elemental areas dA_i and dA_j. Setting equation (1) equal to equation (2) yields

$$dA_i \, F_{dA_i - dA_j} = \frac{I_i \, dA_i \cos\phi_i \, dA_j \cos\phi_j}{W r^2} \tag{3}$$

The definition of a Lambertian radiator states that the total emissive power W is π times the intensity of the emitted radiation. Hence, $W = \pi I$ substituted into equation (3) yields

$$dA_i \, F_{dA_i - dA_j} = \frac{dA_i \cos\phi_i \, dA_j \cos\phi_j}{\pi r^2} \tag{4}$$

To determine the total configuration factor between surfaces i and j in Figure 5, dA_j is integrated over A_j, then dA_j is integrated over A_i. The first integration yields

$$dA_i \, F_{dA_i - A_j} \quad dA_i \int_{A_j} \frac{\cos\Phi_i \, \cos\Phi_j \, dA_j}{\pi r^2} \tag{5}$$

and the second integration yields

$$A_i \, F_{A_i - A_j} \quad A_i \, F_{ij} \quad \int_{A_i} \int_{A_j} \frac{\cos\Phi_i \, \cos\Phi_j \, dA_i \, dA_j}{\pi r^2} \tag{6}$$

Hence the shape factor from surface i to surface j F_{ij} is

$$F_{ij} \quad \frac{1}{\pi A_i} \int_{A_i} \int_{A_j} \frac{\cos\Phi_i \, \cos\Phi_j \, dA_i \, dA_j}{r^2} \tag{7}$$

Therefore, the shape factor is, by definition, a dimensionless coefficient representative of that fraction of the total emitted flux leaving surface i incident on surface j. This is clearly seen by examining the definition of $F_{dA_i - dA_j}$ in equation (2), where F is first defined. Equation (2) rearranged yields

$$F_{dA_i - dA_j} = \frac{dQ_{ij}}{W dA_i} \tag{8}$$

where $dQ_{i \rightarrow j}$ is the heat transfer rate from dA_i to dA_j, and WdA_i is the total rate of heat transfer from dA_i.

The CFP deck calculates shape factors among all suppressor surfaces. The number of shape factors necessary to define the geometry is determined by the number of segments into which the suppressor wall contours are divided and the number of viewing, or aspect, angles for which calculations are desired. Figure 6 is an example of a typical suppressor, illustrating the segment and aspect angles. The number of segments is determined by the number of zones into which the investigator wishes to input separate surface temperatures and/or emissivities. Each segment of the wall contour is defined as a specific geometric shape or body of revolution, and appropriate translation, pitch, roll, and yaw inputs position the segment in the overall suppressor geometry construction. Figure 7 illustrates the input necessary to define, for example, a disc segment. Similar inputs are required for use of any of the geometric options included in the CFP deck.

The degree of accuracy attained in the calculation of the shape factors is also affected by the calculation grid size that is superimposed on each segment. That is, the number of rows and columns into which each segment is divided is also input, thus determining the size of the incremental areas necessary to calculate shape factors and ultimately, the accuracy of the final calculations. The shape factor calculations are then based on the interactions between the individual incremental areas of suppressor segments. Thus, computational complexity (i.e., computer time) is directly proportional to grid fineness. A trade-off study is necessary to determine the number of rows and columns for the segments; the use of an insufficient number of increments results in inaccurate shape factor calculations, but computer time requirements become excessive if the number of incremental areas is large.

IR ANALYSIS PROGRAM

When a matrix of shape factors representative of the suppressor geometry has been calculated, the set of shape factors, along with emissivity and temperature values for each segment of the suppressor, is input to the IRAP deck to obtain the IR signature. An option in the deck allows cooling flow distributions and heat transfer methods to be input in place of segment temperatures, and subroutines are employed to calculate average segment temperatures. Unfortunately, the heat transfer calculation techniques presently incorporated in the IRAP deck are inadequate for this study because different cooling techniques (film, transpiration, and convection), though considered separately, are not considered in combination in the IRAP deck (the ST9 suppressor employs two cooling methods simultaneously - film and convection). Also, the influence of internal cooling wall geometry on convection cooling is not treated in the IRAP deck. This precludes consideration of the fin effect, flow area variation, and coolant property variations associated with internal-wall convection cooling. In the optimization study, previously obtained experimental data and heat transfer technology developed under the ST9 Demonstrator program were used to obtain values of surface temperature for input to the IRAP deck.

The IRAP deck uses the input shape factors, segment temperatures, and emissivity characteristics to generate a matrix of radiation exchange factors, which define the radiation relationships between all segments of the suppressor. The radiant intensities and the IR signature are then calculated from the radiation exchange factors. The radiation exchange factors are defined similarly to the configuration factors, except that they account for multiple reflections in addition to the direct radiant heat transfer.

The main output from the IRAP deck is the calculated IR signature. The input matrix of shape factors defining the suppressor geometry and the calculated matrix of radiation exchange factors, if desired, are also printed out. These factors are useful if the effects of internal radiant heating are desired, since they define the internal radiant heat transfer as well as the heat transfer rate to external viewing locations. The calculated IR signature is also broken down into the percent total and reflected radiation emanating from the individual segments, or predefined grouped segments, which is helpful in a detailed analysis of the suppressor. A complete user's manual and deck listings are provided in Reference 3.

(U) SHAPE FACTOR CALCULATIONS

CONVERSION AND CHECKOUT OF COMPUTER PROGRAMS

The CFP and IRAP portions of the suppressor optimization computer programs previously described were almost completely compatible with the IBM System 360/75 as received. Therefore, little conversion was necessary. The example cases included in the optimization program user's manual (Reference 3) were input and successfully executed, thus verifying the conversion to the programs.

COMPUTATION OF SHAPE FACTORS

The suppressor was segmented for input to the CFP deck as shown in Figure 8. The suppressor geometry is mathematically represented by disc sections for segments 1, 10, and 11 and by polynomials of revolution for the remaining 12 segments comprising the suppressor. The polynomial curve fits were formulated using a least-squares curve-fit computer program with the coordinates from the suppressor blueprint (DKJ-5600) input. The resulting equations were also plotted to ensure that the polynomials were accurate representations of the suppressor geometry.

To calculate the shape factors, the segments must be divided into rows and columns, thereby forming multiple flat-plate elements. The size of the elements determines the accuracy and computing time requirements of the CFP calculations. To determine the optimum number of rows and columns, parametric cases were run for disc-to-polynomial and polynomial-to-polynomial shape factors, with the results presented in Figure 9. These data were obtained by varying the number of rows and columns, individually, on the emitter section, while the receiver grid size remained unchanged. The disc-polynomial shape factor is for Sections 1 and 2 of the suppressor segmentation, and the polynomial-to-polynomial is for Sections 4 and 13. These calculations show that for these segments, a grid size of 72 rows and 25 columns is necessary. Based on these results, grid requirements were chosen for the other segments of the suppressor based on the type of section and its proximity to other sections, which also strongly affects the accuracy of the shape factor calculations.

Table I is a tabulation of the completed shape factor matrix. The zeros in the table indicate that the surfaces do not have "line of sight" between them; hence, the shape factor value is zero. The five viewing angles that were selected as being adequate are shown in Figure 8.

Several basic relationships between shape factors permitted a check to be made on the validity of the calculated F_{ij} values. The two most extensively used were the following:

Proportionality: $F_{ij}A_i = F_{ji}A_j$

Summation Rule: $\sum_{j=1}^{15} F_{ij} = 1.00$

TABLE I. (U) MATRIX OF SHAPE FA(

Area (in.^{2})	Segment No.	Viewing A									
		1	2	3	4	5	6	7	8	9	1(
67.4	1*	0	0.270	0.110	0.026	0.556	0.046	0	0	0	0
146	2	0.124	0	0.022	0.005	0.641	0.158	0	0	0	0
176	3	0.042	0.018	0	0	0.161	0.482	0	0	0	0
172	4	0.010	0.004	0	0	0.006	0.055	0	0	0	0
193	5	0.194	0.487	0.146	0.005	0.061	0.050	0	0	0	0
155	6	0.020	0.149	0.545	0.060	0.062	0.041	0	0	0	0
94.5	7	0	0	0	0	0	0	0	0	0	0
85.3	8	0	0	0	0	0	0	0	0	0	0
91.8	9	0	0	0	0	0	0	0	0	0	0
51.3	10	0	0	0	0	0	0	0	0	0	0
15.9	11	0	0	0	0	0	0	0	0	0	0
107	12	0	0.021	0.363	0.346	0.012	0.040	0	0	0	0
221	13	0	0.013	0.070	0.465	0.008	0.025	0.076	0.066	0.001	0
225	14	0.003	0	0.009	0.119	0.011	0.031	0.279	0.144	0.047	0
206	15	0.001	0	0	0.003	0.008	0.027	0.076	0.196	0.221	0.0

*Row numbers designate suppressor emitter segment.
**Columns 1-15 designate suppressor receiver segment.
Columns 16-20 represent the viewing angles of 0, 15, 30, 45 and 60 deg.

ATRIX OF SHAPE FACTORS

	Viewing Angle Segments**												
	8	9	10	11	12	13	14	15	16	17	18	19	20
	0	0	0	0	0	0	0.010	0.002	0	0	0	0	0
	0	0	0	0	0.015	0.020	0	0	0	0	0	0	0
	0	0	0	0	0.222	0.088	0.010	0	0	0	0	0	0
	0	0	0	0	0.217	0.599	0.156	0.003	0	0	0	0	0
	0	0	0	0	0.007	0.009	0.012	0.009	0	0	0	0	0
	0	0	0	0	0.027	0.035	0.045	0.035	0	0	0	0	0
	0	0	0	0	0	0.177	0.664	0.167	0.107	0.037	0.009	0	0
	0	0	0	0	0	0.015	0.380	0.475	0.191	0.159	0.064	0.016	0.001
	0	0	0	0	0	0.002	0.115	0.496	0.215	0.207	0.173	0.093	0.022
	0	0	0	0	0	0	0	0.073	0.330	0.318	0.283	0.228	0.158
	0	0	0	0	0	0	0	0.047	0.330	0.318	0.283	0.228	0.158
	0	0	0	0	0.020	0.071	0.102	0.030	0.050	0.041	0.021	0.011	0
76	0.066	0.001	0	0	0.035	0.045	0.124	0.075	0	0.050	0.043	0.022	0.008
79	0.144	0.047	0	0	0.048	0.131	0.043	0.057	0	0	0.026	0.047	0.059
76	0.196	0.221	0.018	0.004	0.015	0.080	0.062	0.041	0	0	0.016	0.040	0.063

Preceding Page BLANK - NOT FILMED

The summation rule is only valid for segments that are completely enclosed by other suppressor segments, i.e., none of their radiant heat transfer can escape to the external viewing angles. This includes segments 1 through 6 of the suppressor. (See Figure 8.) Checking the values of the completed shape factors by these two methods verified the accuracy of the CFP deck calculations.

(S) COMPARISONS WITH PREVIOUSLY MEASURED IR SIGNATURES (U)

(U) To indicate the accuracy of the computer programs, the deck calculations were compared with some previously measured IR signatures. The surface emissivity and temperature data from the electrically heated half-scale model tests and the full-scale ST9 Demonstrator suppressor test programs (Reference 1) were input to the IRAP deck, along with the matrix of shape factors. The emissivities for these cases had been previously measured, and the temperatures had been measured with thermocouples on both the cooling louvers and the uncooled surfaces of the suppressors. Although large axial temperature gradients occur on the cooled portions of the walls, there was a sufficient number of thermocouples to calculate average louver temperatures with reasonable accuracy. However, there is generally more uncertainty in the temperature values for these cases than in the emissivity values.

(S) ELECTRICALLY HEATED MODEL COMPARISONS (U)

(U) During the design of the Demonstrator IR suppressor, a half-scale electrically heated model of the suppressor was built and tested to help determine the surface temperatures required to meet the suppression goals. In this rig, electric heating coils and water cooling tubes are brazed to the outer surfaces of the Hastelloy X suppressor walls. These afford the capability to simulate the axial temperature gradients that occur with the convection/film cooling scheme of the suppressor without the need for hot exhaust flow. Hot-parts emissions can thereby be measured directly. A number of IR signatures were measured corresponding to the simulation of a wide range of coolant distributions to the visible suppressor surfaces. The test program also included tests with and without a high-emissivity paint applied to the visible suppressor walls. The results of these tests (Reference 1, Table XII) thus provide the IR signatures attained from a wide range of surface temperatures and two different visible-surface emissivities.

(S) The deck predictions, in terms of the agreement of maximum signature levels, are compared in Table II for the 2-3 and 3-5μ bandwidths. (The 3-5μ data for the unsuppressed test are not presented because the radiometer was overdriven when this point was recorded.) Although consistently higher than the measured maxima, the computer program predictions were generally in excellent agreement, especially since the uncertainty in IR signature measurements has been shown to be $\pm 24^{\circ}$ (Reference 4). The 2-3μ bandwidth predictions are consistently less accurate than the higher-absolute-magnitude 3-5μ bandwidth results, but this inaccuracy is probably due to radiometric uncertainties rather than deficiencies in the deck. These comparisons are considered to be the best verification of the IRAP deck's capabilities, since the measured data used in these comparisons are actual radiometric measurements with no corrections for exhaust plume emission/attenuation effects.

(S) DEMONSTRATOR SUPPRESSOR COMPARISONS (U)

(U) During the test program, the ST9 suppressor test rig was tested at four power settings and several cooling flow rates, as well as with no cooling flow. Suppressed and unsuppressed IR data were recorded with both a broadband and a spectral radiometer, and hot-parts radiation levels were calculated for the 2-3μ

and 3-5μ bandwidths by using data recorded in bandwidths where plume emissions do not occur. (See Reference 1.)

(S) The results of the IRAP deck predictions for the full-scale suppressor tests are compared in Table III. As with the electrically heated model comparisons, the 2-3μ results show consistently greater variations than do the higher-magnitude 3-5μ values, probably for the reasons stated previously. Note, however, that the large percentage errors in the 2-3μ band are small differences in absolute magnitude. When the magnitude of the 2-3μ radiation is large, as in the unsuppressed case, the predicted signature agrees with the measured within 6% . These results further verify the accuracy of the IRAP deck predictions.

(S) A summary comparison of the predicted and measured IR signatures is presented in Figure 10 for the electrically heated and suppressor data in the 2-3μ and 3-5μ bandwidths. For values less than 10 w/sr (not shown in the figure), the scatter attributed to the measurement uncertainties causes the comparison to become poor. However, the comparison shows that, except for a few isolated points, the measured and predicted signature levels agree within ±20%, and the vast majority of the points in the 10 to 20 w/sr range are within ±10% of perfect agreement. The data from 10 to 100 w/sr appear to be randomly scattered above and below the zero error line, but the values above 100 w/sr indicate that the predicted signature is consistently higher than the measured, regardless of aspect angle.

(U) All of the data comparisons were also prepared as individual polar plots for each test, and are presented in Appendix I.

TABLE II. (S) COMPARISON OF MAXIMUM MEASURED AND PREDICTED IR LEVELS FOR ELECTRICALLY HEATED MODEL TESTS (U)

Run No.*	Description of Test	Maximum Measured J- w/sr 2-3μ Bandwidth	Maximum Measured J- w/sr 3-5μ Bandwidth	Maximum Predicted J- w/sr 2-3μ Bandwidth	Maximum Predicted J- w/sr 3-5μ Bandwidth	Percent Error 2-3μ Bandwidth	Percent Error 3-5μ Bandwidth
1	Unsuppressed Signature**	230	-	250	540	8.7	-
2	Suppressed Signature	13	55	14	50	7.7	9.1
3	Total Reflected Radiation - All Viewable Surfaces Cold	6.3	24	10	25	58.7	4.2
-	Total Reflected Radiation With Exposed Surfaces Black - All Viewable Surfaces Cold	1.8	5	2.1	6.1	16.7	22.0
8	Suppressed Signature With Exposed Surfaces Black	9.0	42	7.5	35	-16.7	-16.7
9	Reduced Wall Temperature Corresponding to Increased Cooling Flow, Exposed Surfaces Black	3.	18	3.9	19	18.2	5.6
10	Increased Outer Wall Temperature - Final Suppressor Signature, Exposed Surfaces Black	4.4	23	4.5	23	2.3	0

*From Reference 1, Table XII.
**Uncooled wall temperatures for all tests were equal to exhaust gas temperature at MRP conditions.

Page 24 of 120 Pages

TABLE III. (S) COMPARISON OF MAXIMUM MEASURED AND PREDICTED IR LEVELS FOR DEMONSTRATOR SUPPRESSOR TESTS (U)

Run No.*	Description of Test	Maximum Measured J-w/Sr		Maximum Predicted J-w/Sr		Percent Error	
		2-3μ Bandwidth	3-5μ Bandwidth	2-3μ Bandwidth	3-5μ Bandwidth	2-3μ Bandwidth	3-5μ Bandwidth
4.01	MRP With Hot Cooling Flow	-	64	11	59	-	-7.8
7.03	MRP With Maximum Cooling Flow	4.6	34	6.8	35	47.8	2.9
9.09	83% MRP With Design Cooling Flow	2.3	22	3.1	22	34.8	0
16.01 16.02	MRP, Unsuppressed	180	430	190	470	5.6	9.3

*From Reference 1, Table XII.

(S) PARAMETRIC OPTIMIZATION STUDY (U)

(U) Using the completed shape factor matrix, which defines the suppressor geometry, as input to the IRAP deck of the optimization computer program, a complete parametric study of the effects of coolant distribution and suppressor surface emissivities was conducted.

(U) TEMPERATURES AND EMISSIVITIES USED IN THE PARAMETRIC STUDIES

Emissivity Values

Three levels of emissivity were varied parametrically. The values were chosen to correspond to known emissivities of three coating candidates that are representative of a wide range of possible emissivities. Hence, the study was conducted with the following emissivities:

Low, ϵ = 0.1 (Hanovia Gold)

Intermediate, ϵ = 0.5 (Magnesium Zirconate)

High, ϵ = 0.9 (PTI-404A Black Paint)

Surface Temperatures

The temperatures of the cooled segments as a function of cooling flow rate were determined using the heat transfer technology developed during the ST9 Demonstrator engine program. Specifically, the louver wall temperature profiles measured during the runs at NRP (9.01-9.10) of the suppressor test program (Reference 1), combined with analytical predictions, were used to determine the average heated surface temperature for each louver as a function of the total coolant flow rate to that region. The coolant flow rates to each of the three cooled zones were expressed as a percentage of the total coolant flow (which was held constant), and the average individual louver wall temperatures were then expressed in terms of these flow-rate percentages.

The cooling louver temperatures used in the parametric study are presented in Figures 11, 12, and 13 for the inner wall, outer wall, and base respectively. These plots are graphical representations of experimental and analytical results from the previous tests of the suppressor. In some cases, the analytical predictions did not agree with the measured data, i.e., the predicted curves did not pass through the measured data points. In these cases, the predicted curves were simply translated vertically to pass through the data points, so that the extrapolations to smaller or larger coolant flow rates could be made with confidence. This technique was applied to all cooled segments of the suppressor, unless the analytical and measured data agreed exactly.

Coolant flow distributions for the parametric study were selected such that a wide range of possible combinations would be considered. However, the overall range of coolant flow splits was limited by the structural integrity of the cooling air plenums, which were not designed for high-pressure operation. Other factors considered in the selection of the high and low limits for the inner/outer wall distribution

were the wall temperatures attained. After consideration of these factors, coolant distributions of 10, 20, 30, and 40 were chosen for the inner wall louvers; 50 through 90 in 5 increments for the outer wall louvers; and 0, 5, and 10 for the base. The application of these coolant flows to the parametric study will be explained in subsequent paragraphs. All percentages represent the fraction of the total design value of cooling airflow, 0.778 lb/sec.

The temperatures input for the uncooled segments were those measured during the previous tests. The turbine was simulated as being at exhaust gas temperature with an emissivity of 1.0. This value is justified when one considers that in the test rig the turbine is simulated by a straight-pipe section upstream of the suppressor inlet, the walls of which are radiating at exhaust gas temperatures. This isothermal cavity in place of the power turbine is very nearly representative of a true blackbody source.

(U) GENERAL DESCRIPTION OF METHODOLOGY

One of many useful options of the suppressor optimization computer program IRAP deck allows the user to input individual segments, for which separate shape factors are defined, as a grouped surface. When using this option, several suppressor segments are redefined as a grouped surface for which single emissivity and temperature inputs are required, thus conserving computer and input time. This option was utilized in the parametric study, in which the nonvisible inner and outer wall segments were each grouped, thus forming two input regions from five individual shape factor segments. Further, the visible inner and outer walls, and the base, were considered to be grouped surfaces in the sense that individual emissivities for these regions were used, rather than attempting to vary each louver emissivity individually. However, these regions were not input to the IRAP deck as grouped surfaces, since the option precludes the ability to input separate louver surface temperatures. To present the parametric results, then, the suppressor geometry shown in Figure 11 was used. Regions I, II, and III are the nonvisible turbine, inner wall, and outer wall, and regions IV, V, and VI are the visible inner wall, base, and outer wall.

Using the segmentation by regions as the definition of the variables for the parametric study, there are five regions for which the emissivities must be optimized (II-VI) and three regions for which the temperatures (cooling distribution) must be optimized (IV, V, and VI). Furthermore, these two variables are not independent of each other. Hence, the method of determining the optimum emissivity/coolant distribution values must consider the combined, or interacting, effects of emissivity and cooling distribution. A complete parametric variation of the terms described above would result in a total of nearly a thousand possible combinations, assuming that an adequate number of cooling distributions were investigated. However, it was possible to reduce this number to less than 200 IRAP deck cases with no reduction in the total scope of the parametric study. This was accomplished by conducting two studies to determine the radiation contributions of (1) the nonvisible, uncooled surfaces, and (2) the visible, cooled surfaces, and then adding the results. These two studies could be conducted independently because the radiation emanating from the nonvisible surfaces (regions I, II, and III, Figure 11), and reflected to the environs by the visible surfaces, is independent of the temperatures of the visible surfaces. Therefore, since the temperatures

of the nonvisible surfaces remain constant, the reflected radiation can be minimized by simply parametrically varying the emissivities of all suppressor surfaces (defined as regions) until a combination of surface emissivities which minimizes reflected radiation is found.

Further, the radiation of the visible surfaces emanating directly to the environs is independent of the emissivities of the nonvisible surfaces, assuming the effects of internal radiant heating are negligible. Therefore, a study was conducted to determine the radiation of the visible, cooled surfaces by parametrically varying their emissivities and cooling distributions while the temperatures of the nonvisible surfaces were held at zero. The independence of these two studies reduced the number of computer runs necessary to conduct a complete parametric study by more than 80%.

Reflected Radiation From the Nonvisible Regions I, II, and III

The conditions of this study were as follows:

1. The temperatures of the visible surfaces (regions IV, V, and VI) were input as zero.
2. Nonvisible surface temperatures (regions I, II, and III) were held constant at the value equal to measured temperatures from the Demonstrator tests at NRP.
3. Power turbine emissivity was assumed to be 1.0 for all cases.

A typical reflected radiation study matrix is shown in Figure 15. Each element JR_{ij} in this reflected radiation matrix represents the source radiant intensity prediction for the i^{th} row and j^{th} column emissivity conditions. Since visible surface temperatures are input as zero for this study, the results of the JR matrix represent the true prediction of reflected emissions from internal sources, independent of the distribution of cooling flow to regions IV, V, and VI.

Radiation From the Cooled Regions IV, V, and VI

The conditions of this study were as follows:

1. The temperatures of the nonvisible surfaces (regions I, II, and III) were input as zero.
2. The temperature of region V (the base) was input as a function of the cooling flow remaining after regions IV and VI were supplied.

A typical study matrix is shown in Figure 16. Each element JD_{ij} of the matrix represents the source radiant intensity prediction for the i^{th} row emissivity conditions and the j^{th} column cooling flow distribution to regions IV and VI, i.e., the visible portions of the inner and outer wall. Note that the radiation of the visible base area (region V) has been omitted. From examination of the geometry of the suppressor, it was determined that the base area of the centerbody acts

only as a specular reflecting surface at aspect angles between 66 and 80 deg. The projected visible surface area of the base is relatively small at these large aspect angles, and it was concluded that the radiation reflected from the base was negligible. This conclusion is verified by the small values of the shape factors from segment 15 (the last louver of the outer wall) to the base segments (Figure 8), which is indicative of low diffuse reflections. Since the base contributes direct radiation, the obvious optimum value of emissivity is 0.1, or the lowest emissivity attainable with coatings. Thus, the only study necessary for the base is the effect of cooling flow. This study was not conducted separately, but was combined with the computer runs that comprise the JD matrix. Each column j of the JD matrix has a specific percent W_c assigned to the inner and outer cooled walls. Obviously, all columns do not total 100%. The difference represents the amount of cooling air supplied to the base for that particular case. Thus, column 1 computer runs included the base segment temperatures that correspond to 10% base cooling flow; column 2 included 5% base cooling, etc. Hence, the JD matrix elements represent predicted source radiant intensity levels from all visible surfaces, independent of the temperatures and emissivities of the nonvisible surfaces. The total number of input cases required to generate the JR and JD matrices presented above was 189.

Since the radiant intensities of the JR and JD matrices are independent of each other, they may be systematically added, or combined, into an expanded matrix that is representative of a complete parametric study of all the variables included in the two constituent matrices. The common denominator between the JR and JD matrices is the region IV and VI emissivity combinations, which define the rows of both matrices; e.g., the radiant intensity predictions in any row i of JR are compatible with those in row i of JD. The resulting three-dimensional matrix expansion may be generalized as $JT_{nkj} = JR_{nk} + JD_{nj}$ for each row n, column k of JR, and row n, column j of JD. However, since the objective was to determine the combination of emissivities and cooling distributions resulting in the minimum value of JT, a complete expansion, which would result in 972 possible total source radiant intensities, was not required. Rather, the minimum, or optimum JT_{njk} value, was determined as follows:

1. The minimum value from each row of the JR and JD matrices was selected.
2. The corresponding row values $(JR_n + JD_n)_{minimum}$ rows 1 to 9 were added.
3. The optimum configuration was then the minimum value from the resulting nine possibilities.

Since the computer program IRAP deck allows the user to select two bandwidths, JR and JD matrices were formed for both the 2-3 and 3-5μ bands. The complete matrix expansions for all viewing angles and radiation bandwidths are presented in Appendix II, along with the combined optimum for each aspect angle and wavelength band.

(S) OPTIMIZATION RESULTS (U)

(U) Before the reflected radiation (JR) and direct radiation (JD) matrices were combined to determine the optimum configuration for the suppressor, several conclusions were obvious from examining the individual matrices. The JR matrix results clearly showed that the cooled outer wall must have a high emissivity to reduce the potentially large reflected radiation emanating primarily from the uncooled inner wall. In addition, the reflected radiation matrix showed that the optimized emissivity for the uncooled inner wall was 0.1, thus further reducing the reflected radiation. Results of the JD matrix were not so easily interpreted. There are no "obviously optimized" emissivities and/or coolant distributions, since the emissivity/coolant distribution combinations have interacting effects, and also because the trends with aspect angle are not consistent. However, it was clear from the JD results that 5% base flow was slightly superior to the 10%, which was tested in the Demonstrator suppressor program, and the 0%. The 0% resulted in an intolerably large signature from the base.

(S) Results of the combined matrix are presented in Figures 17 through 20 for the 15-deg aspect angle. These show typical effects of inner and outer wall emissivity variations for the four coolant flow distributions. Figure 17 shows that for low coolant flow rates to the inner wall (resulting in higher inner wall temperatures), the emissivity of this surface should be as low as possible. The same trend is apparent in Figure 18, but the effect of the inner emissivity is negligible, since the three curves almost converge at the minimum IR level of 21 w/sr. In Figures 19 and 20, the trend is reversed and the minimum IR signature occurs when the visible inner wall has a high emissivity. All of these curves show the desirability of a high emissivity coating on the visible outer wall, since this reduction in IR signature is due to decreased reflections, which are independent of the coolant distribution. However, because these are for the 15-deg aspect angle only, a comparison of the absolute levels of these four figures, which would indicate that the 40/55/5 percent coolant distribution is optimum, is misleading. Nevertheless, the relationships represented in these graphs do demonstrate that the optimum emissivity combinations are not independent of the coolant flow distribution.

(S) Figures 21, 22, and 23 show the IR signature results in the 3-5 μ bandwidth as a function of aspect angle for the three most promising emissivity combinations. In each figure, the nonvisible outer wall emissivity is 0.5 (representative of no emissivity-control coating - just bare metal), the visible outer wall emissivity is 0.9, and the base emissivity is 0.1. Further, the base flow rate is held constant at 5% in all three graphs. Hence, the only variable factors are the inner/outer wall percent coolant split (the abscissa of each graph) and the emissivity of the visible inner wall, which are 0.1, 0.5, and 0.9, respectively. A comparison of these three figures shows that the emissivity combination of 0.9 on both visible walls (Figure 23) clearly yields the minimum IR signature of only 17 w/sr, which is 26% below the 23 w/sr maxima of the Demonstrator suppressor design.

(S) A comparison of Figures 21 and 23 shows the interdependence of surface emissivity and coolant distribution, illustrating that these two variables cannot be "optimized" independently. The optimum coolant distribution in Figure 21 is 17/78 (inner/outer wall percent coolant flow), resulting in a maximum IR signature

of 21 w/sr at 0 and 15 deg. The optimum coolant distribution in Figure 23 is 29/66. Thus, the change in the cooled inner wall emissivity between these two figures radically changed the optimum coolant distribution, which illustrates the interdependence of these two variables. This comparison also illustrates that the optimum choice cannot be based on a single aspect angle, but that the overall trend of the IR signature with aspect angle must be considered. This is a factor which is also optimized with the 29/66 percent coolant distribution and the high emissivity visible walls shown in Figure 23. Using the parameters defined in Figure 23 as a starting point, additional IRAP deck cases were run with small coolant distribution changes to further refine the IR signature optimization. Figures 24 and 25 present the results with the base flow held at 3%, while the distribution to the inner and outer cooled walls is varied. These results, though slightly higher overall than those previously presented and showing less sensitivity to the coolant distribution, are essentially identical to the levels with 5% base flow. Considering the limitations in the measurement accuracy of hot-parts IR radiation, the differences observed in the maxima are negligible; however, since the predicted maximum signature occurs over a smaller range of aspect angles with 3% base flow, the 29/68/3 distribution was selected as the optimum coolant distribution for the test program. With less than 3% base flow, substantially higher signatures result, since the base temperature increases very rapidly.

(S) The optimized IR signature is shown in Figures 26 and 27 for the 2-3 and 3-5 μ bandwidths. The measured IR signature from the ST9 Suppressor Program is also plotted on these graphs for comparison. The optimized design gives a 25% reduction in the maximum IR signature in the 3-5μ bandwidth, and a 13% reduction in the 2-3μ bandwidth. Whereas the maximum signatures previously occurred at zero deg aspect angle, the optimization yields an essentially constant level from 20 to 50 deg. Table IV shows how the IR signatures were decreased in terms of the change in emissivity and coolant flow distribution from the Demonstrator design to the optimized suppressor. The two changes that give the largest signature reduction are (1) coating the nonvisible inner wall with a low-emissivity coating, which substantially reduces the reflected radiation, and (2) changing the cooling flow distribution from 22/68/10 to 29/68/3 percent, which substantially reduces the direct radiation.

(S) After the emissivity-control coatings were chosen, the computer program IRAP deck was rerun with the actual coating emissivities of 0.05 and 0.95. The results are presented in Figures 28 and 29, along with the signatures based on the 0.1 and 0.9 emissivities. The trends are the same, at a slightly lower overall level in the 3-5μ bandwidth and a significantly lower level in the 2-3μ bandwidth, resulting in final predicted signature reductions of 26 and 28% in the 2-3 and 3-5μ bandwidths, respectively. As previously discussed, this maximum occurs over a large aspect angle, approximately 20 to 50 deg. Hence, the final emissivity/coolant distribution values that minimize the IR signature are (1) 0.05 emissivity on the uncooled, nonvisible inner wall and the cooled plug base, (2) 0.95 emissivity on the cooled, invisible inner and outer walls, and (3) a 29/68/3 (inner wall/outer wall/base) percent coolant distribution. The results of the parametric study indicated that the emissivity of the uncooled, nonvisible portion of the outer wall had no appreciable effect on the reflected radiation. For this reason, emissivity control was not deemed necessary for this surface.

[illegible] 30 of 120 Pages

Page 31 of 120 Pages

TABLE IV. (S) COMPARISON OF ORIGINAL AND OPTIMIZED IR SUPPRESSORS (U)

Grouped No.	Surface Name	Surface ε's		Change in Coolant Flow (%)	Change in Radiant Intensity at the 15-deg Aspect Angle	
		Original	Optimized		(w/sr)	(%)
1	Turbine	1.0	Not Changeable	-	0.20	200
2	Nonvisible Inner Wall	0.4-0.6	0.1	-	-2.20	-60
3	Nonvisible Outer Wall	0.4-0.6	0.4-0.6	-	0.0	0
4	Visible Inner Wall	0.9	0.9	33	-2.90	-28
5	Plug Base	0.4-0.6	0.1	-70	-0.30	-42
6	Visible Outer Wall	0.9	0.9	1	-0.30	-4
Total Change		-	-	0	-5.50	-25

(S) SELECTION AND APPLICATION OF EMISSIVITY-CONTROL COATINGS (U)

(U) Two emissivity-control coatings had to be selected for application to the suppressor. The selections were made based on the emissivity values of the coatings investigated under an Army-sponsored program (Reference 2) as being capable of withstanding turbine exhaust gas temperatures for prolonged periods of time. Of the coatings recommended for IR suppressors, the highest and lowest emissivity coatings were selected: the phosphate-bonded ceramic coating for the high-emissivity coating, and the gold film over a zirconium diffusion barrier for the low-emissivity coating.

(U) The recommended surface preparation and coating application techniques described in Reference 2 were followed to the extent possible with the full-scale suppressor. However, before the coatings were applied, an application study using sample coupons of Hastelloy X FINWALL and sheet stock was conducted to evaluate the use of Hastelloy X as a substrate and to investigate alternate methods of surface preparation. The best samples were then subjected to a 1200°F exhaust plume environment for 12 hours to determine their durability under actual test conditions. There was no change 'n the appearance of the coatings at the end of the 12-hour test, thereby indicating the acceptability of Hastelloy X.

(S) The changes in recommended surface preparation included using a hand-polished surface preparation, instead of the stipulated electropolishing for the low-emissivity coating. This change was necessary because the struts and the complex curve surface of the suppressor precluded electropolishing without significant development time and expense. Also, after recommended application of the gold film and the low temperature bake, an additional baking operation at 800°F for 20 minutes was found to be required to produce a high gloss gold surface.

(S) The high-emissivity coating was applied to the suppressor surfaces in accordance with instruction. The ferric chloride etching process stipulated by the Army-sponsored coating investigation for preparation of this coating was not used because of the possibility of damaging the 0.005-in. louver material. A grit blast was substituted. Bend tests and 12-hour exhaust environment endurance tests of coupon samples indicated that the coating adherence was comparable to that demonstrated in the Army-sponsored program.

(U) The details of the surface preparation, application, and baking procedures used are outlined in the following paragraphs. Figure 30 shows how the suppressor was disassembled to facilitate application of the coatings. The coated suppressor is shown in Figures 31, 32, and 33.

(S) HIGH-EMITTANCE COATING (U)

(U) The phosphate-bonded ceramic coating was applied to the four cooling louvers that make up the outer wall and to the three cooling louvers of the inner wall.

(S) Surface Preparation (U)

Louver surfaces were prepared as follows:

1. Mask all surfaces except those to be cleaned.
2. Grit blast exposed areas with No. 90 silicon carbide grit at 30-50 psig nozzle pressure.
3. Clean any areas missed by the grit blast with 80-grit silicon carbide paper.
4. Wipe all exposed surfaces with cloth dampened with perchlorethylene.

(S) Coating Application (U)

The ceramic coating application is as follows:

1. Pour off excess solvent such that the Sermetal material to be applied consists of 50% solvent and 50% solid particles by volume.
2. Using a soft camel's hair brush, apply a uniform coat to surface (coating was applied to the inner wall louvers by using a spray gun rather than a brush).
3. Allow coating to dry in air for 30 minutes.
4. Bake in air-atmosphere furnace for 1.0 hour at 300°F.
5. Repeat steps 2-4 four times.

(S) LOW-EMITTANCE COATING (U)

(S) Eight coats of zirconium oxide diffuser barrier material were sprayed and baked on the highly polished surfaces of the base and uncooled inner wall. One coat of gold resinate was then brushed onto both surfaces and baked to produce a high gloss gold finish.

(S) Surface Preparation (U)

The surfaces were prepared as follows:

1. Remove oxide layer from uncooled inner wall by using a very fine grade emery cloth.
2. Polish uncooled inner wall and base with buffing wheels and compound until a mirror-like surface is obtained.

(S) Application of Diffusion Barrier (U)

The diffusion barrier is applied as follows:

1. Thoroughly mix one part zirconium resinate (Hanovia No. 5437) with seven parts cineole (eucalyptus oil) by weight and filter solution to remove foreign particles.
2. Clean uncooled inner wall and base with clean cloth dampened in Varsol (refined kerosene) to remove polishing compound.
3. Remove Varsol by wiping surfaces with a clean cloth dampened with perchlorethylene.
4. Spray a very thin coat of zirconium resinate solution on uncooled inner wall and base.
5. Air dry for 15 minutes.
6. Bake part in a dust-free, air-atmosphere furnace at 200°F for 25 minutes.
7. Bake part in a dust-free, air-atmosphere furnace at 960°F for 20 minutes.
8. Vacuum clean surfaces after part has cooled to 140°F or less.
9. Repeat steps 4-8 a total of eight times.

(S) Application of Gold Film (U)

The gold film is applied as follows:

1. Clean zirconium oxide surfaces with cloth dampened in acetone. Vacuum clean to remove dust.
2. Brush on one coat of gold resinate (Hanovia "N") over uncooled inner wall and base.
3. Air dry for 45 minutes.
4. Bake part in dust-free, air-atmosphere furnace at 392°F for 15 minutes.
5. Bake part in dust-free, air-atmosphere furnace at 800°F for 30 minutes.

(U) TEST PROGRAM

MOUNT AND CHECKOUT

The tests were conducted in the D-32 stand at Pratt & Whitney Aircraft's Florida Research and Development Center. Figure 34 shows the suppressor test rig mounted in the stand with a swirl generator mounted just upstream of the suppressor. The swirl generator, shown in Figure 35, has adjustable vanes to swirl the flow entering the suppressor, simulating the turbine exhaust flow at off-design power settings. The downstream end of the swirl generator is instrumented to define the flow conditions at the suppressor inlet.

The main air supply for the D-32 stand is compressor bleed air from a J57 slave engine. Maximum airflow capability is 15 lb/sec at 100 psia, which is more than adequate to simulate the ST9. A JP-4-fueled heater burner is installed in the main supply line to heat the air before entering the suppressor test rig. Thus, through appropriate controls, the flow entering the suppressor duplicated the engine exhaust flow rate, temperature, pressure, and swirl angle.

Cooling air for the test rig is supplied by two centrifugal blowers connected in series and regulated by remote-controlled butterfly valves. The cooling air is then split into three separate lines: one for the outer wall, one for the inner wall, and one for the base. Each supply line has a flow-measuring orifice and a hand control valve to permit individual control of the coolant flow to each cooled section of the suppressor.

All data were taken by manually recording manometer readings for pressure data and potentiometer readings for thermocouple data.

Plywood shielding painted with flat black paint was installed such that rig and stand parts were hidden from the field of view of the radiometers. A sketch of the shielding relative to the suppressor and radiometers is shown in Figure 36. The suppressor exit after installation of shielding but prior to the first checkout tests is shown in Figure 37.

After completion of mounting and instrumentation hookup, six hot-flow checkout tests were conducted at a simulated engine operating condition of 837 MRP. The test log, presented in Table V, gives the test conditions for all the tests. Different total coolant flow rates were run in the checkout tests to provide orifice data needed for setting the total coolant flow at the design value of 0.788 lb/sec. During the checkout tests, satisfactory performance of the test stand heater burner, cooling air supply system, and the suppressor was verified by recording and analyzing all data needed for running the test program. The only irregularities detected during the checkout tests were that wall temperatures of the base louvers and the last outer wall louvers were about 100°F lower than predicted, and the coolant ΔP had increased over that of previous tests of the suppressor.

TABLE V. (U) OPTIMIZED IR SUPPRESSOR TI

Date	Run No.	Test Objectives	Hot Gas Flow Conditions: Power Setting % MRP	Swirl Angle (deg)	Flow Rate (lb/sec)	Total Temperature (°F)	Mach No.	OW Flow Rate (lb/sec)	IV Flow (lb/
10/11/71	1.01	Test Rig Checkout	83	16	7.08	1030	0.335	0.552	0.2
10/11/71	1.02	Test Rig Checkout	83	16	7.13	1035	0.338	0.640	0.2
10/11/71	1.03	Test Rig Checkout	83	16	7.23	1030	0.342	0.453	0.1
10/13/71	1.04	Test Rig Checkout	83	16	7.96	1030	0.381	0.563	0.2
10/13/71	1.05	Test Rig Checkout	83	16	7.61	1030	0.361	0.531	0.2
10/13/71	1.06	Test Rig Checkout	83	16	7.45	1035	0.431	0.459	0.1
10/13/71	2.01	Performance and IR Signature at 83% MRP	83	16	7.82	1035	0.373	0.528	0.2
10/13/71	2.02		83	16	7.07	1035	0.374	0.532	0.2
10/14/71	2.03	Performance and IR Signature With Adjusted Coolant Flows	83	16	7.70	1035	0.368	0.545	0.2
10/14/71	2.04		83	16	7.72	1035	0.369	0.548	0.2
10/15/71	3.01	Performance and IR Signature at 100% MRP	100	21	8.48	1145	0.416	0.517	0.2
10/15/71	3.02		100	21	8.39	1140	0.412	0.529	0.2
10/15/71	4.01	Performance and IR Signature at 40% MRP	40	21	6.52	835	0.281	0.522	0.2
10/15/71	4.02		40	21	6.52	835	0.281	0.514	0.2
10/18/71	5.01	Performance and IR Signature at 60% MRP	60	0	7.01	925	0.320	0.518	0.2
10/18/71	5.02		60	0	7.07	925	0.322	0.521	0.2

IZED IR SUPPRESSOR TEST LOG

Mach No.	Coolant Flow Conditions					Hot Time (hr)	Remarks
	OW Flow Rate (lb/sec)	IW Flow Rate (lb/sec)	Base Flow Rate (lb/sec)	Total Flow Rate (lb/sec)	Total Temperature (°F)		
0.335	0.552	0.233	0.026	0.811	115	0.5	Test Objectives Achieved
0.338	0.640	0.270	0.030	0.940	118	1.0	Test Objectives Achieved
0.342	0.453	0.191	0.023	0.667	110	1.5	Test Objectives Achieved
0.381	0.563	0.238	0.014	0.816	90	2.0	Test Objectives Achieved
0.361	0.531	0.225	0.026	0.782	120	2.5	Test Objectives Achieved
0.431	0.459	0.192	0.022	0.673	120	3.0	Test Objectives Achieved
0.373	0.528	0.220	0.025	0.772	135	4.1	Initial Coolant Flow Split Resulted in High Inner Wall Temperatures and Low Base Temperatures
0.374	0.532	0.208	0.025	0.765	110	5.3	
0.368	0.545	0.233	0.013	0.790	110	6.2	Base Flow Reduced and Inner Wall Flow Increased; Test Objectives Achieved
0.369	0.548	0.234	0.015	0.797	100	8.0	
0.416	0.517	0.226	0.016	0.759	107	9.3	Test Objectives Achieved
0.412	0.529	0.225	0.016	0.770	106	9.6	Test Objectives Achieved
0.281	0.522	0.230	0.017	0.769	115	10.7	Test Objectives Achieved
0.281	0.514	0.226	0.016	0.756	110	11.0	Test Objectives Achieved
0.320	0.518	0.243	0.016	0.777	100	11.7	Test Objectives Achieved
0.322	0.521	0.242	0.016	0.778	100	12.2	Test Objectives Achieved

Preceding Page BLANK - NOT FILMED

TEST

As shown in the Test Log, 10 hot-flow tests were conducted with the optimized suppressor. Due to the time required to make a radiometer traverse to take IR data at five aspect angles, two sets of pressure and temperature data are recorded for each IR traverse. In tests 2.01-2.02 at 83% MRP, the optimum coolant distribution determined in the analytical study, 29/68/3 (% to inner wall/outer wall base), was used. However, the data showed that the base temperatures were about 100°F lower than predicted. Since the predicted IR signature was based on wall temperatures rather than flow rates, the base coolant flow rate was reduced until base temperatures near those predicted were attained. Two additional tests at 83% MRP (2.03-2.04) were then conducted, and are considered the "design point" tests for comparison with the predicted IR signature. The temperature of the last two outer wall louvers still ran somewhat low, however.

Using essentially the same cooling flow-rate distribution developed during tests 2.03-2.04, tests were run at power settings of 100, 10, and 60% MRP, as shown in the test log. No difficulties with the stand, suppressor, or radiometric equipment occurred during these tests, and the planned test program was thus completed with test 5.02.

After completion of the test program, the suppressor was demounted and the coatings examined to determine if any deterioration had occurred. As shown in the photograph of the suppressor exit in Figure 38, a discolored area appeared in the gold coating on the outer base louver at about the 1 to 3 o'clock position. Close examination of this area indicated that the thin gold film had come off during testing. However, this defect appeared early in the test program and did not increase significantly in size after it was first observed. Apparently, improper coating application or contamination resulted in poor bonding of the gold to the diffusion barrier in this area. The high-emissivity coating, with the exception of a few small areas where the coating chipped off, showed no deterioration from the 12 hours of hot-flow tests. Examination of the upstream, inlet end of the suppressor revealed that a layer of rust-type dust had been deposited all over the gold-coated surface of the uncooled inner wall. However, removal of the dust with a cloth showed that the gold film was still in excellent condition. Photographs taken before and after removal of the dust are shown in Figures 39 and 40. Although the dust layer probably increased the emissivity of the coating, the good agreement between predicted and measured IR signatures indicates that a major increase in emissivity did not occur before completion of the 83% MRP design point test.

(S) TEST RESULTS (U)

(U) COOLING SYSTEM PERFORMANCE

The results of the analytical study showed that the optimum cooling flow split was 29/68/3 (% to inner wall/outer wall base), which, for the design total flow rate of 0.778 lb/sec, translates to flow rates of 0.230 0.530 0.020 lb/sec. However, the analytical study was based on the surface temperatures predicted as a function of flow rate, not on flow rate specifically. The initial tests showed that the cooling flow split had to be changed to obtain the surface temperatures approximating those shown to be optimum in the analytical study. Unfortunately, the resulting wall temperatures were still somewhat different from the predicted, or optimum, values shown in Figures 41, 42, and 43 for the inner wall, outer wall, and base respectively. These data, at the design point of 837 MRP, show that the first inner wall louver was cooler than predicted, but that louvers 2 and 3 were hotter than predicted. The average louver temperatures, shown in Table VI, differed by 45° to 85°F. The net effect of these inner wall differences was a small increase in the IR signature at the low aspect angles where the inner wall is visible.

The main discrepancy with the outer wall temperatures (Figure 42) was that the last two louvers were about 100°F cooler than predicted, resulting in a reduced IR signature at high aspect angles. The base temperatures (Figure 43) agreed fairly well with predicted values.

The difference was unexpected since the predictions were based on previous test data at nearly the same coolant flow rates (Reference 1). The main reason the temperatures didn't agree with the predicted values is believed to be the grit-blasting operation (recommended in Reference 2) used to prepare the surface of both the inner and outer wall louvers for the high-emissivity coating. The force of the 30-psi grit blast could have reduced the cross-sectional area of the coolant passages by slightly collapsing the 0.005-in.-thick FINWALL skin. Although close inspection of the louvers did not reveal any obviously depressed areas, a few thousandths reduction can make a large difference in the 0.040-in. coolant passage height. The increase in coolant plenum pressures (also listed in Table VI) required to obtain the desired coolant flow rates supports this belief. The very high inner wall plenum pressure was noted immediately during the check-out tests. It was first thought that the coating (which is a liquid applied by spraying or brushing) had plugged the coolant passages. Accordingly, all the coolant passages were then rodded out with a piece of wire. However, only insignificant plugging was found, and only a slight decrease in the coolant ΔP was achieved.

Since the grit blasting was a manual operation, it is probable that the various louvers were affected randomly. Thus, the ΔP of some louvers could have been more seriously degraded than others, resulting in some louvers running cooler and some hotter than predicted. (The amount of cooling flow an individual louver passes is not controlled; it is a function of its cross-sectional area and the plenum pressure.)

TABLE VI. (U) ST9 SUPPRESSOR COOLING SYSTEM PARAMETER COMPARISON

Parameter	Predicted Value	Measured Value-Run 2.04
Coolant Supply Temp, °F	120	125
Total Coolant Flow Rate, lb/sec	0.778	0.797
INNER WALL		
Coolant Rate, lb/sec	0.230	0.234
Coolant Plenum Pressure, psia	16.2	18.4
Average Surface Temp - Louver 1, °F	510	435
Average Surface Temp - Louver 2, °F	310	395
Average Surface Temp - Louver 3, °F	395	440
Uncooled Surface Temp - °F	970	990
OUTER WALL		
Coolant Flow Rate, lb/sec	0.530	0.548
Coolant Plenum Pressure, psia	15.6	15.9
Average Surface Temp - Louver 1, °F	430	445
Average Surface Temp - Louver 2, °F	465	450
Average Surface Temp - Louver 3, °F	530	455
Average Surface Temp - Louver 4, °F	480	370
Uncooled Surface Temp - °F	850	780
BASE		
Coolant Flow Rate, lb/sec	0.020	0.015
Coolant Plenum Pressure, psia	14.8	14.9
Average Surface Temp - Louver 1, °F	360	335
Average Surface Temp - Louver 2, °F	350	315

These results negate the analytical optimization study as to the optimum cooling flow distribution. However, the primary objective of attaining a significant decrease in the IR signature with no increase in cooling flow was achieved.

The remainder of the test at the other power settings proceeded without further anomalies. The surface temperatures, as expected, generally varied directly with power setting, as shown in Figures 44, 45, and 46 for the inner wall, outer wall, and base. The only exception was the inner wall, which ran cooler at 60% than at 40%. This is consistent with the Demonstrator test results, and is due to the better film cooling achieved with the 0-deg swirl angle at 60% MRP. With the high swirl angle of the other power settings, the cooling film discharged from each louver tends to be washed away and quickly degraded. Thus, the 21-deg swirl angle at 40% power reduces the film cooling effectiveness more than enough to offset the 90°F reduction in exhaust gas temperature. This effect is more pronounced on the inner wall because it has a severe adverse pressure gradient that also degrades the film. The fact that the third inner wall louver is film cooled only also makes the inner wall more susceptible to film cooling effectiveness changes.

(S) IR SIGNATURE (U)

(U) Infrared radiation measurements were made using a Mark IX spectral radiometer and a R8K broadband radiometer. The spectral radiometer uses a variable 1.6-5.3μ filter, and the broadband data were taken using 2-3, 3-5, and 3.79-4.0μ filters.

(U) The radiometers were traversed from 0 deg (dead aft) to 80 deg on an arc approximately 200 feet from the suppressor exit, with data recorded at five equally spaced aspect angles for each IR signature measured. All radiation measurements were made at night to minimize the background radiation.

(U) A calibration source made from a flat copper plate 10 in. in diameter was placed adjacent to the suppressor. PTI404 paint was used as a high-emissivity coating on the copper plate, and calibrated thermocouples were imbedded in the plate for accurate temperature measurement. Measurement of the IR emissions of the calibration source was made consecutively with each measurement of the suppressor.

(U) Data Reduction Procedures

The radiant intensity of the calibration source, in units of watts/steradian, was calculated from its temperature and emissivity using standard gray-body radiation formulae. The responsivity factors of the broadband radiometer, in units of watts/steradian/millivolt, were then calculated by dividing the reading of the radiometer (in millivolts), when viewing the calibration source, into the calculated radiant intensity of the calibration source for each band-pass filter:

$$\text{Responsivity factor, } R = J_{calib}/V_{calib}, \quad w/sr/mv$$

The spectral data were recorded on a strip chart recorder. Responsivity factors for the spectral data were calculated by measuring the areas under the spectral

plots for the bandwidths of interest with a planimeter, and dividing the calculated radiant intensity for the same bandwidths by the measured areas. Spectral data were calibrated for the 2-3, 3-5, and 3-4μ bandwidths.

The source radiant intensity of the suppressor, in units of w/sr, was then calculated by multiplying the readings of the broadband radiometer (in mv) by the appropriate responsivity factors, and multiplying the areas under the spectral plots by the spectral radiometer responsivity factors. In this manner, the true radiant intensity of the suppressor was measured. The atmospheric attenuation did not have to be corrected because the path length from the calibration source to the radiometers is the same as the path length from the suppressor to the radiometers.

Since the measured emissions in the 2-3 and 3-5μ bandwidths include large plume contributions, hot-parts emissions were calculated using the 3.79-4.0 and 3-4μ data, where the exhaust plume emissions are negligible. This was accomplished using standard blackbody radiation formulae to calculate an effective temperature for the suppressor from the emissions in these two bandwidths. This effective temperature was then used to calculate the hot-parts radiant intensity over the 2-3 and 3-5μ bandwidths. Because the broadband and spectral calculations are based on data from different bandwidths, the answers do not agree exactly; they are only an approximation of the "correct" answer. The spectral values are considered more accurate, however, since large absolute levels are used in the extrapolation. This same procedure was used in the ST9 Demonstrator program, and is described in detail in Reference 1.

In addition to the bandwidth radiation calculations described above, the spectral data were used to calculate the spectral distribution of the emissions. The calibration technique described above was used, except that the absolute levels (height) of the various wavelengths on the spectral plots were used to calculate responsivity factors, as opposed to the areas used for the bandwidth calibrations. Standard gray-body radiation formulae were used to calculate the calibration source emissions at the specific wavelengths, and these values were divided by the measured heights on the spectral plot at the same wavelengths. A bandwidth of 0.1μ was used for wavelengths other than the plume emission bandwidths around 2.7 and 4.3μ, where increments of 0.05μ were used to better define the steep slopes of the plume emission spikes.

(S) Test Results (U)

(U) The measured IR signature of the optimized suppressor is compared with that of the original Demonstrator suppressor design in Figures 47 and 48 for the 2-3 and 3-5μ bandwidths at the design point of 83% MRP. Those data show that the optimized suppressor gave a reduction in the IR signature of 22% or more in both bandwidths, which is a significant reduction, especially since it was attained with no degradation in engine performance.

(S) The measured IR signatures for the two bandwidths are compared with those predicted from the analytical study in Figures 49 and 50. These data show that the measured IR signature is slightly higher than the predicted signature at aspect angles between 0 and 30 deg. At aspect angles from 30 to 90 deg, however, the measured IR signature decreased considerably more rapidly than did the predicted

signature. The reason for this is the measured wall temperature distributions (Figures 41 and 42), which show that the temperatures of the last two outer wall louvers were lower, and the temperatures of similar inner wall louvers higher, than those predicted and used in the optimization study. Since the last two outer wall louvers contribute most of the IR signature at high aspect angles, the reduced temperature of these louvers reduced the radiant intensity at high angles. Conversely, the increased inner wall temperatures increased the signature at the low aspect angles. The IRAP deck was therefore rerun with the measured values of wall temperature; the results are presented in Figures 51 and 52. The agreement is much better, and these results verify the accuracy of the IRAP deck.

(S) The spectral data for the 83% MRP tests were also reduced to obtain curves of source spectral radiant intensity ($w/sr/\mu$), as shown in Figures 53 through 57 for all five aspect angles recorded. Because the measurements were made at a distance of 200 feet from the target, the intervening atmosphere significantly attenuated the measured emissions in the H_2O and CO_2 bandwidths around 2.7 and 4.3μ. Therefore, the readings received at the radiometer for these wavelengths were nearly zero for the target and zero for the calibration source. Because of these low levels, the radiometer data in these regions cannot be considered valid; therefore, only dashed lines are shown in the figures near the plume emission peaks at 2.7 and 4.3μ.

(S) The blackbody radiation curves superimposed on the spectral traces of Figures 53 through 57 illustrate the method used to calculate the hot-parts radiation. These curves are for the effective temperature corresponding to the radiation between 3.0 and 4.0 μ, where plume emissions are negligible, and the radiation can be attributed to hot parts alone. The blackbody curves are then integrated from 2-3 and from 3-5μ to obtain the hot-parts radiation for these bandwidths. Note that the blackbody curves agree reasonably well with the measured data in the 3-4μ range. The agreement is not exact because the radiating hot parts are not actually at a constant temperature, and there is also reflected radiation emanating from the much hotter uncooled portions of the suppressor.

(S) The IR signature at 100% MRP is presented in Figures 58 and 59, along with the results from the Demonstrator suppressor. The IR signature from the optimized suppressor is higher than that of the Demonstrator suppressor at aspect angles between 0 and 20 deg and lower at angles greater than 20 deg. The increase in IR emissions at low aspect angles was caused primarily by the high base temperature, which was 500°F during the test at 100% MRP. This was caused by the reduction in base cooling flow from 0.08 to 0.02 lb/sec. This optimized the IR emissions at 83% MRP, but it is not an optimum coolant distribution at 100% MRP, as might be expected. The optimum cooling distribution for the suppressor is obviously dependent on the power setting, i.e., the exhaust gas temperature at which the optimization is conducted.

(S) Similar comparisons of IR signatures from the optimized suppressor and the Demonstrator suppressor are presented in Figures 60 and 61 for the 40% power setting and in Figures 62 and 63 for 60% MRP. These data are the total measured emissions, i.e., including the contributions of the plume. The comparisons show that the emissivity/coolant distribution optimization made only a small improvement in the maximum IR levels. This is because the reduction in the temperature of the nonvisible surfaces and the turbine at low power settings reduces the reflected radiation to a small percentage of the total. Thus, the reduction due to emis-

sivity control coatings is much less. The trend of lower emissions at high aspect angles occurred because of the lower-than-expected temperatures of the last two outer wall louvers, consistent with the results at 83% and 100% MRP.

(U) In general, the emissivity/coolant distribution optimization resulted in significant reductions in IR emissions at the design point of 83% MRP, lesser reductions at lower power settings, and an increase in the maximum signature at 100% MRP. These results, which clearly demonstrate that the optimum configuration is a function of the power setting, indicate that future optimization studies should also consider the engine operating regime, i.e., range of exhaust gas temperatures, as a criterion for choosing the optimum emissivity/coolant distribution values.

43 120 Pages

(U) AERODYNAMIC PERFORMANCE

The aerodynamic performance of a diffuser is measured by the ratio of the static pressure increase from the inlet to the exit of the diffuser ($p_2 - p_1$) to the inlet dynamic pressure (q_1). This ratio is termed the pressure recovery coefficient, Cp:

$$Cp \quad \frac{p_2 - p_1}{q_1} \tag{9}$$

The numerator of this coefficient is determined by assuming that the exit pressure p_2 of subsonic flow exhausting to the atmosphere is equal to ambient pressure, and by calculating an average of the measured inlet static pressures (p_1). The determination of the denominator, q_1, given by

$$q_1 = P_{t_1} - p_1 \tag{10}$$

requires an average inlet total pressure (P_{t_1}). Values of P_{t_1} are computed from measurements of the two inlet total pressure rakes, which implies that the conditions at the rake locations are representative of the conditions around the entire inlet annulus. This was not the case, however, for some of the tests in this program apparently because of inaccurate settings of the individually adjustable swirl-generator vanes. This was determined by comparisons of q_1 with a dynamic pressure computed from the measured mass flow rate for each test assuming a uniform flow across the inlet. The mass-flow dynamic pressure, q_{flow}, was computed from the relations

$$V = \dot{w}/(\rho A_1 \cos \alpha) \tag{11}$$

and

$$q \quad \rho V^2/2 \tag{12}$$

as

$$q_{flow} \quad (\rho/2)\left(\frac{\dot{w}}{A}\right)^2 \left(\frac{1}{\cos^2 \alpha}\right) \tag{13}$$

Note that a correction for swirl angle, $\cos \alpha$, has been included, since $\dot{w}/\rho A$ represents only a mass-average axial component of velocity.

A comparison of q_{flow} and q_1 for any test should show that $q_1 > q_{flow}$. This is because dynamic pressure is a function of the square of the velocity; a nonuniform velocity profile, therefore, has a higher dynamic pressure than the same average velocity with a uniform profile. In other words, it takes more energy to drive a nonuniform flow through a duct than a uniform flow.

In general, the ratio q_1/q_{flow} has varied between 1.01 and 1.15 during previous small-scale and full-scale diffuser tests. Occasionally, values of q_1/q_{flow} between 0.9 and 1.0 occur because of circumferential distortions in total pressure. In these cases, the inlet total pressure rake is located in the wake of a swirl vane and the recorded total pressures are less than the circumferential average. Therefore, a $q_1/q_{flow}<1.0$ is the result.

A tabulation of Cp's (based on q_1) and ratios of q_1/q_{flow} is given in Table VII for all tests of the coated suppressor and for selected tests conducted at the same power settings during the Demonstrator program. All tests of the coated suppressor at 83% MRP had q_1/q_{flow} values less than unity and Cp's about 6% higher than the value used in the Demonstrator program from test 9.10 (Cp = 0.62). This indicates that wakes from swirl vanes impinged on one, or both, of the installed inlet total pressure rakes. However, the good agreement of these data with the average q_1/q_{flow} from Demonstrator tests 9.01 and 9.11 (q_1/q_{flow} = 0.98) indicates that a similar problem existed in some of the Demonstrator tests. Since the swirl vane angle was reset between Runs 9.01 and 9.11 to repair a broken swirl vane, a slight change in swirl vane angle could have occurred. Hence, the large variation in q_1/q_{flow} experienced in the Demonstrator program was probably due to shifting of wake locations relative to the rakes. In this coated suppressor program, where swirl vane angle was not changed between runs 1.01 and 2.04, only small variations in Cp and q_1/q_{flow} (attributable to recording accuracy) occurred during those tests. Therefore, the relatively high Cp's at 83% MRP are attributed to wakes impinging on the total pressure rakes.

In tests 3.01 and 3.02, the coated suppressor was tested at conditions simulating 100% MRP. Table VII shows a large reduction in Cp (nearly 40%) from that obtained at 83% MRP. This was expected because a similar loss occurred in the Demonstrator program caused by large wakes from the flow separation from the six struts due to the high swirl angle (21 deg). However, the coated suppressor performance (Cp = 0.408) was about 10% below that of the average of Demonstrator runs 7.03 and 12.02 (Cp = 0.453). These differences in Cp can be explained by analysis of the variation of Cp with swirl angle in Figure 64, which shows the variation in the Cp of the coated suppressor as the power setting is increased from 40 to 100% MRP. Note that Cp drops very rapidly between 83 and 100% MRP even though swirl angle changes only 5 deg. Thus, in this area, a small variation in swirl angle produces a large variation in Cp. It is estimated that the accuracy of setting the swirl vanes is about ± 1.0 deg. As shown in Figure 64, a 1.0-deg error on either side of 21 deg would result in Cp values ranging between 0.32 and 0.50, or a 22% variation about the average. This indicates that the differences in Cp probably resulted from errors in swirl angle setting.

At 40% MRP, both Cp and q_1/q_{flow} are very close to the average between tests 8.01 and 11.01 of the Demonstrator suppressor, as shown in Table VII. Note that the Cp at 40% MRP is about 20% higher than that obtained at 100% MRP, although the swirl angle is the same at both power settings. This is because the inlet Mach number at 40% MRP is about 0.28, while at 100% MRP it is 0.41, as shown in Table V. Previous data from the Demonstrator program and from scale model tests have shown that Cp losses increase with M_1 at high swirl angles (Reference 5).

TABLE VII. (U) AERODYNAMIC PERFORMANCE DATA

		Coated Suppressor			Demonstrator Suppressor		
% MRP	Swirl Angle (deg)	Run No.	Cp	q_1/q_{flow}	Run No.	Cp	q_1/q_{flow}
83	16	1.01	0.643	0.977	9.01	0.714	0.917
83	16	1.02	0.647	0.964	9.10	0.624	1.051
83	16	1.03	0.637	0.967	9.11	0.622	1.056
83	16	1.04	0.664	0.988			
83	16	1.05	0.661	0.950			
83	16	1.06	0.665	0.956			
83	16	2.01	0.662	0.973	9.01	0.714	0.917
83	16	2.02	0.661	0.959	9.10	0.624	1.051
83	16	2.03	0.655	0.999	9.11	0.622	1.056
83	16	2.04	0.658	0.989			
100	21	3.01	0.407	1.080	7.03	0.385	1.148
100	21	3.01	0.408	1.079	12.02	0.520	1.023
40	21	4.01	0.504	1.083	8.01	0.459	1.144
40	21	4.02	0.507	1.079	11.01	0.560	1.012
60	0	5.01	0.649	1.140	10.01	0.571	1.121
60	0	5.02	0.648	1.117	14.01	0.564	1.118

The last two data points presented in Table VII (runs 5.01 - 5.02) were obtained at zero swirl angle simulating 60% MRP. These results show that the Cp from the coated suppressor was 14% higher than Demonstrator Cp's from runs 10.01 and 14.01. Although q_1/q_{flow} from the coated suppressor is higher than at other power settings, these data show good agreement with q_1/q_{flow} data from the Demonstrator tests. The reason for the higher performance is not known, but in general, performance losses in suppressors can be attributed to two effects: (1) flow separation due to too much curvature of the walls or too high an angle of attack on the struts, and (2) total pressure losses due to wall friction. Since the swirl angle was zero in runs 5.01 - 5.02, stall of the struts should not have occurred. However, a reduction in surface friction due to modification of the uncooled inner wall from a relatively rough, oxidized surface to a highly polished surface could produce higher performance; e.g., a previously undetected area of separation could have been eliminated by reduced boundary layer thickness, or a lower total pressure loss could have resulted from reduced wall skin friction. Either of these effects would tend to raise Cp without affecting q_1/q_{flow}. Hence, the improved performance at 60% MRP could be due to reduced surface friction of the uncooled inner wall.

The above results suggest that greater accuracy in Cp data would have been possible if a better swirl generator had been available. Several improvements in swirl generator design would improve accuracy: (1) connect all swirl vanes to a synchronizer ring having a vernier adjustment capability, and (2) use airfoil-shaped swirl vanes rather than the flat sheet-metal vanes currently used. Although an increase in complexity and cost would result, these changes would reduce Cp errors by improving swirl angle repeatability and reducing the size of wakes off swirl vanes. In general, the differences in Cp data between the coated and Demonstrator suppressor discussed above would have a negligible effect on engine horsepower. For the ST9 Demonstrator Engine, a 50% reduction in Cp results in only a 2.0% loss in shp or sfc. Therefore, the greatest difference in Cp between Demonstrator and coated suppressor tests (a 14% increase at 60% MRP) would affect shp and sfc only about 0.5%.

(U) CONCLUSIONS AND RECOMMENDATIONS

CONCLUSIONS

1. The objectives of this program were met. A significant reduction (22%) in the maximum IR signature at normal rated power (83% MRP) was attained through optimizing the surface temperature/emissivity of the suppressor.

2. There was a smaller reduction in the maximum IR signature at the lower power settings, and an increase at 100% MRP.

3. The CFP and IRAP decks provide an accurate and reliable means of predicting the IR signature of an infrared suppressor when surface emissivities and wall temperatures are known.

4. To minimize IR emissions at any viewing angle, a parametric study involving complete variation of emissivities and cooling flow distributions is desirable. The method of minimizing the reflected and direct emissions separately significantly reduces computing requirements necessary to optimize emissivity/coolant distribution values, and may be applied to any suppressor design.

5. Both the high and low emittance coatings used in this program showed good durability under simulated engine exhaust conditions. Use of emittance-control coatings on internal surfaces of an IR suppressor will reduce the IR signature with no increase in total coolant flow, weight, or complexity.

6. Periodic cleaning of coated surfaces may be required to prevent increases in IR signature due to accumulation of dust or other deposits on low emittance coated surfaces.

7 Application of coatings apparently increased aerodynamic performance at zero swirl, but had little effect on performance at swirl angles between 16 and 21 deg.

RECOMMENDATIONS

1. An analytical study should be conducted with increased total coolant flow rate (through a redesigned cooling louver system) to reduce the IR signature to the levels required of more advanced suppressor designs.

2. Infrared suppressors should be optimized such that the selected cooling flow and emissivity distributions provide the minimum IR signature at all power settings rather than at only one power setting.

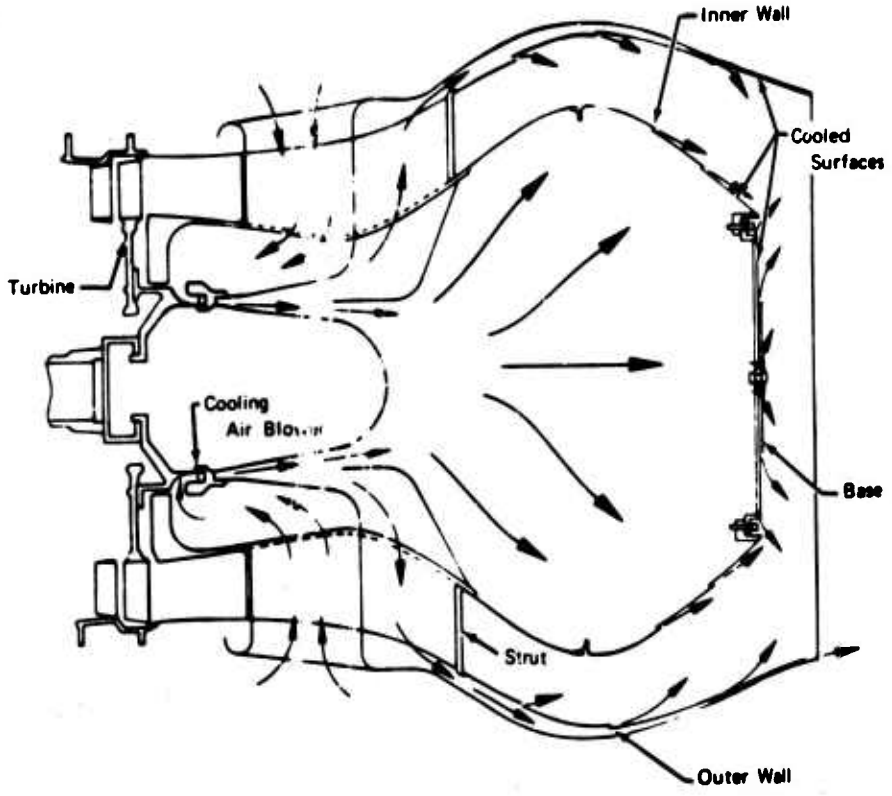

Figure 1. (U) ST9 Demonstrator IR Suppressor.

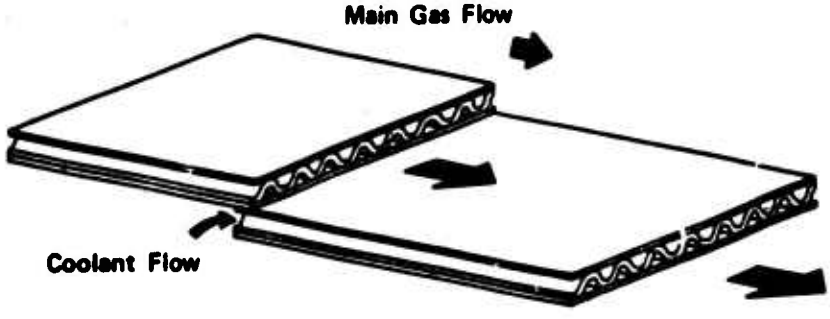

Figure 2. (U) TRANSWALL™ Louvers.

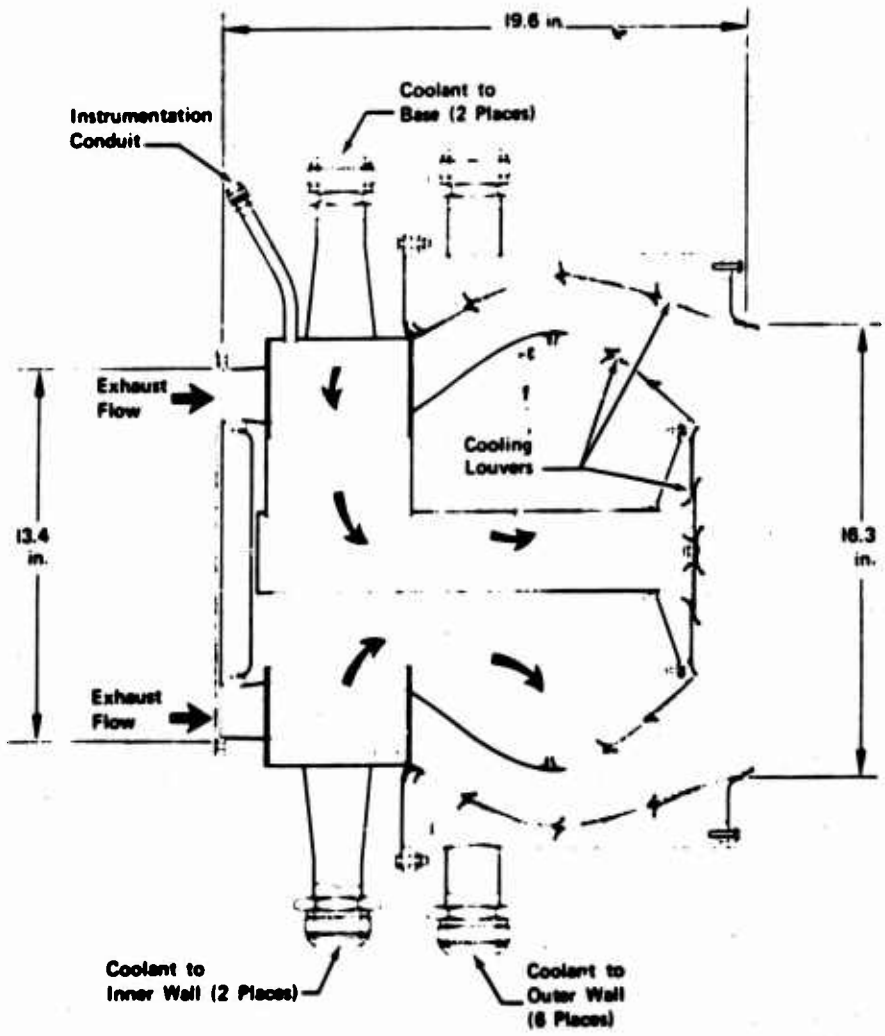

Figure 3. (U) ST9 Demonstrator IR Suppressor Test Rig.

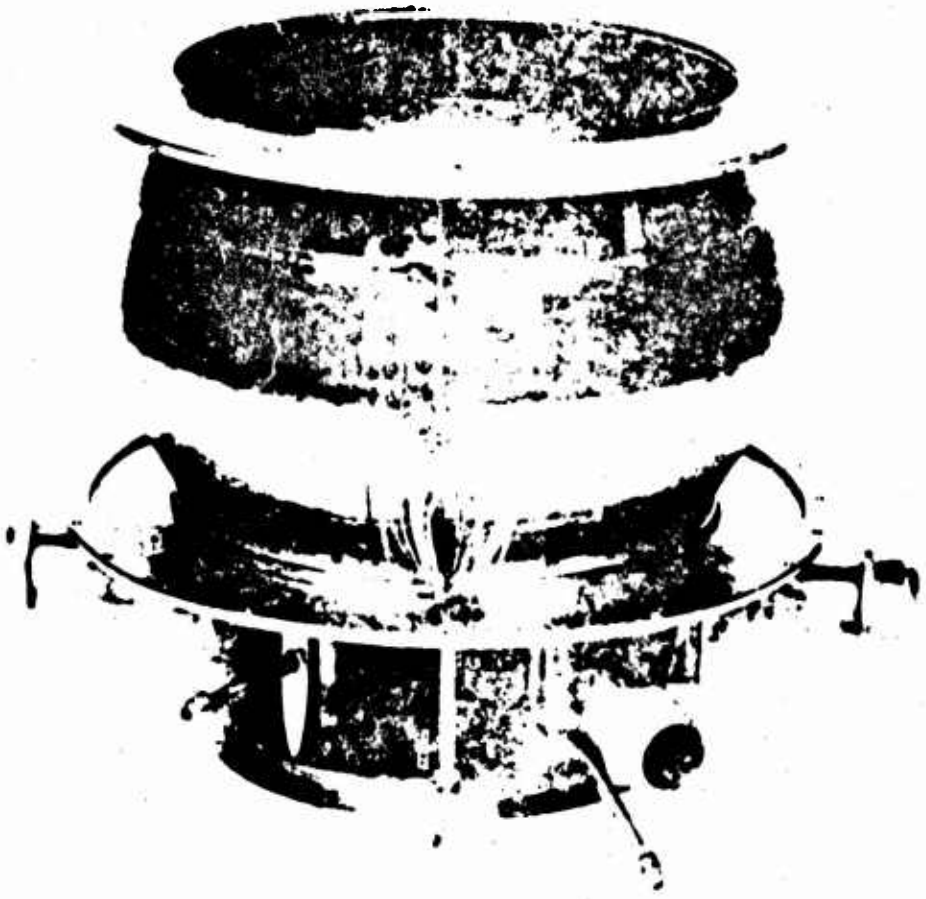

Figure 4. (U) ST9 Demonstrator IR Suppressor Test Rig (With Outer Wall Plenum Removed).

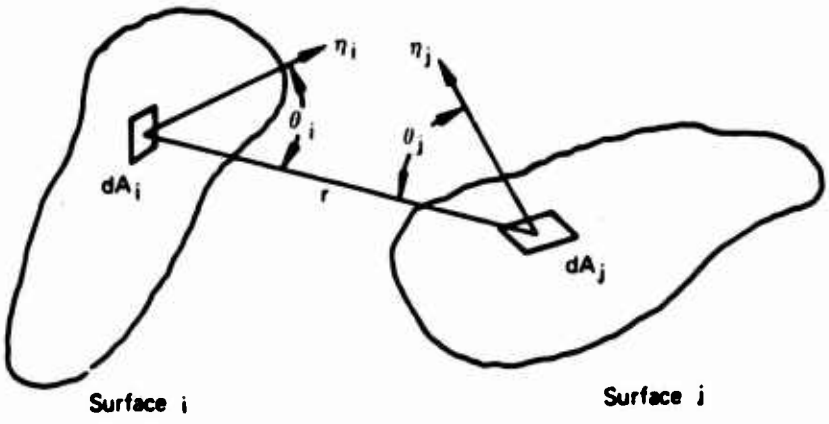

Figure 5. (U) Basic Lambertian Radiation Geometric Relationships

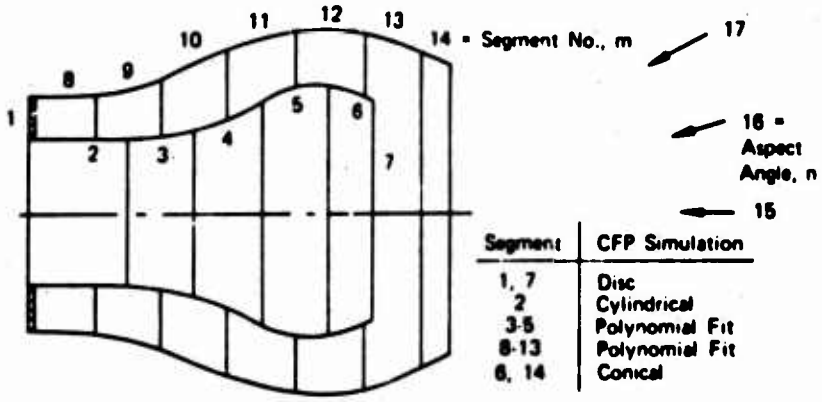

Figure 6. (U) Illustration of IR Suppressor Optimization Program CFP Deck Segmentation Capabilities and Relationship of Shape Factors to Segments.

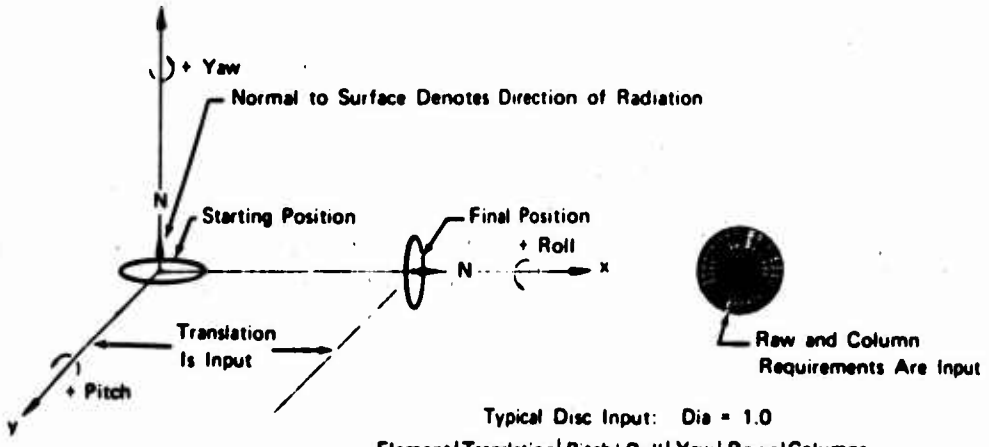

Typical Disc Input: Dia = 1.0

Element	Translation	Pitch	Roll	Yaw	Rows	Columns
No. 7 Disc	x = +3.4 y = z = 0	-90°	0°	0°	10	20

Figure 7. (U) Illustration of Geometry Input to IR Suppressor Optimization Program CFP Deck.

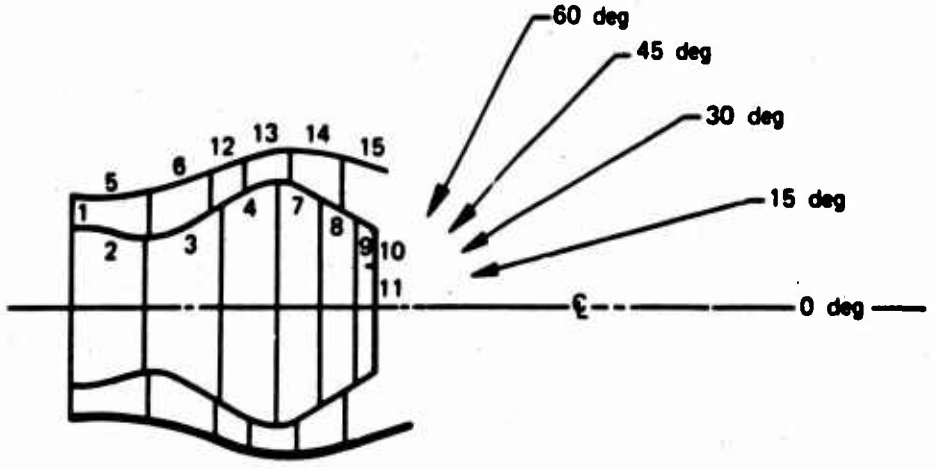

Figure 8. (U) ST9 Suppressor Segmentation for CFP Deck.

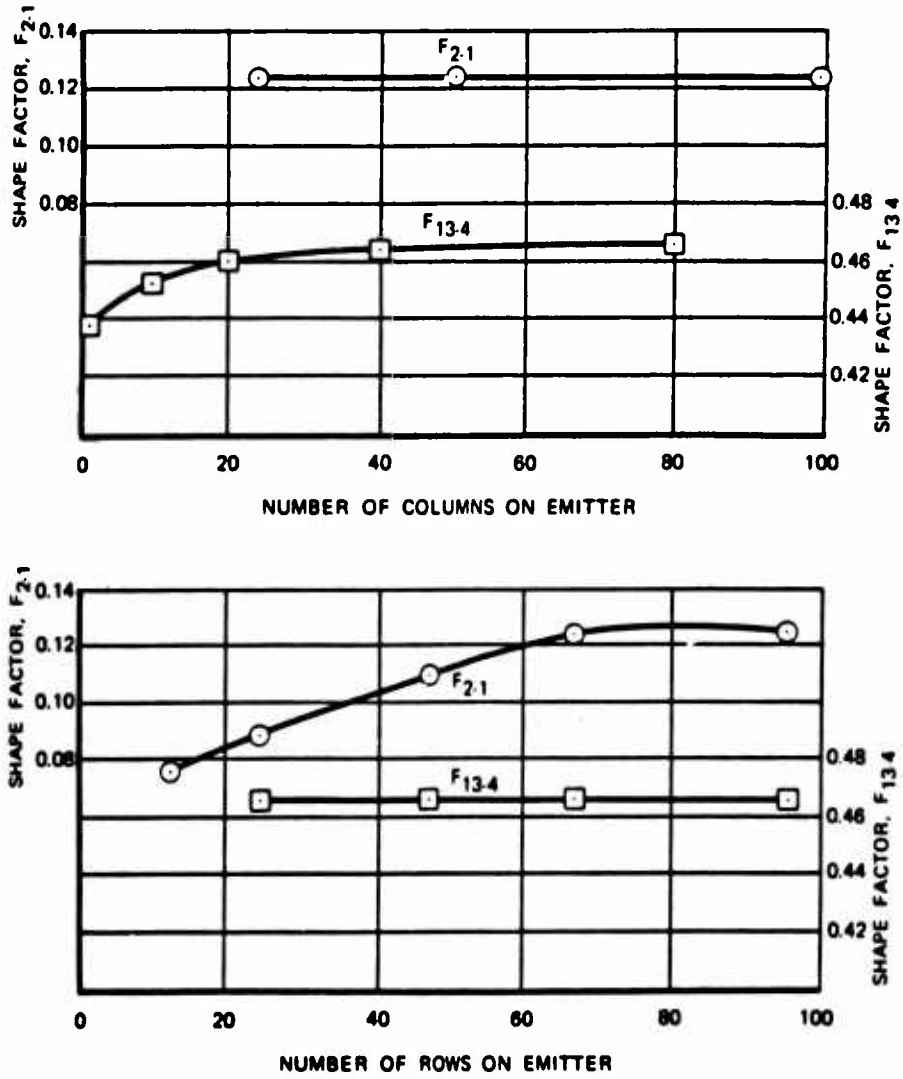

Figure 9. (U) Row and Column Effects on Shape Factor Accuracy.

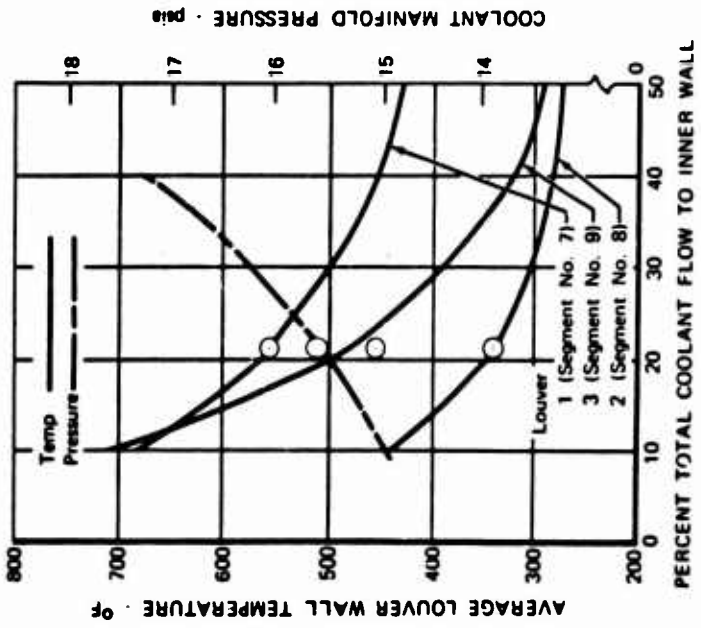

Figure 11. (U) ST9 IR Suppressor Predicted Average Inner Wall Temperatures.

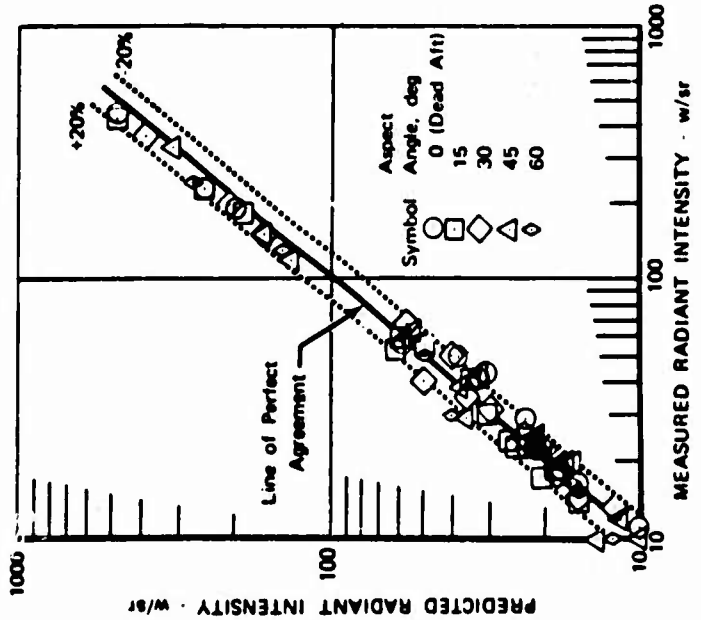

Figure 10. (S) Comparison of Measured and Predicted IR Signatures From Previous Suppressor Tests (U).

Page 55 of 120 Pages

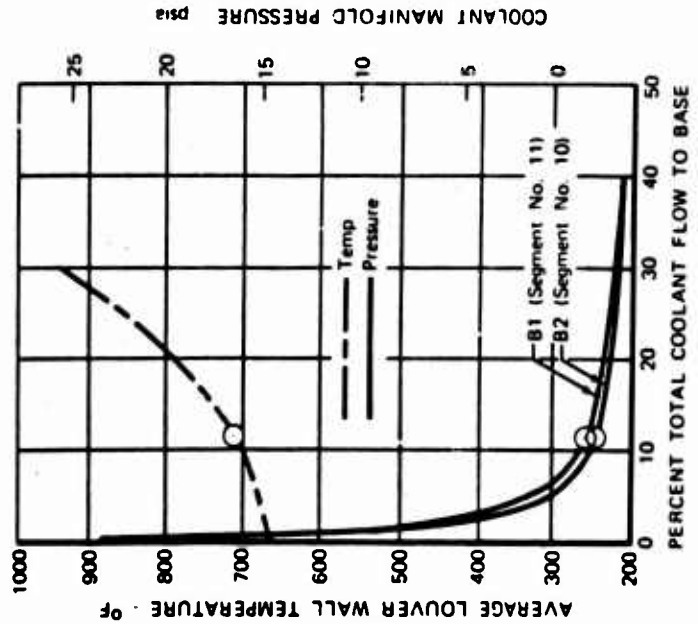

Figure 13. (U) ST9 IR Suppressor Predicted Average Base Temperatures.

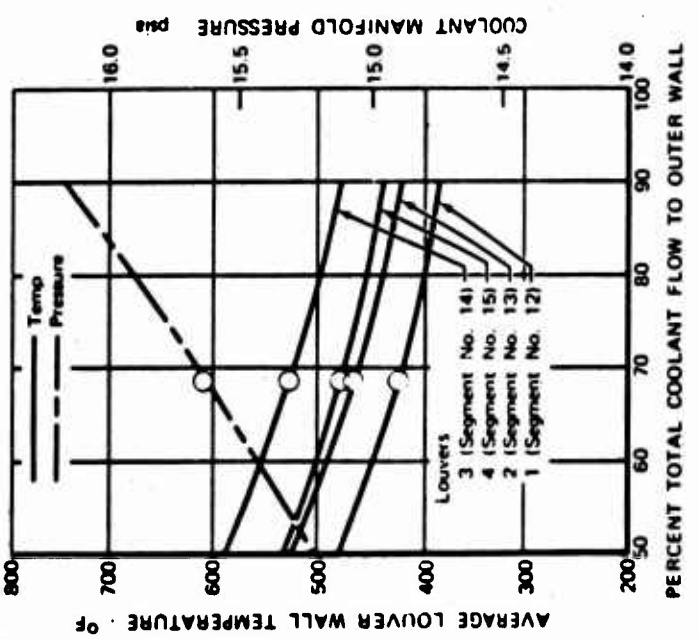

Figure 12. (U) ST9 IR Suppressor Predicted Average Outer Wall Surface Temperatures.

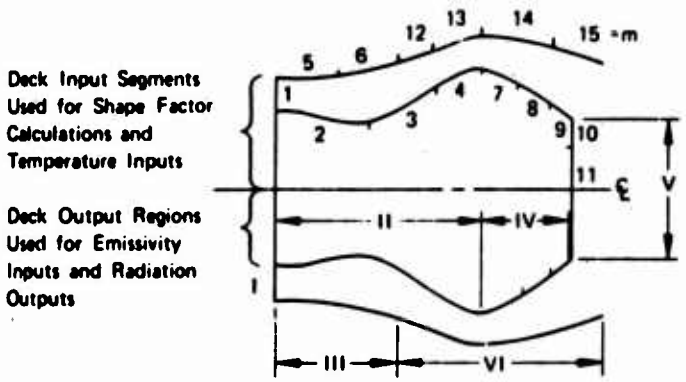

Figure 14. (U) Suppressor Optimization Computer Program IRAP Deck Output Regions.

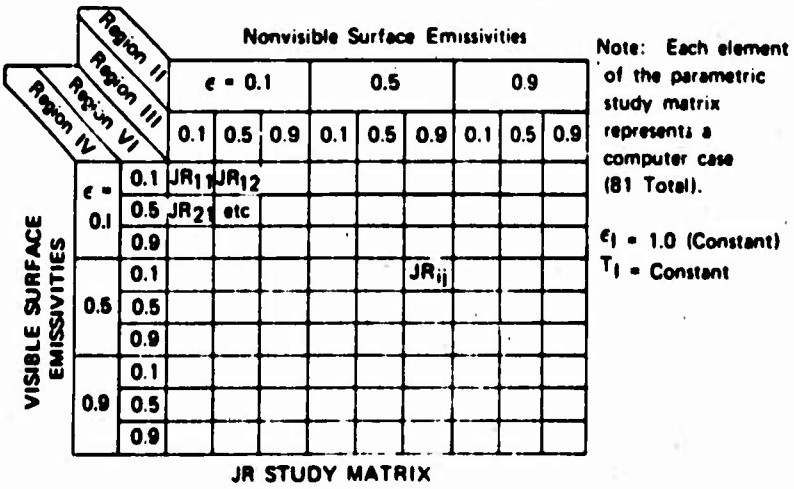

Figure 15. (U) Study Set I - Reflected Radiation, Suppressor Surfaces I, II, and III.

57 120 Pages

Coolant Flow Distributions, % Total W_c

Region IV		10			20			30			40		
VISIBLE SURFACE EMISSIVITIES	VI	80	85	90	70	75	80	60	65	70	50	55	60
0.1	0.1	JD_{11}	JD_{12}										
	0.5	etc	JD_{22}										
	0.9												
0.5	0.1												
	0.5							JD_{ij}					
	0.9												
0.9	0.1												
	0.5												
	0.9												

JD STUDY MATRIX

Note: Each element in the study matrix represents a computer case (108 Total).

Figure 16. (U) Study Set II - Direct Radiation, Suppressor Surfaces IV, V, and VI.

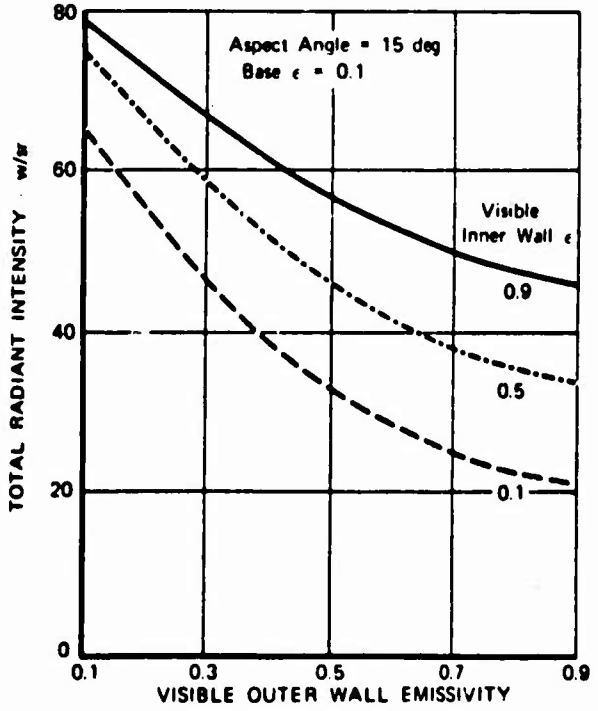

Figure 17. (S) ST9 Suppressor IR Signature in 3-5μ Bandwidth for Various Visible Surface Emissivities With 10/85/5 Coolant Distribution (U).

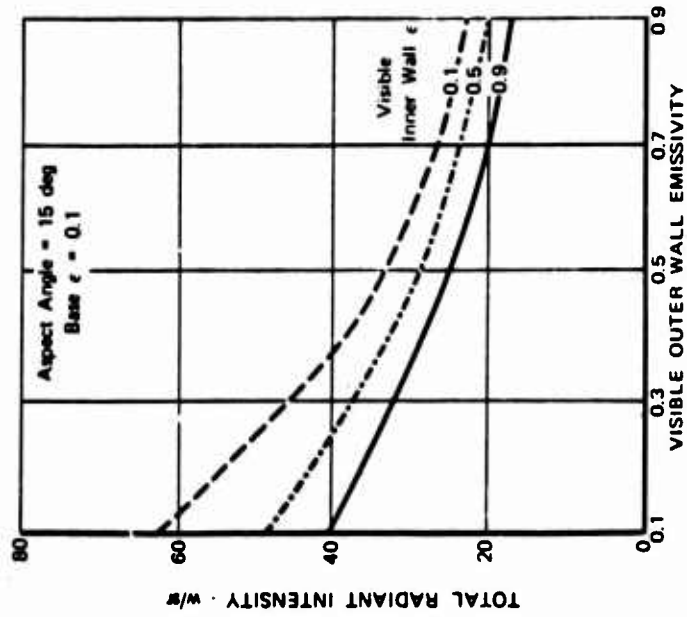

Figure 19. (S) ST9 Suppressor IR Signatures in 3-5μ Bandwidth for Various Visible Surface Emissivities With 30/65/5 Coolant Distribution (U).

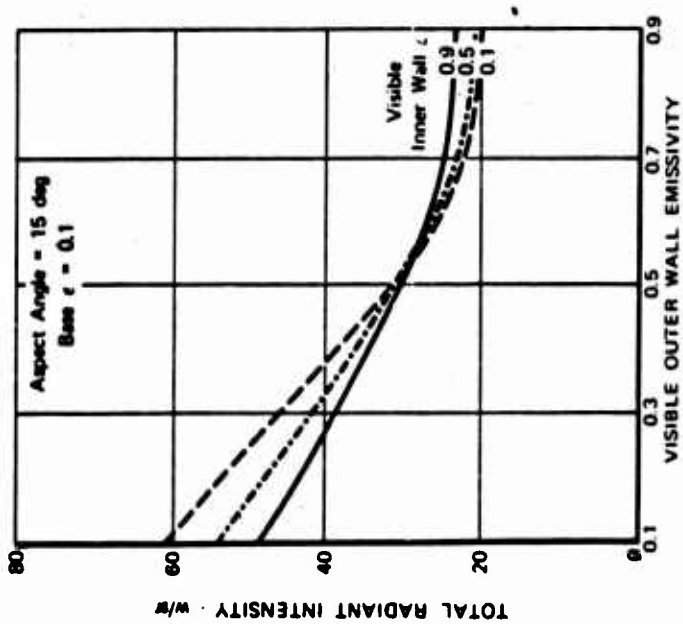

Figure 18. (S) ST9 Suppressor IR Signatures in 3-5μ Bandwidth for Various Visible Surface Emissivities With 20/75/5 Coolant Distribution (U).

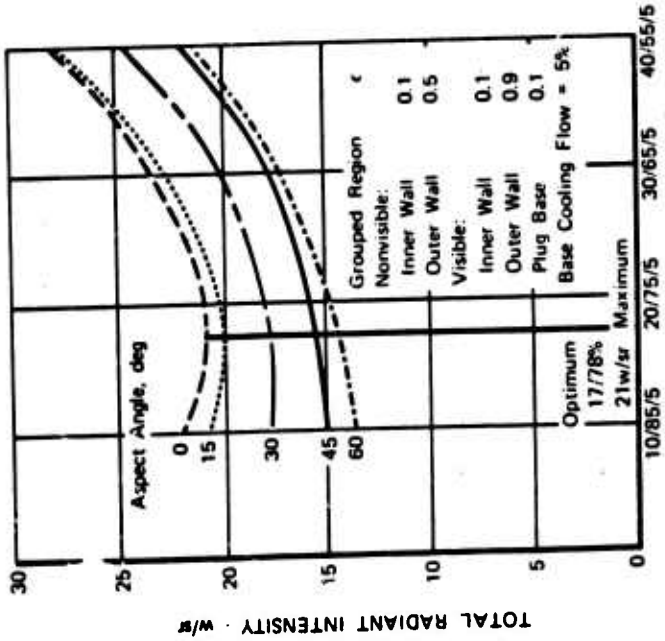

Figure 21. (S) ST9 Suppressor IR Signatures in 3-5μ Bandwidth for Various Coolant Distributions With 0.1 Cooled Inner Wall Emissivity (U).

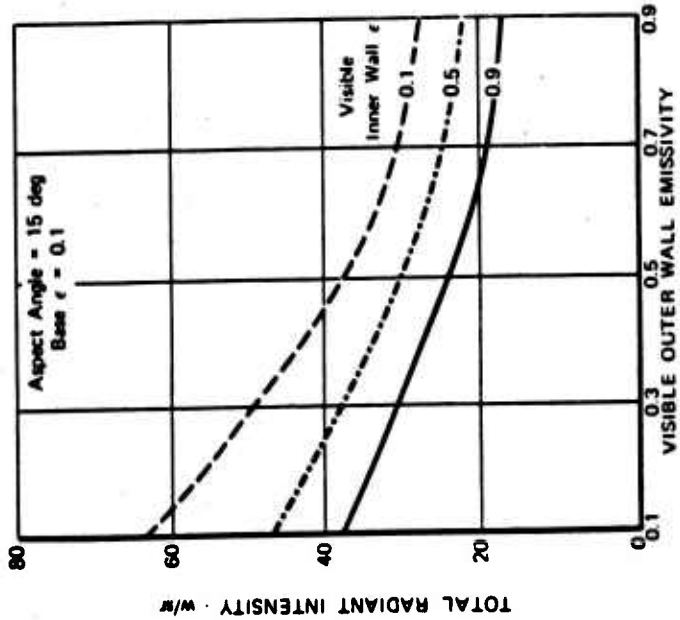

Figure 20. (S) ST9 Suppressor IR Signatures in 3-5μ Bandwidth for Various Visible Surface Emissivities With 40/55/5 Coolant Distribution (U).

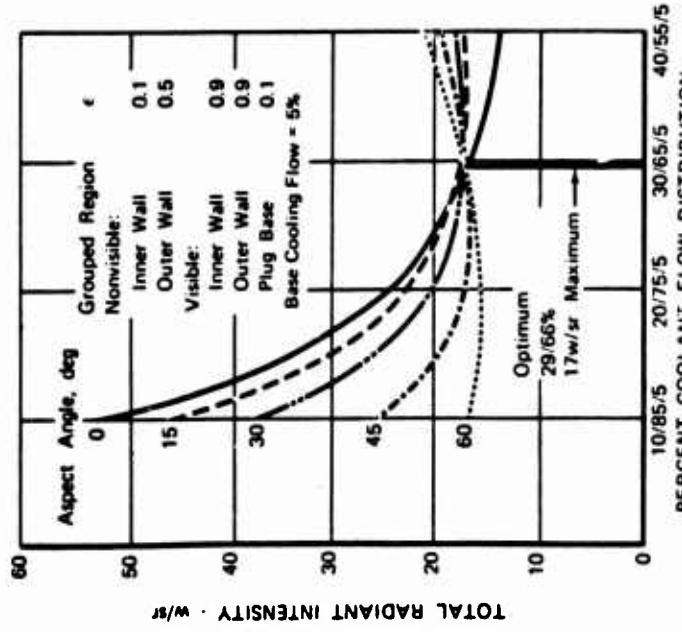

Figure 23. (S) ST9 Suppressor IR Signatures in 3-5μ Bandwidth for Various Coolant Distributions With 0.9 Cooled Inner Wall Emissivity (U).

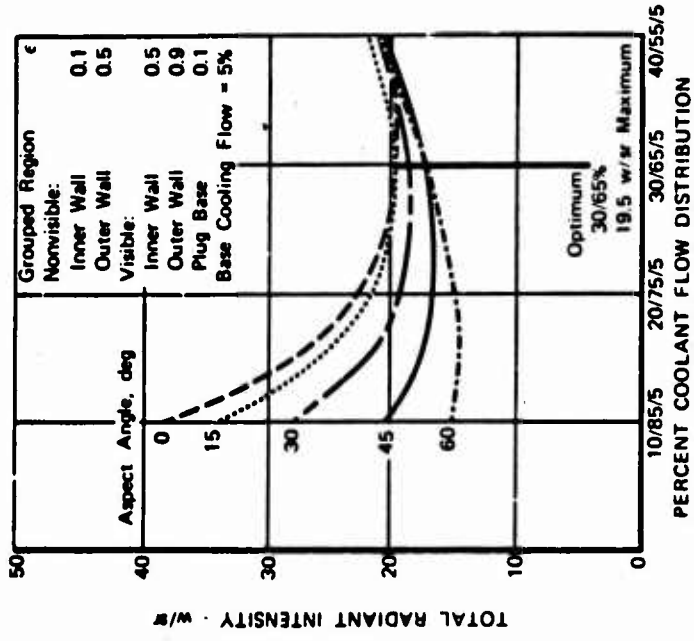

Figure 22. (S) ST9 Suppressor IR Signatures in 3-5μ Bandwidth for Various Coolant Distributions With 0.5 Cooled Inner Wall Emissivity (U).

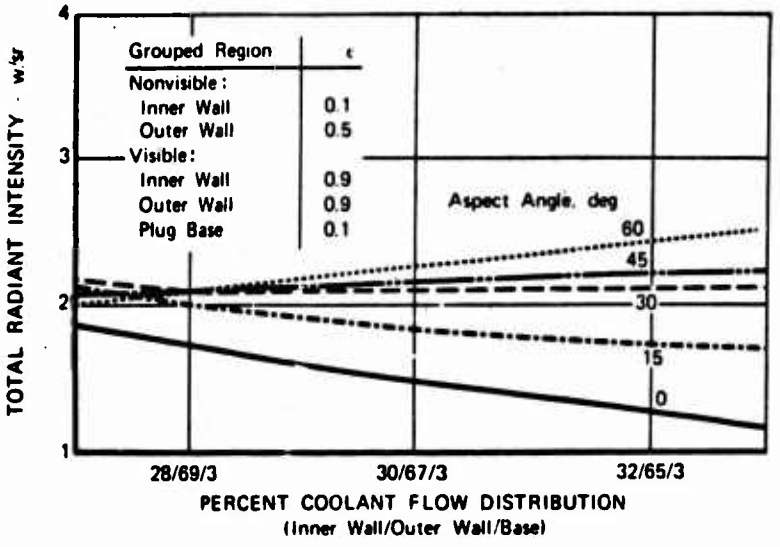

Figure 24. (S) ST9 Suppressor IR Signature in 2-3μ Bandwidth for Changes in Coolant Flow Distribution (U).

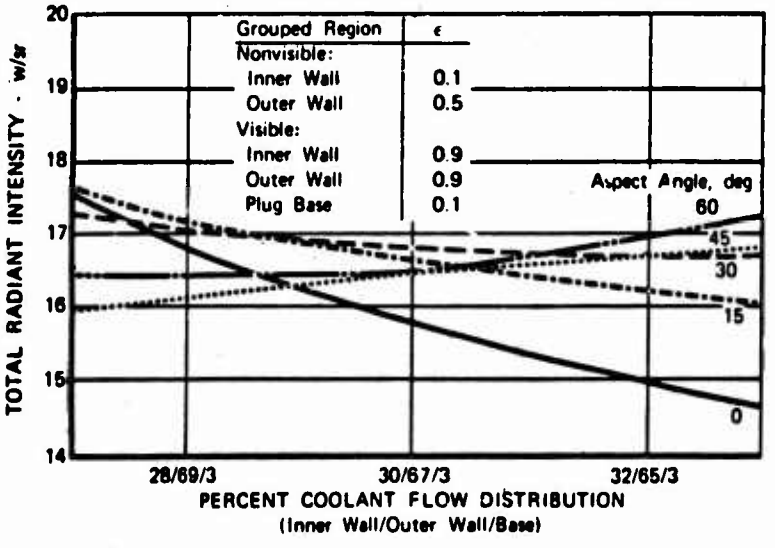

Figure 25. (S) ST9 Suppressor IR Signature in 3-5μ Bandwidth for Changes in Coolant Flow Distribution (U).

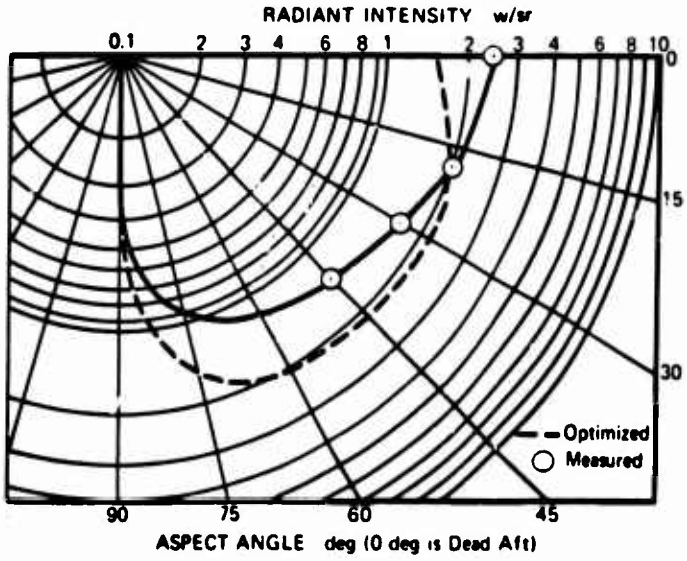

Figure 26. (S) ST9 Suppressor IR Signature Comparison in 2-3μ Bandwidth at 83% MRP (U).

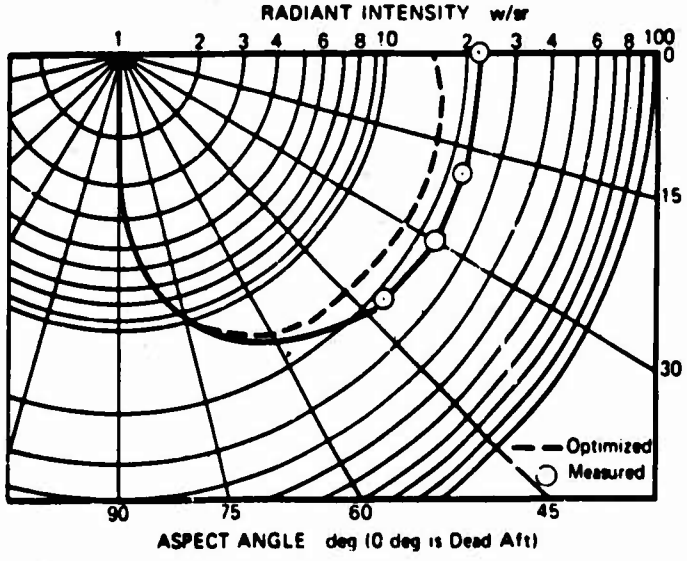

Figure 27. (S) ST9 Suppressor IR Signature Comparison in 3-5μ Bandwidth at 83% MRP (U).

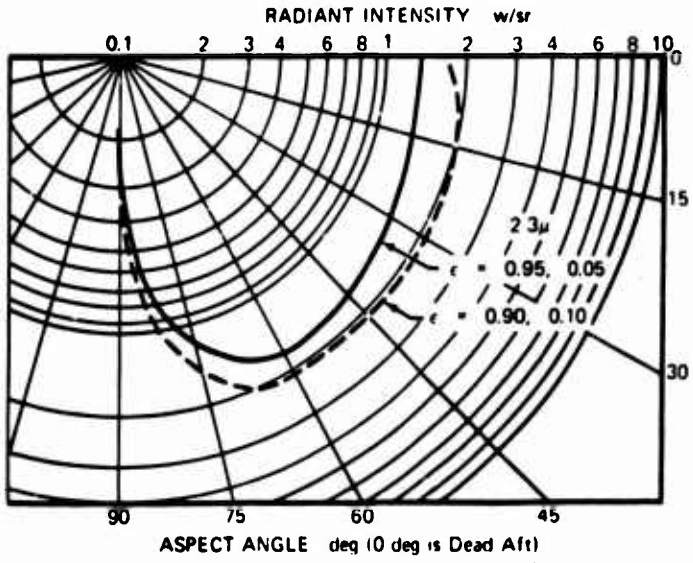

Figure 28. (S) ST9 Suppressor Optimized IR Signatures in 2-3μ Bandwidth for Actual Coating Emissivities (U).

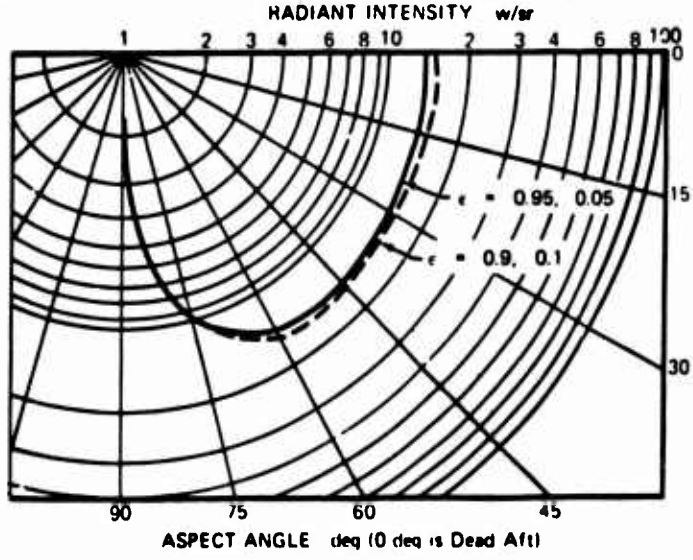

Figure 29. (S) ST9 Suppressor Optimized IR Signatures in 3-5μ Bandwidth for Actual Coating Emissivities (U).

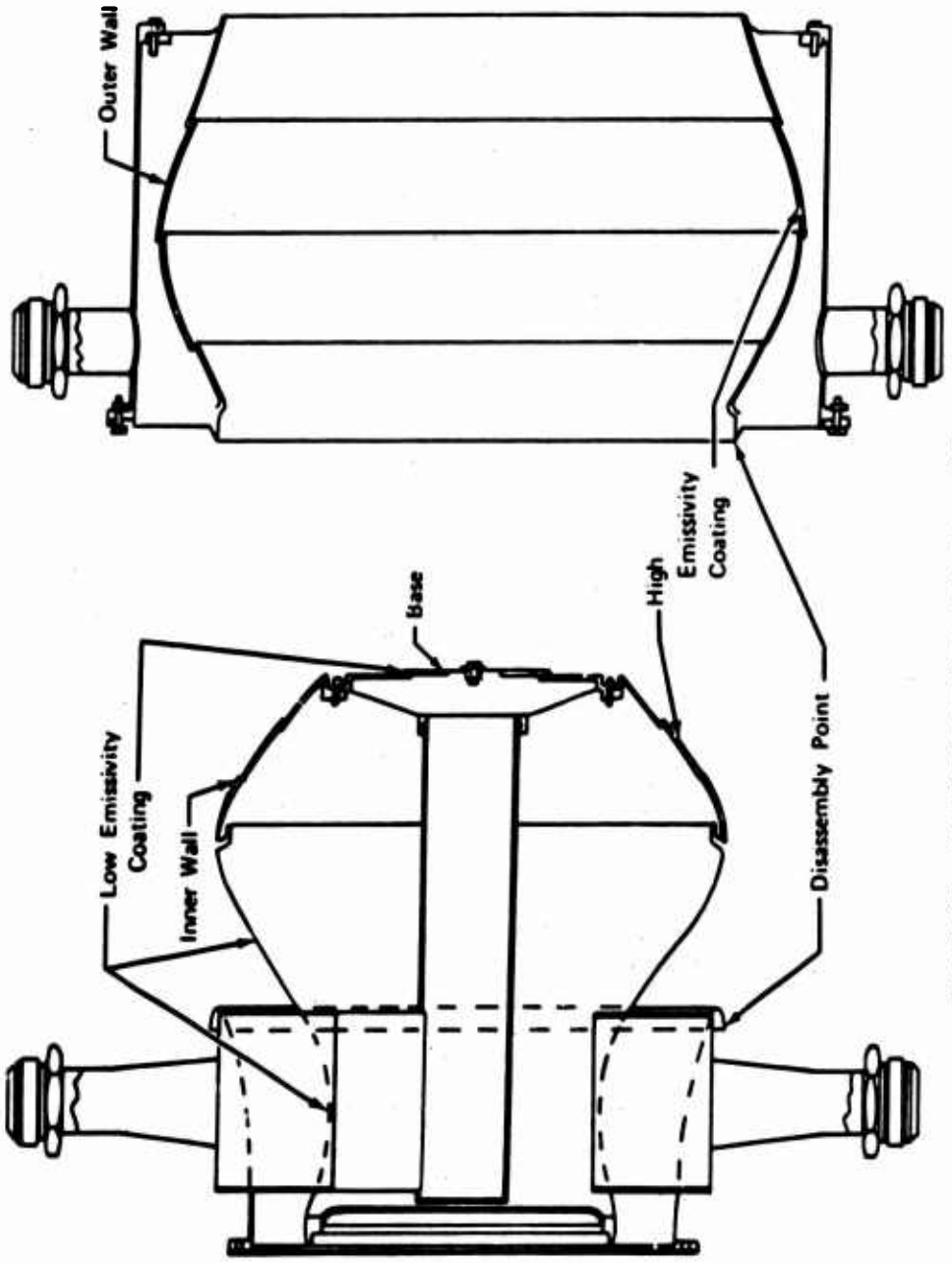

Figure 30. (U) Disassembly and Coating of Demonstrator IR Suppressor

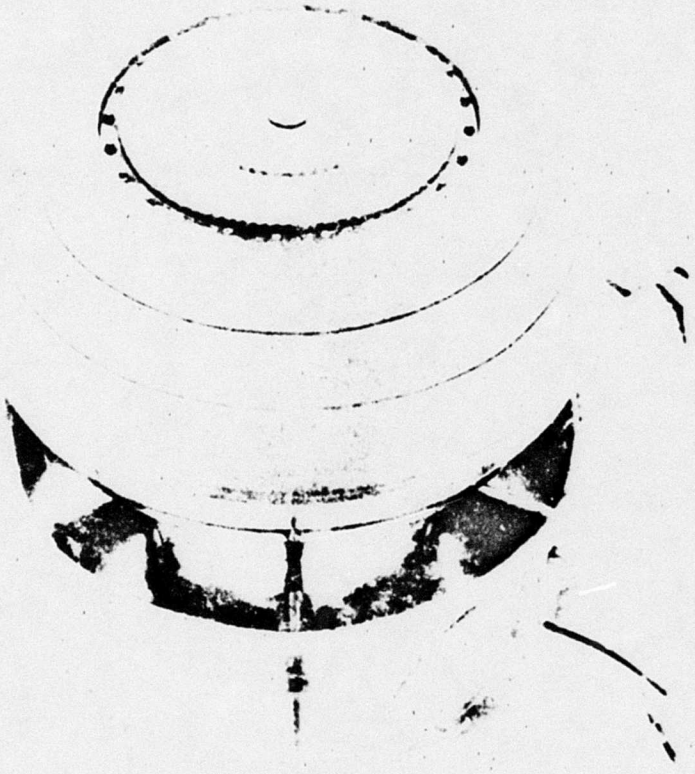

Figure 31. (U) SF9 Silicone Ablator Coated Inner Wall.

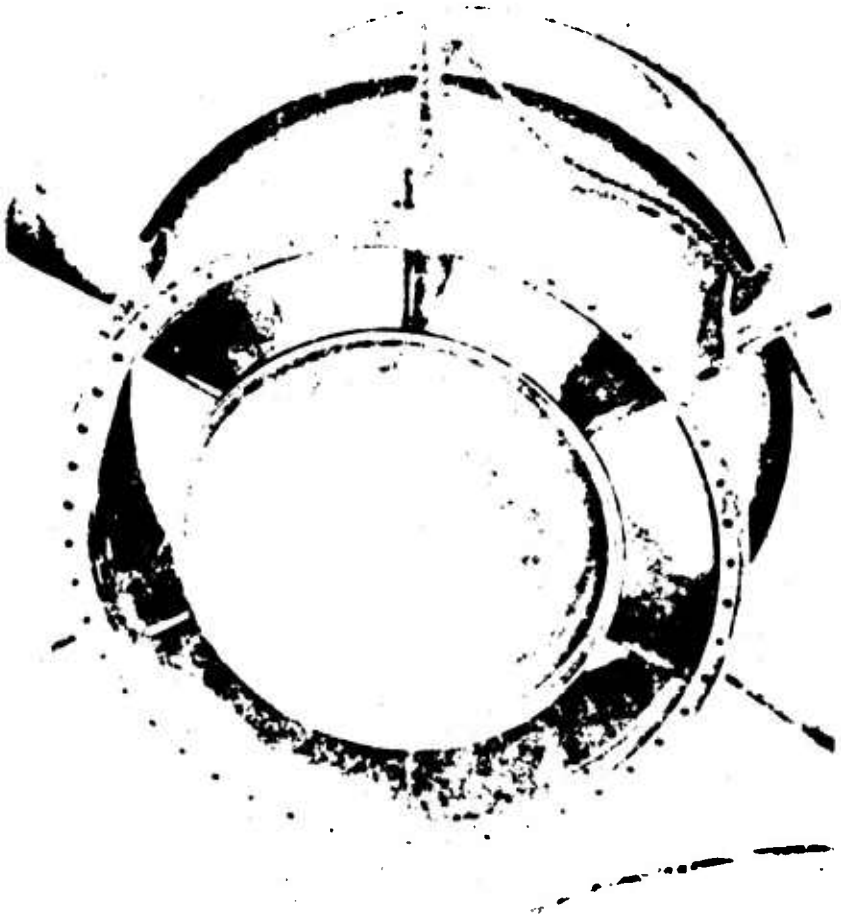

Figure 3[illegible] [illegible] Coated Inner Wall
[illegible] Team).

Figure 33. (U) ST9 Suppressor Coated Outer Wall.

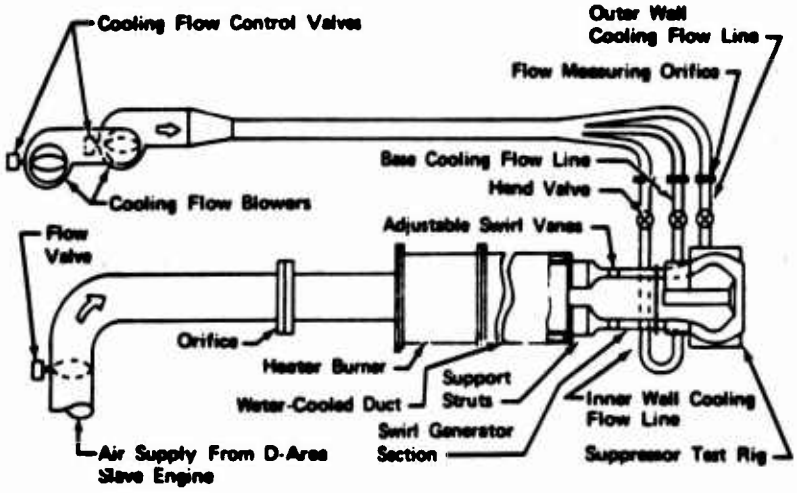

Figure 34. (U) ST9 Demonstrator IR Suppressor Test Stand Installation

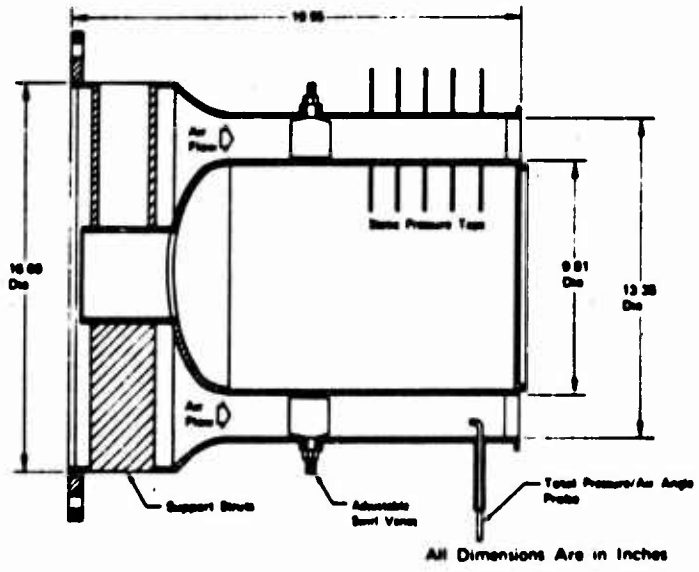

Figure 35. (U) ST9 IR Suppressor Test Rig Swirl Generator Section

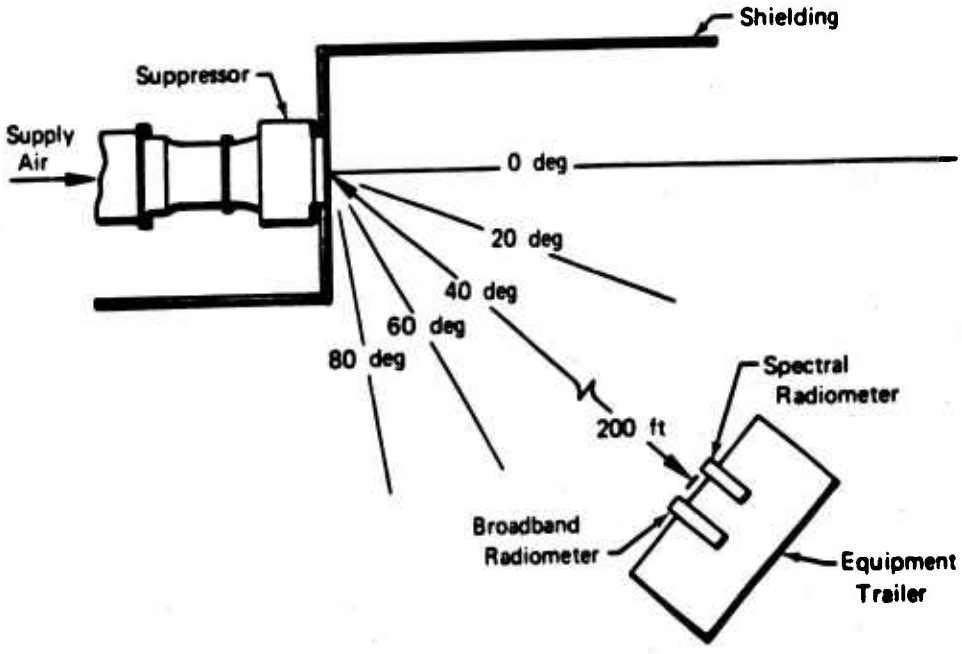

Figure 36. (U) ST9 Suppressor Test Setup and Layout Showing Method of Recording IR Data

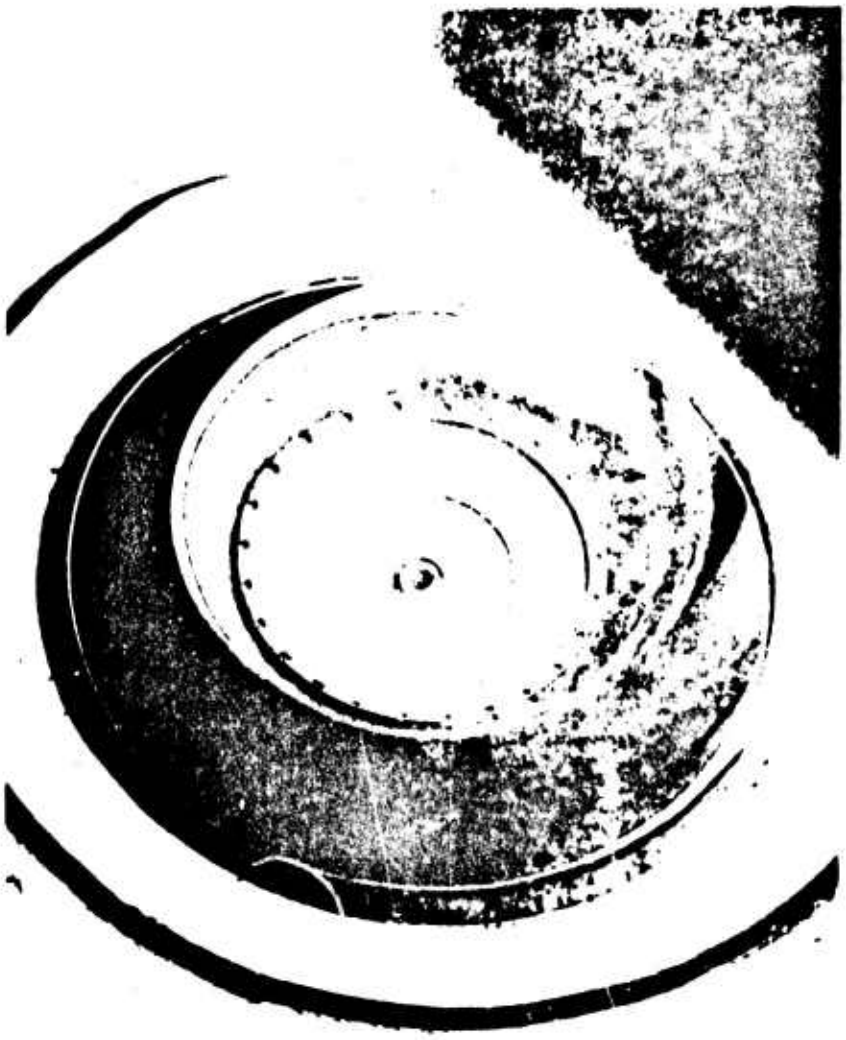

Figure 37. (U) ST9 Suppressor Mounted on Test Stand Before Testing.

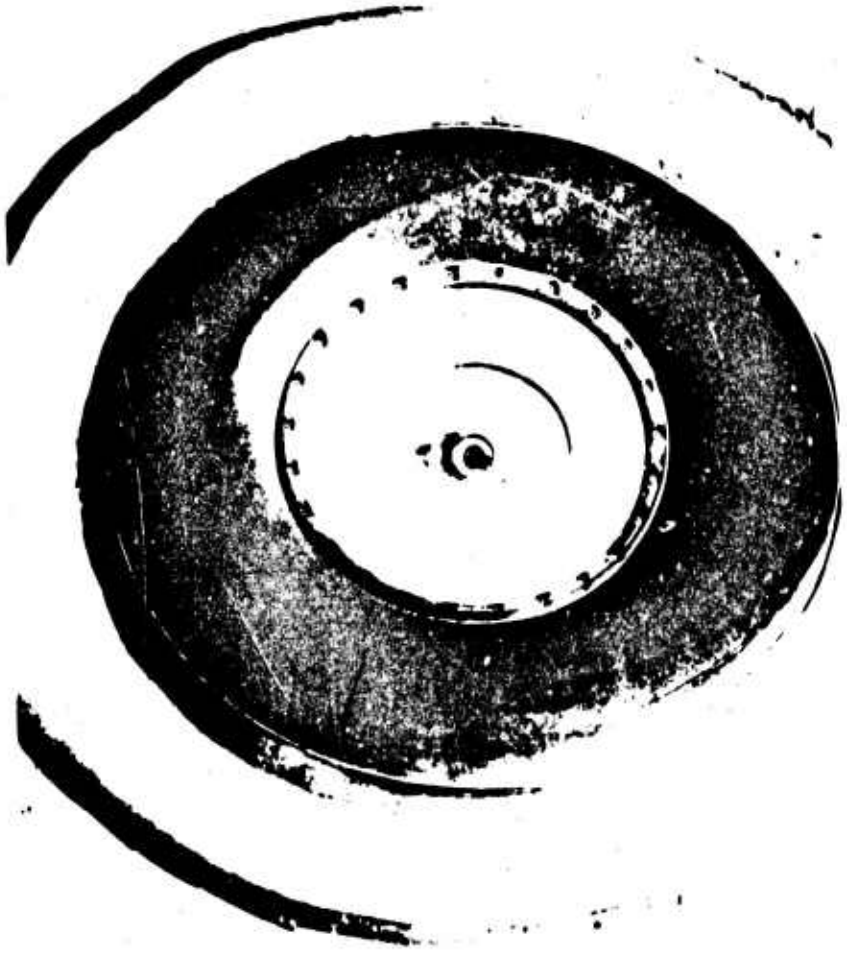

Figure 38. (U) ST9 Suppressor Exit After Testing.

Figure 39. (U) ST9 Suppressor Inlet After Testing, Showing Dust on Inner Wall of Cowling.

Figure 10. (U) [illegible]29 Support [illegible] After Testing; Dust Removed From Outer Wall (at 2 O'clock).

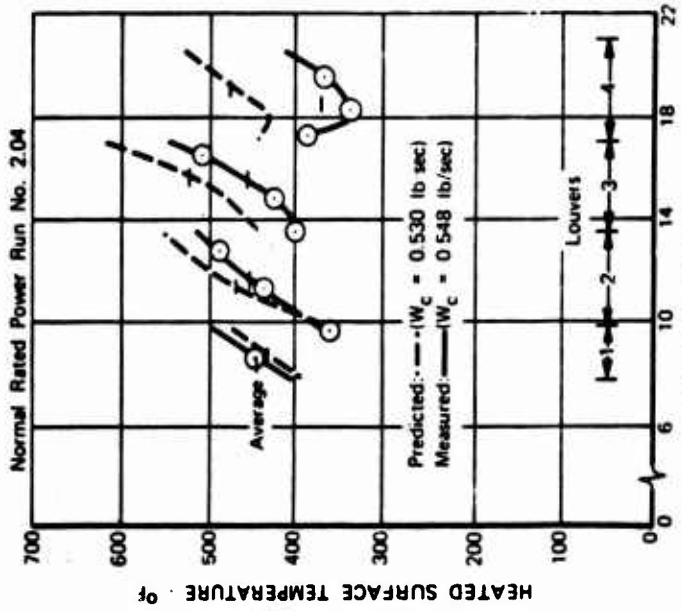

Figure 42. (U) ST9 Suppressor Outer Wall Surface Temperature Comparison.

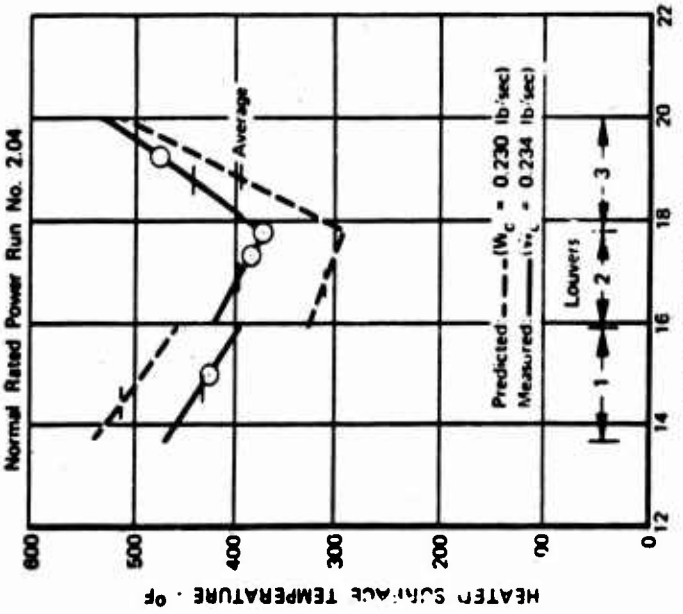

Figure 41. (U) ST9 IR Suppressor Inner Wall Surface Temperature Comparison.

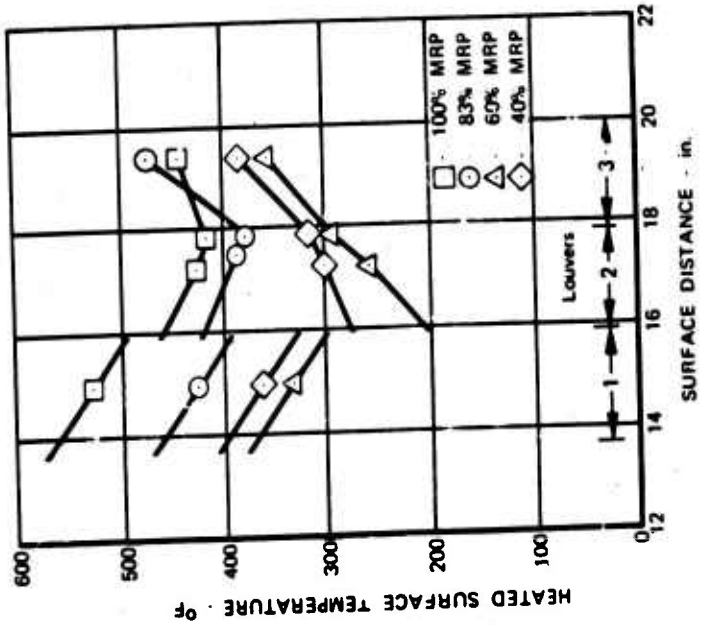

Figure 44. (U) ST9 Suppressor Measured Inner Wall Surface Temperatures.

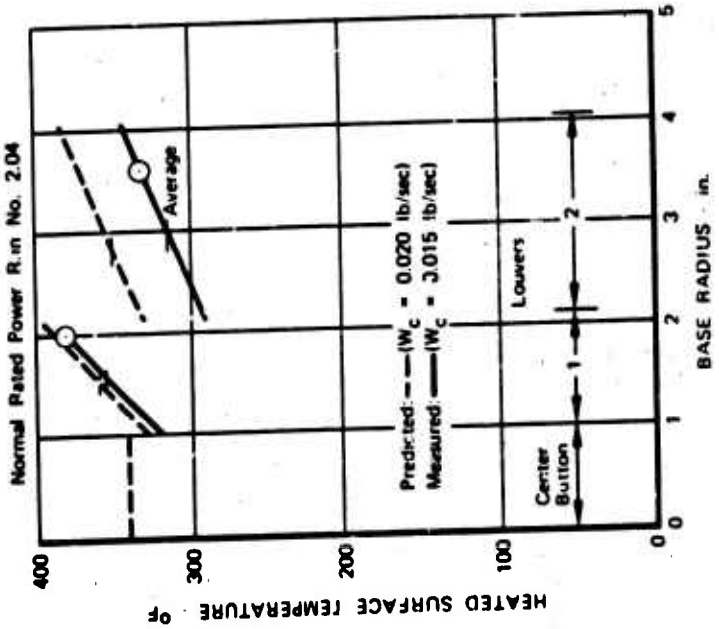

Figure 43. (U) ST9 Suppressor Base Surface Temperature Comparison.

Page 76 of 126 Pages

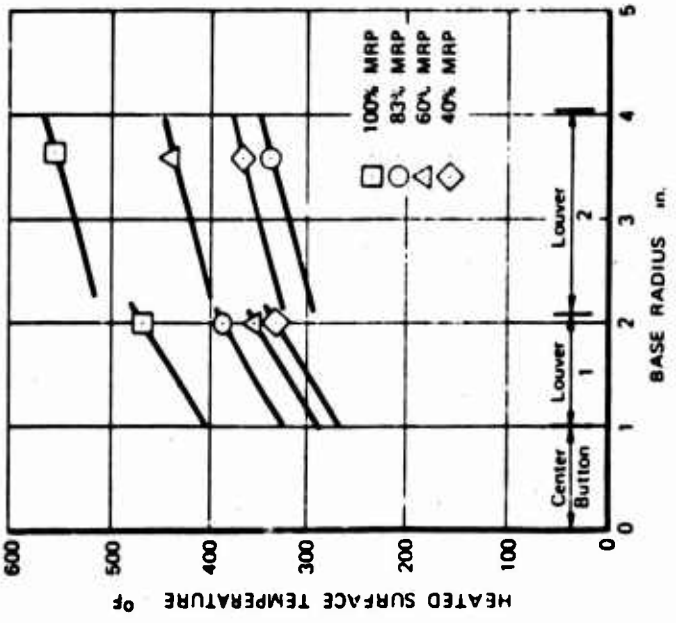

Figure 46. (U) ST9 Suppressor Measured Base Surface Temperatures.

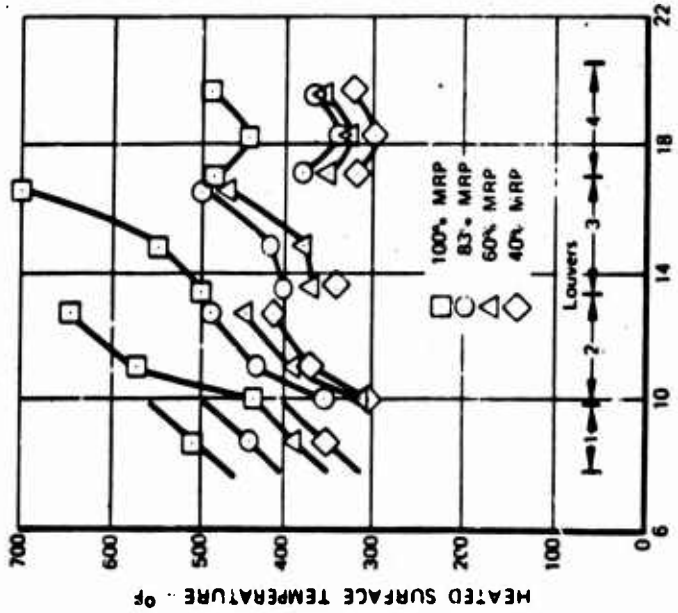

Figure 45. (U) ST9 Suppressor Measured Outer Wall Surface Temperatures.

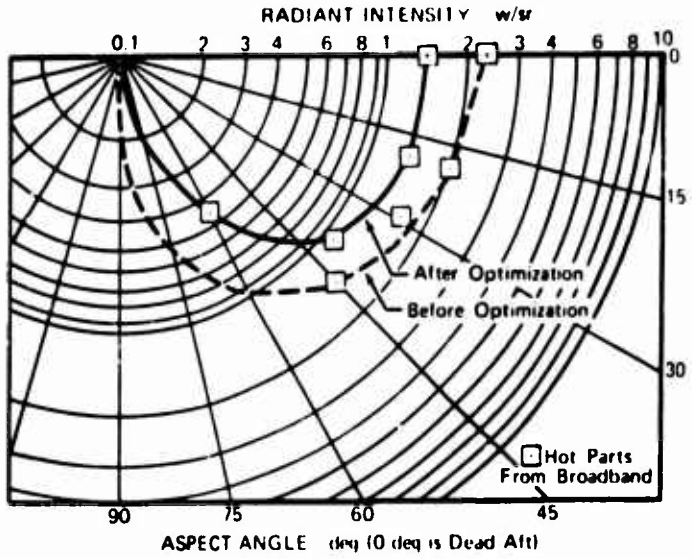

Figure 47. (S) ST9 Suppressor IR Signature Comparison in 2-3μ Bandwidth (U).

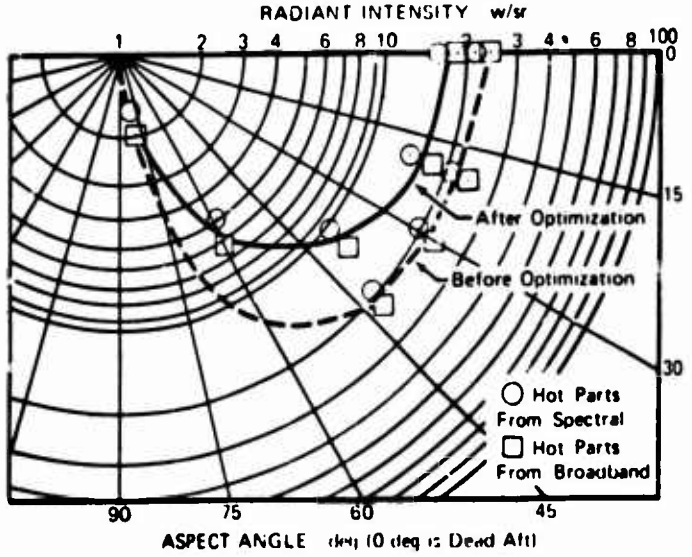

Figure 48. (S) ST9 Suppressor IR Signature Comparison in 3-5μ Bandwidth (U).

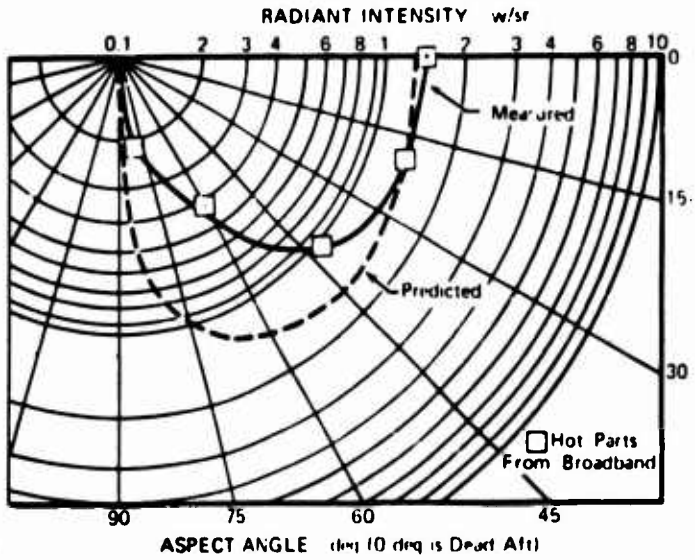

Figure 49. (S) ST9 Suppressor IR Signature Comparison for Predicted Surface Temperatures in 2-3μ Bandwidth (U).

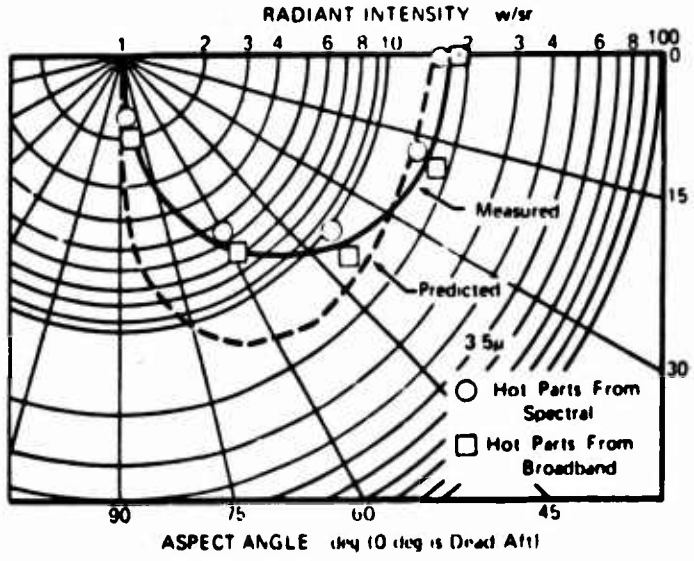

Figure 50. (S) ST9 Suppressor IR Signatures for Predicted Surface Temperatures in 3-5μ Bandwidth (U).

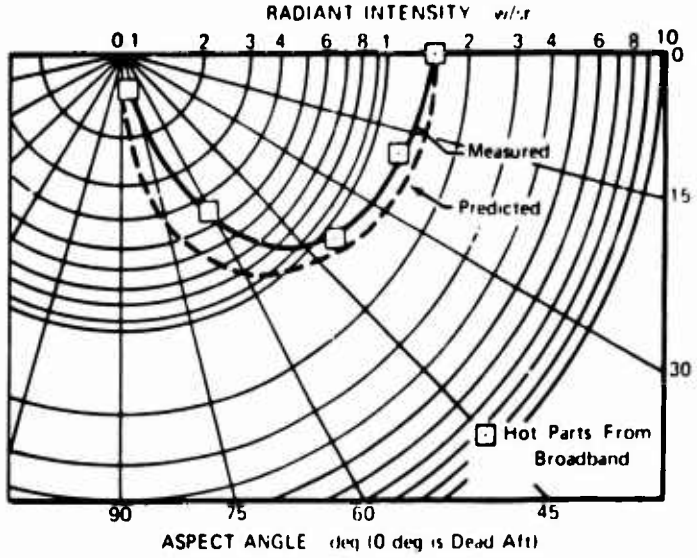

Figure 51. (S) ST9 Suppressor IR Signature Comparison for Measured Surface Temperatures in 2-3μ Bandwidth (U).

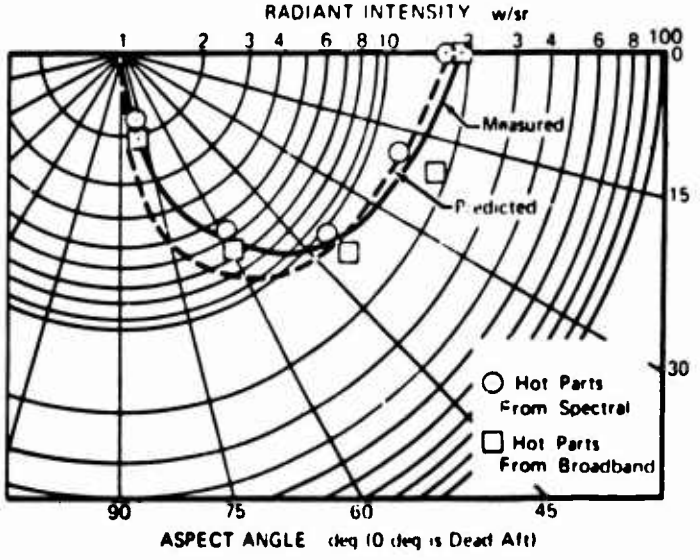

Figure 52. (S) ST9 Suppressor IR Signature Comparison for Measured Surface Temperatures in 3-5μ Bandwidth (U).

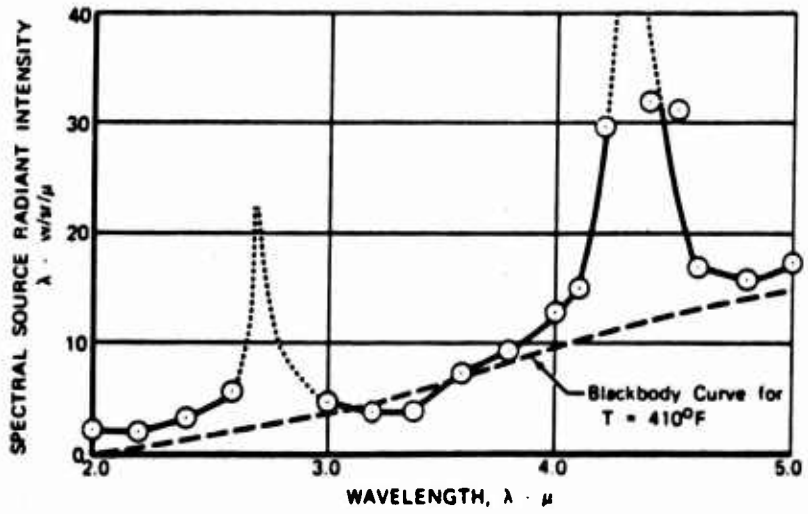

Figure 53. (S) ST9 Suppressor Spectral Intensity at Zero Deg Aspect Angle (U).

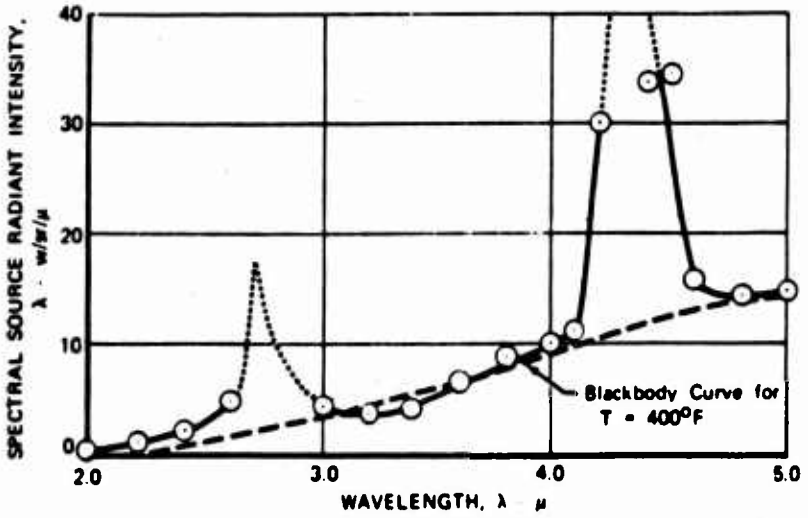

Figure 54. (S) ST9 Suppressor Spectral Intensity at 20 Deg Aspect Angle (U).

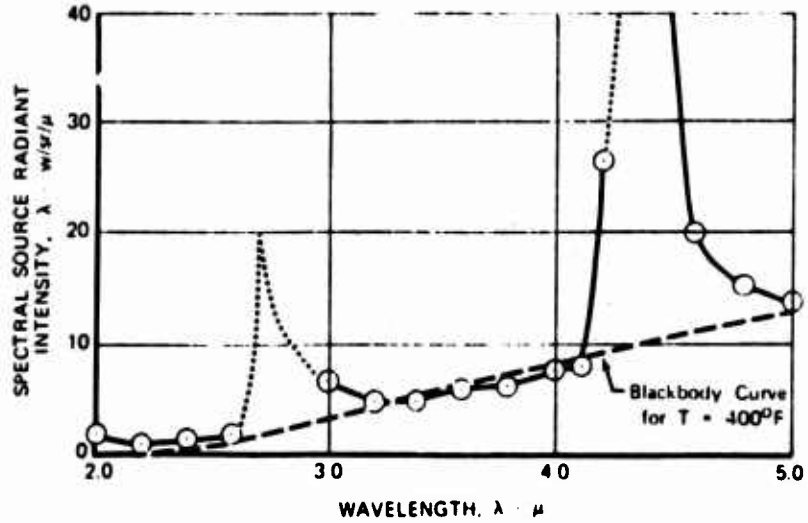

Figure 55. (S) ST9 Suppressor Spectral Intensity at 40 Deg Aspect Angle (U).

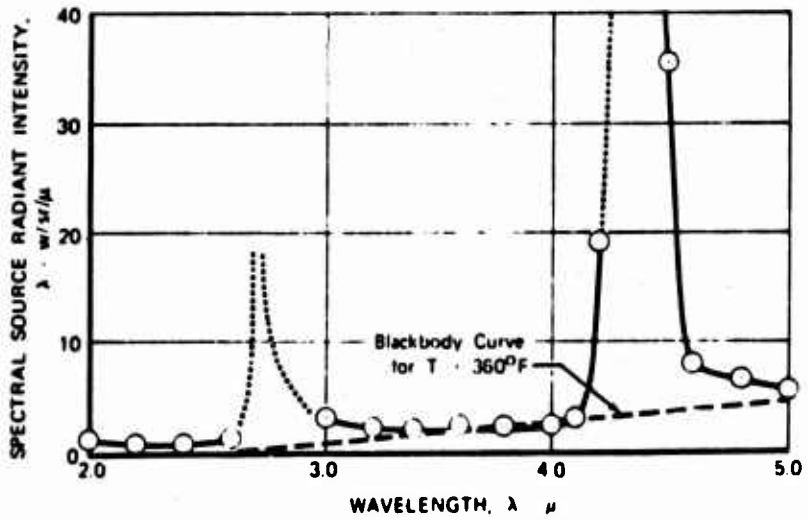

Figure 56. (S) ST9 Suppressor Spectral Intensity at 60 Deg Aspect Angle (U).

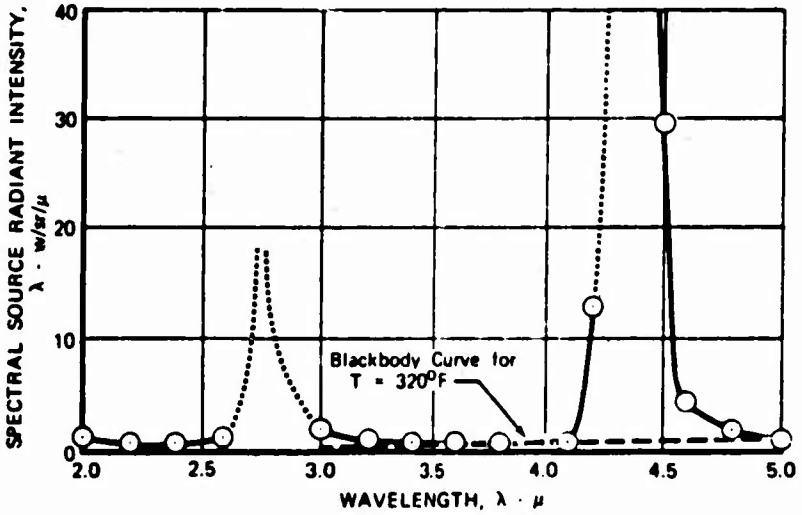

Figure 57. (S) ST9 Suppressor Spectral Intensity at 80 Deg Aspect Angle (U).

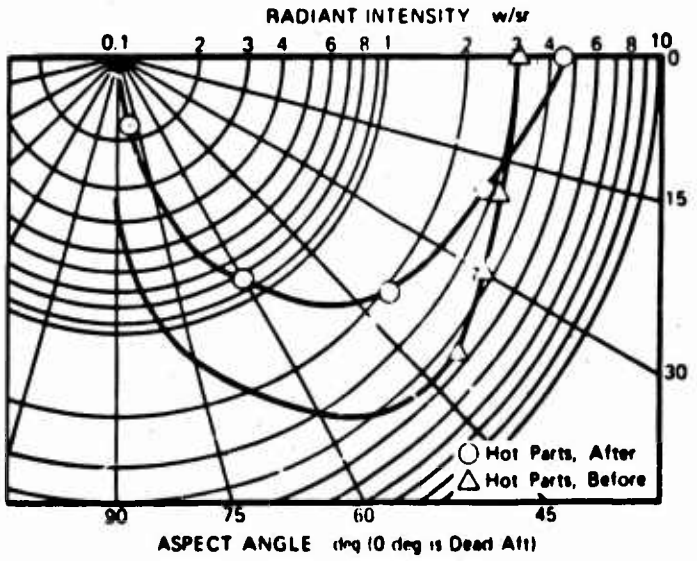

Figure 58. (S) ST9 Suppressor IR Signature Comparison at 100% MRP, 2-3μ Bandwidth (U).

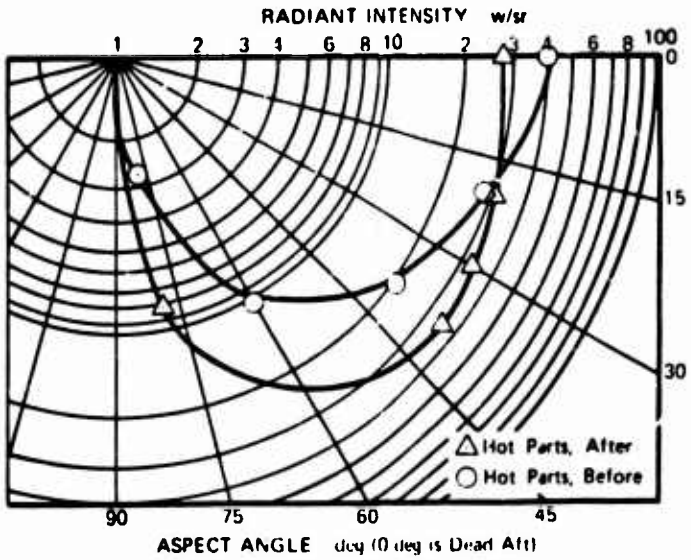

Figure 59. (S) ST9 Suppressor IR Signature Comparison at 100% MRP, 3-5μ Bandwidth (U).

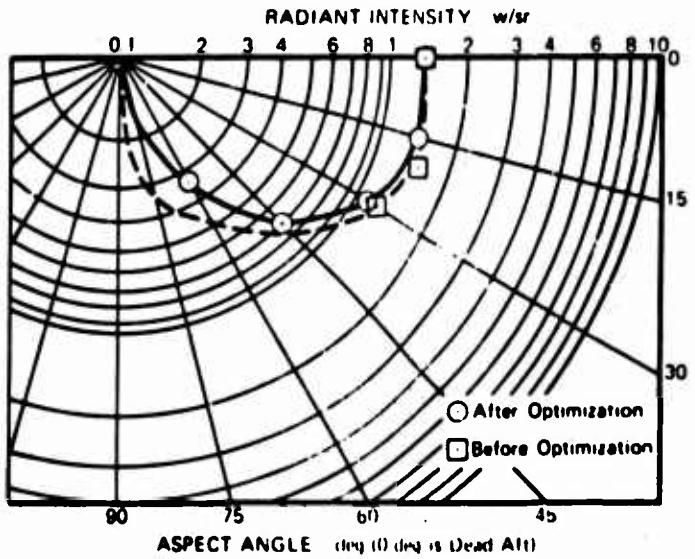

Figure 60. (S) ST9 Suppressor IR Signature Comparison at 40% MRP, 2-3μ Bandwidth (U).

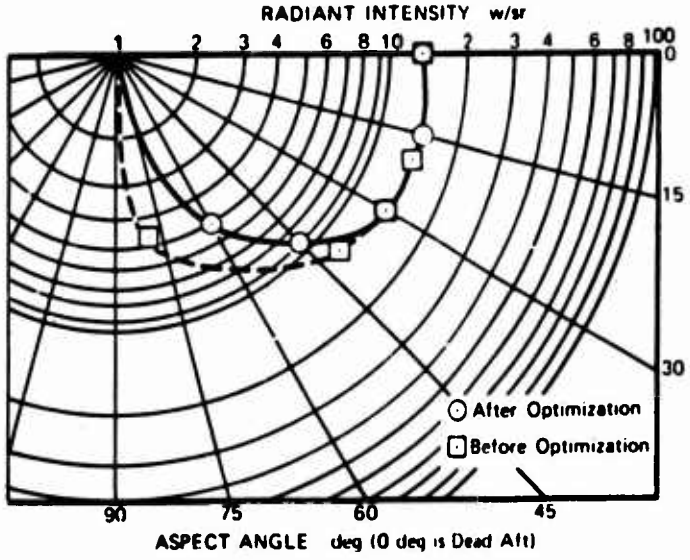

Figure 61. (S) ST9 Suppressor IR Signature Comparison at 40% MRP, 3-5μ Bandwidth (U).

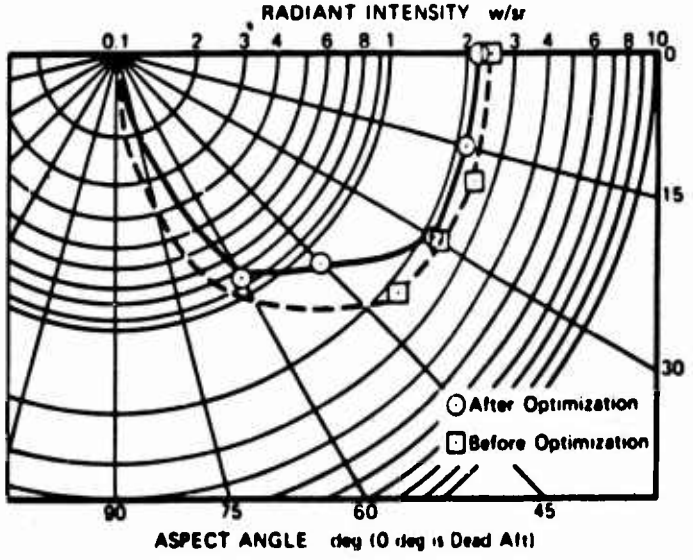

Figure 62. (S) ST9 Suppressor IR Signature Comparison at 60% MRP, 2-3μ Bandwidth (U).

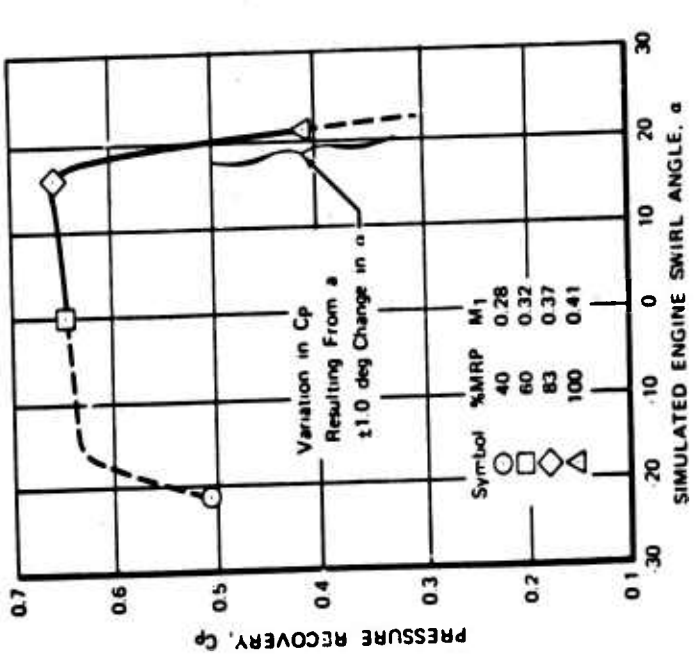

Figure 64. (U) ST9 Suppressor Mach No. and Swirl Angle Effects on Cp.

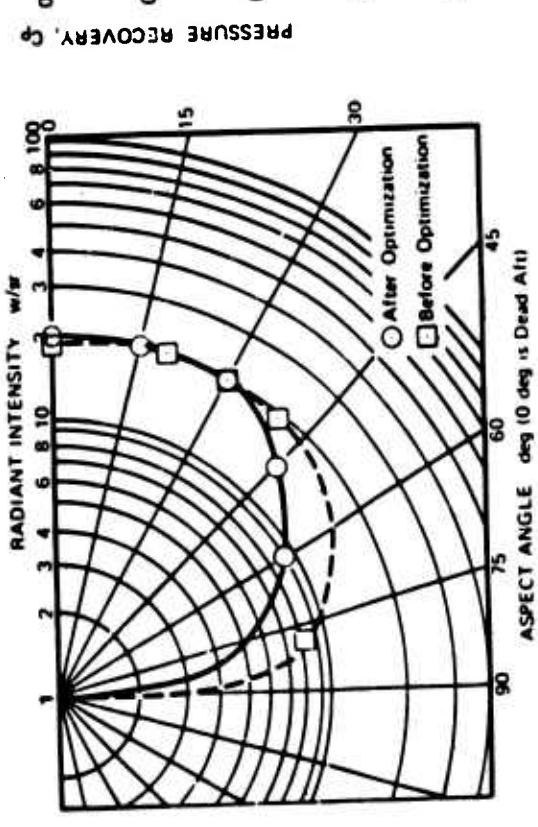

Figure 63. (S) ST9 Suppressor IR Signature Comparison at 60% MRP, 3-5μ Bandwidth (U).

(U) LITERATURE CITED

1. Booz, D. E., ST9 INFRARED SUPPRESSION HARDWARE EVALUATION (U), USAAMRDL Technical Report 71-32, Contract DAAJ02-68-C-0001, U. S. Army Air Mobility Research and Development Laboratory, Fort Eustis, Virginia, January 1972.(CONFIDENTIAL)

2. Duncan, T. C., et al., IR SUPPRESSOR OPTIMIZATION THROUGH IR SIGNATURE ANALYSIS AND SURFACE EMITTANCE CONTROL (U), General Dynamics Report TM-6-332-60.28-2, Contract DAAJ02-69-C-0077, August 10, 1970. (SECRET)

3. Duncan, T. C., USER'S MANUAL FOR THE IR SUPPRESSOR SIGNATURE PREDICTION DIGITAL COMPUTER PROGRAMS, General Dynamics Report No. TM-6-332-5.30-1, 1971.

4. Rackauskas, R., and D. Stowell, COMPARISON OF A-4B INFRARED RADIATION MEASUREMENTS (U), NAVSO P-2315, Vol 16, No. 1, p 343, October 1971. (CONFIDENTIAL)

5. Thayer, E. B., EVALUATION OF CURVED-WALL ANNULAR DIFFUSERS, ASME Paper No. 71-WA/FE-35, November 1971.

APPENDIX I
(S) ST9 SUPPRESSOR AND SCALE MODEL PREDICTED AND MEASURED IR SIGNATURE COMPARISONS (U)

(U) Figures 65 through 75 present comparisons of the predicted and measured radiant intensities from the electrically heated half-scale model and the Demonstrator suppressor program. Data are presented for both the 2-3 and 3-5μ bandwidths. These comparisons were used to validate the accuracy of the CFP and IRAP computer decks. They show that in addition to accurately predicting the maximum emission levels, the deck predictions also follow the same trends with aspect angle as the measured data.

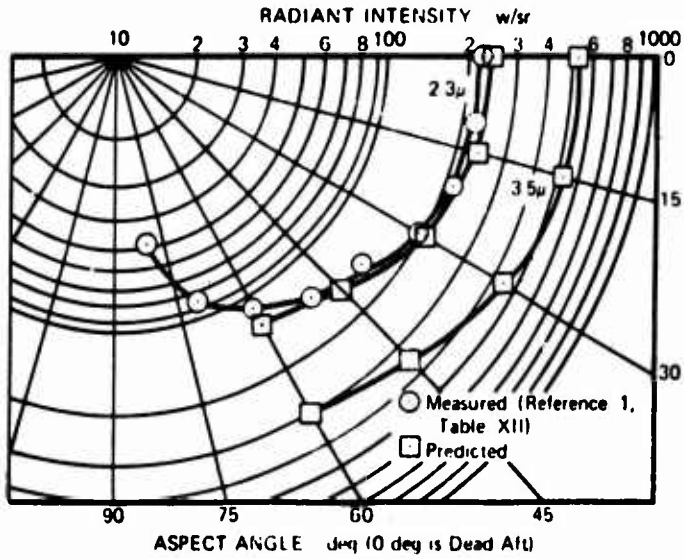

Figure 65. (S) Comparison of Measured and Predicted IR Signatures (MRP Unsuppressed), Electrically Heated Model Run 1 (U).

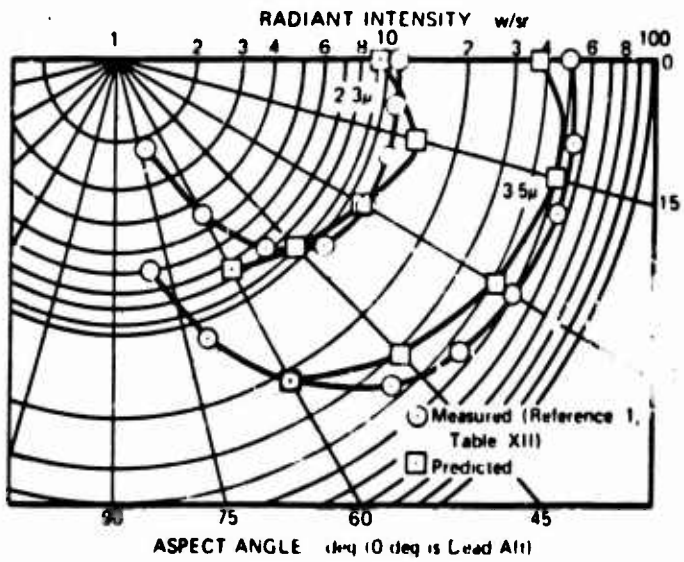

Figure 66. (S) Comparison of Measured and Predicted IR Signatures (MRP Suppressed), Electrically Heated Model Run 2 (U).

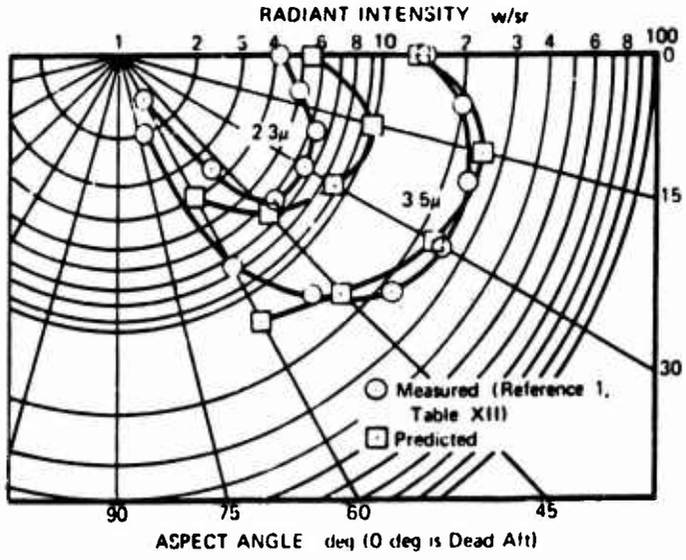

Figure 67. (S) Comparison of Measured and Predicted IR Signatures (MRP Suppressed), Electrically Heated Model Run 3 (U).

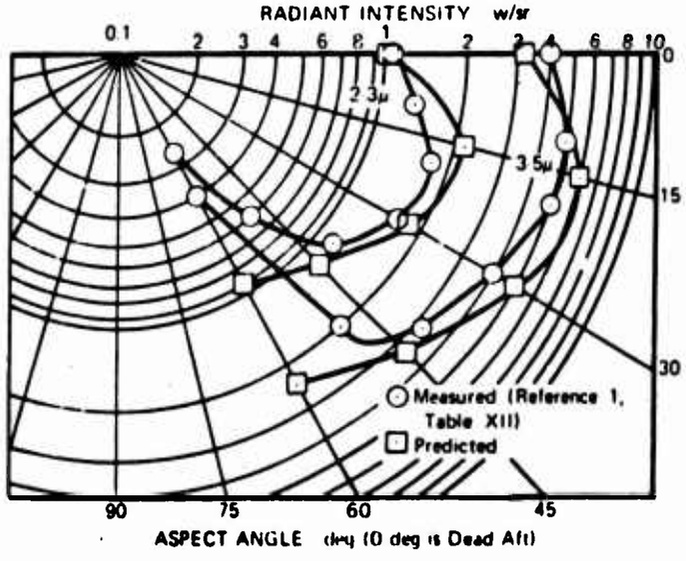

Figure 68. (S) Comparison of Measured and Predicted IR Signatures (MRP Suppressed), Electrically Heated Model Run 7 (U).

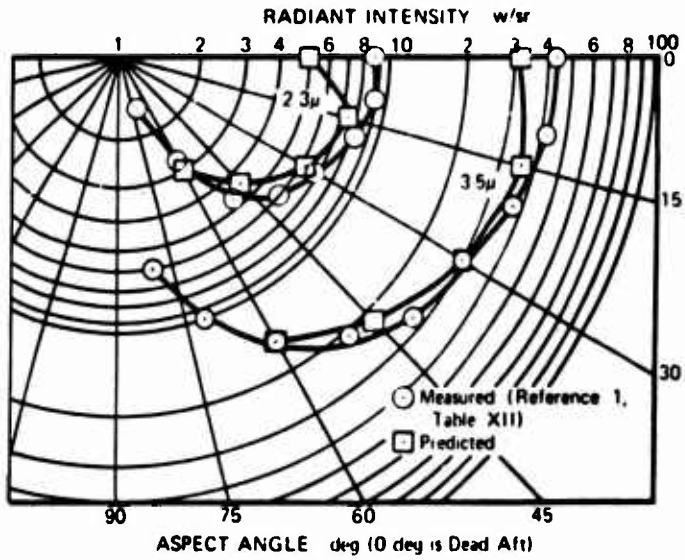

Figure 69. (S) Comparison of Measured and Predicted IR Signatures (MRP Suppressed), Electrically Heated Model Run 8 (U).

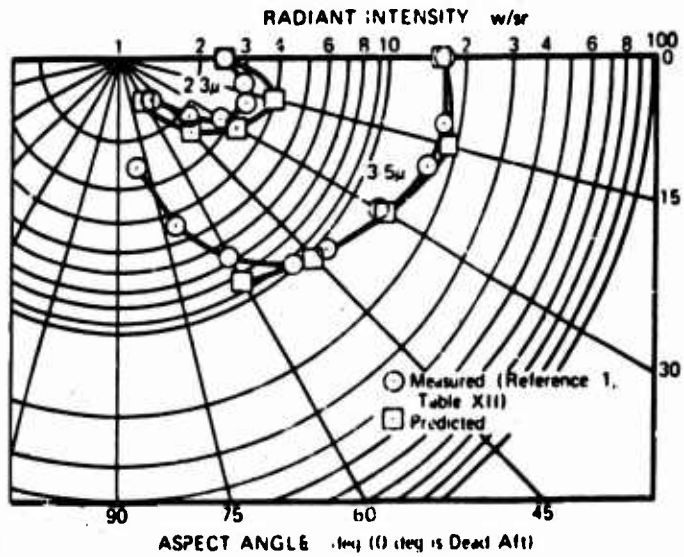

Figure 70. (S) Comparison of Measured and Predicted IR Signatures (MRP Suppressed), Electrically Heated Model Run 9 (U).

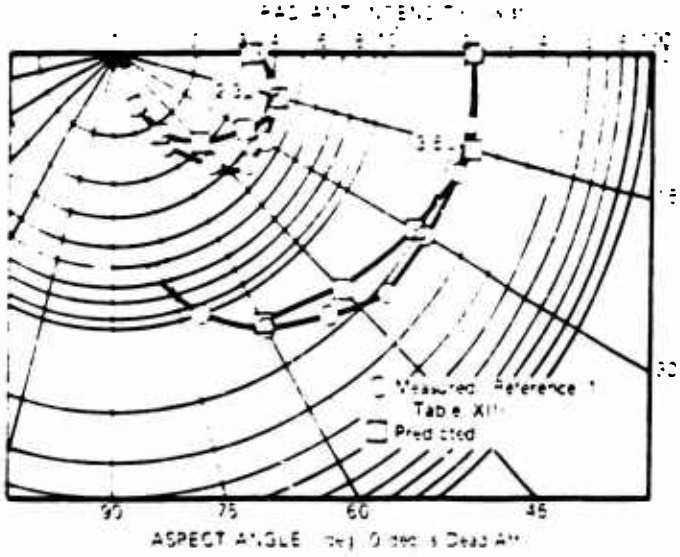

Figure 71. (S) Comparison of Measured and Predicted IR Signatures (MRP Suppressed), Electrically Heated Model Run 10 (U).

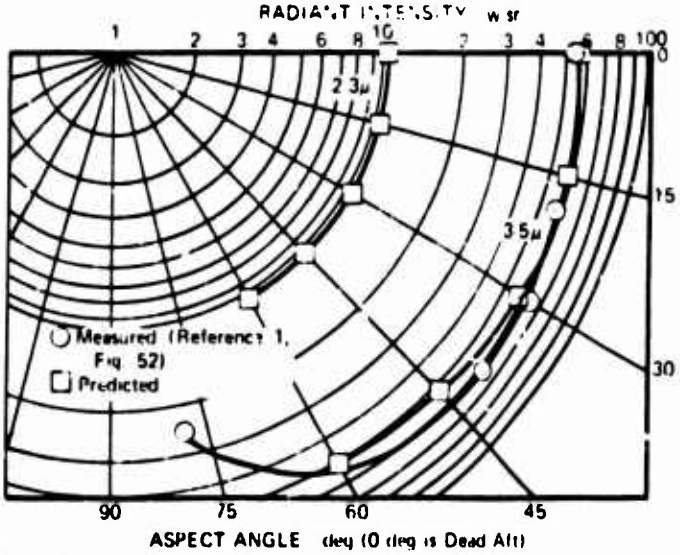

Figure 72. (S) Comparison of Measured and Predicted IR Signatures (MRP With Design Cooling Flow), Full-Scale Run 4.01 (U).

UNCLASSIFIED
SECRET

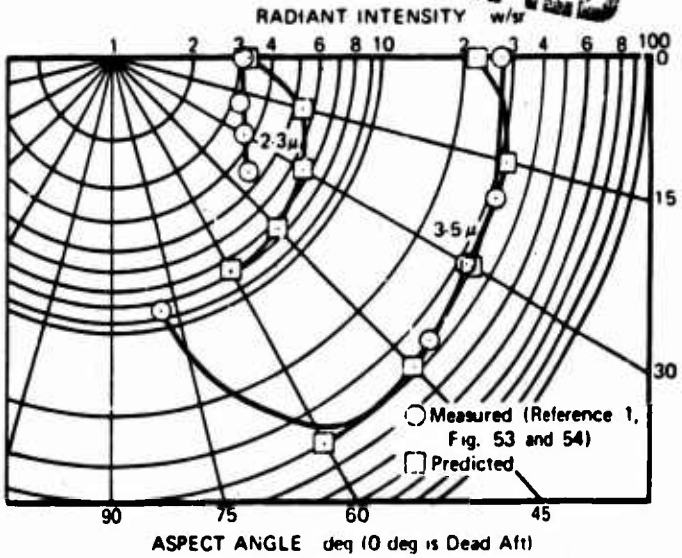

Figure 73. (S) Comparison of Measured and Predicted IR Signatures (MRP With Maximum Cooling Flow), Full-Scale Run 7.03 (U).

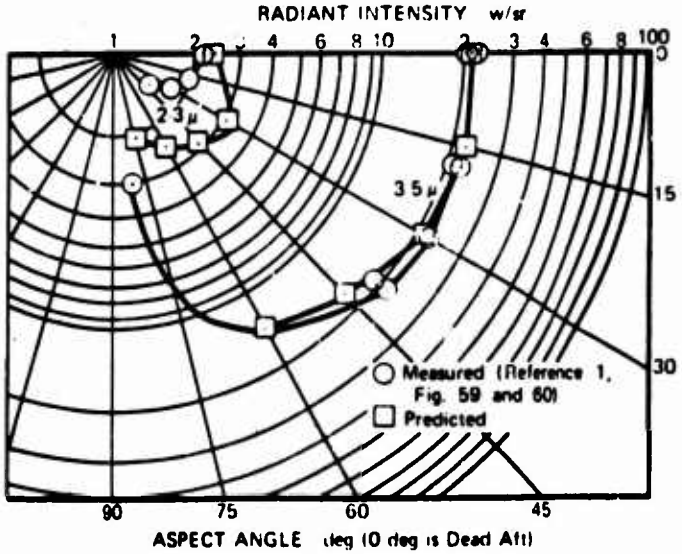

Figure 74. (S) Comparison of Measured and Predicted IR Signatures (83% MRP With Design Cooling Flow), Full-Scale Run 9.09 (U).

SECRET
UNCLASSIFIED
Page 93 of 120 Pages

UNCLASSIFIED
SECRET

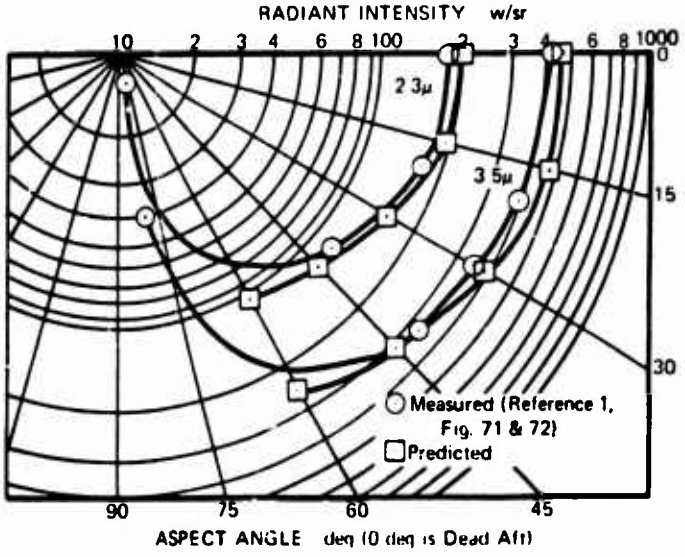

Figure 75. (S) Comparison of Measured and Predicted IR Signatures (MRP Unsuppressed), Full-Scale Runs 16.01 and 16.02 (U).

UNCLASSIFIED
SECRET

SECRET
(This page is Unclassified)

APPENDIX II
(S) COMPLETE EMISSIVITY/COOLANT DISTRIBUTION OPTIMIZATION MATRICES (U)

(U) Tables VIII through XVII present the complete results of the reflected radiation study matrix. Values were determined for all five aspect angles and the two wavelength bandwidths. Tables XVIII through XXVII present the direct radiation parametric study results for the five aspect angles considered and the two bandwidths. These two sets of tabulations were systematically combined, to find the optimum IR signatures corresponding to each emissivity condition defined by the rows of both parametric studies. This combination is presented in Tables XXVIII and XXIX. The optimum values for the different wavelength bandwidths and aspect angles did not necessarily occur at the same emissivity/coolant distribution conditions. Hence, graphical methods of determining the optimum suppressor configuration were used to show the combined effects of emissivity/coolant distribution and aspect angle on the IR signature.

SECRET
(This page is Unclassified)
95 120 Pages

Page 96 of 120 Pages

SECRET

TABLE VIII. (S) REFLECTED RADIATION MATRIX FOR THE 2-3μ BAND AT 0 DEGREES ASPECT ANGLE (U)

Visible Surface Emissivities (Inner Wall/Outer Wall)	Nonvisible Surface Emissivities (Inner Wall/Outer Wall)								
	0.1/0.1	0.1/0.5	0.1/0.9	0.5/0.1	0.5/0.5	0.5/0.9	0.9/0.1	0.9/0.5	0.9/0.9
0.1/0.1	*16.78	14.57	13.69	24.98	23.11	21.87	28.71	27.57	26.59
0.1/0.5	4.34	4.03	3.92	8.04	7.53	7.19	10.53	10.13	9.79
0.1/0.9	0.55	0.52	0.52	1.09	1.03	0.99	1.54	1.48	1.43
0.5/0.1	9.47	8.30	7.83	14.43	13.40	12.71	16.76	16.18	15.67
0.5/0.5	3.02	2.80	2.73	5.55	5.21	4.98	7.23	6.99	6.79
0.5/0.9	0.42	0.41	0.40	0.84	0.79	0.76	1.18	1.14	1.11
0.9/0.1	5.16	4.55	4.31	7.89	7.37	7.03	9.18	8.95	8.75
0.9/0.5	1.95	1.82	1.77	3.53	3.34	3.20	4.56	4.46	4.36
0.9/0.9	0.31	0.29	0.29	0.60	0.57	0.55	0.83	0.81	0.80

*Matrix values represent the reflected radiation, in w/sr, corresponding to the emissivity combinations shown.

SECRET

TABLE IX. (S) REFLECTED RADIATION MATRIX FOR THE 3-5μ BAND AT 0 DEGREES ASPECT ANGLE (U)

Visible Surface Emissivities (Inner Wall/Outer Wall)	Nonvisible Surface Emissivities (Inner Wall/Outer Wall)								
	0.1/0.1	0.1/0.5	0.1/0.9	0.5/0.1	0.5/0.5	0.5/0.9	0.9/0.1	0.9/0.5	0.9/0.9
0.1/0.1	*44.60	42.32	41.59	66.94	63.69	61.52	77.04	74.90	73.06
0.1/0.5	11.55	11.76	12.00	21.58	20.81	20.32	28.29	27.57	26.95
0.1/0.9	1.48	1.55	1.62	2.95	2.87	2.82	4.15	4.05	3.97
0.5/0.1	25.19	24.13	23.83	38.68	36.92	35.75	45.00	43.91	42.96
0.5/0.5	8.05	8.20	8.37	14.90	14.36	14.03	19.41	18.98	18.64
0.5/0.9	1.16	1.22	1.26	2.29	2.23	2.19	3.20	3.13	3.07
0.9/0.1	13.75	13.25	13.12	21.19	20.31	19.72	24.68	24.24	23.87
0.9/0.5	5.23	5.32	5.43	9.51	9.22	9.03	12.28	12.09	11.92
0.9/0.9	0.86	0.89	0.93	1.65	1.61	1.59	2.27	2.24	2.21

*Matrix values represent the reflected radiation, in w/sr, corresponding to the emissivity combinations shown.

SECRET
87
Page 97 of 120 Pages
UNCLASSIFIED

Page 98 of 120 Pages

SECRET

88

TABLE X. (S) REFLECTED RADIATION MATRIX FOR THE 2-3μ BAND AT 15 DEGREES ASPECT ANGLE (U)

Visible Surface Emissivities (Inner Wall/Outer Wall)	Nonvisible Surface Emissivities (Inner Wall/Outer Wall)								
	0.1/0.1	0.1/0.5	0.1/0.9	0.5/0.1	0.5/0.5	0.5/0.9	0.9/0.1	0.9/0.5	0.9/0.9
0.1/0.1	*19.68	17.17	16.17	29.85	27.85	26.51	28.71	27.57	26.59
0.1/0.5	4.34	4.96	4.83	10.43	9.87	9.50	13.95	13.55	13.21
0.1/0.9	0.69	0.66	0.66	1.53	1.46	1.41	2.24	2.18	2.13
0.5/0.1	13.68	12.07	11.43	21.56	20.25	19.37	25.38	24.69	24.10
0.5/0.5	4.36	4.07	3.97	8.66	8.23	7.94	11.64	11.36	11.11
0.5/0.9	0.61	0.58	0.58	1.37	1.31	1.27	2.01	1.97	1.93
0.9/0.1	10.20	9.07	8.63	16.53	15.63	15.02	19.70	19.29	18.94
0.9/0.5	3.60	3.37	3.29	7.25	6.93	6.72	9.80	9.62	9.46
0.9/0.9	0.53	0.51	0.50	1.21	1.17	1.13	1.79	1.76	1.74

*Matrix values represent the reflected radiation, in w/sr, corresponding to the emissivity combinations shown.

SECRET

TABLE XI. (S) REFLECTED RADIATION MATRIX FOR THE 3-5 μ BAND AT 15 DEGREES ASPECT ANGLE (U)

Visible Surface Emissivities (Inner Wall/Outer Wall)	Nonvisible Surface Emissivities (Inner Wall/Outer Wall)								
	0.1/0.1	0.1/0.5	0.1/0.9	0.5/0.1	0.5/0.5	0.5/0.9	0.9/0.1	0.9/0.5	0.9/0.9
0.1/0.1	*52.32	49.72	48.89	80.00	76.51	74.18	92.68	90.56	88.73
0.1/0.5	14.15	14.34	14.65	27.97	27.14	26.60	37.46	36.74	36.12
0.1/0.9	1.86	1.95	2.02	4.12	4.03	3.97	6.03	5.93	5.84
0.5/0.1	36.39	34.94	34.52	57.80	55.54	54.04	68.11	66.83	65.73
0.5/0.5	11.61	11.80	12.02	23.24	22.57	22.15	31.21	30.72	30.31
0.5/0.9	1.65	1.72	1.78	3.69	3.62	3.57	5.43	5.55	5.28
0.9/0.1	27.14	26.22	25.99	44.33	42.79	41.77	52.88	52.13	51.48
0.9/0.5	9.60	9.75	9.93	19.48	19.00	18.69	26.32	26.00	25.72
0.9/0.9	1.45	1.51	1.56	3.29	3.23	3.19	4.85	4.80	4.75

*Matrix values represent the reflected radiation, in w/sr, corresponding to the emissivity combinations shown.

SECRET
Page 99 of 120 Pages
99
SECRET

Page 100 of 120 Pages

UNCLASSIFIED SECRET RESTRICTED DATA

TABLE XII. (S) REFLECTED RADIATION MATRIX FOR THE 2-3 μ BAND AT 30 DEGREES ASPECT ANGLE (U)

Visible Surface Emissivities (Inner Wall/Outer Wall)	Nonvisible Surface Emissivities (Inner Wall/Outer Wall)								
	0.1/0.1	0.1/0.5	0.1/0.9	0.5/0.1	0.5/0.5	0.5/0.9	0.9/0.1	0.9/0.5	0.9/0.9
0.1/0.1	*16.36	14.28	13.45	24.89	23.21	22.09	28.84	27.86	27.01
0.1/0.5	4.24	3.95	3.86	8.38	7.92	7.62	11.25	10.91	10.61
0.1/0.9	0.53	0.51	0.50	1.18	1.13	1.09	1.75	1.70	1.65
0.5/0.1	11.91	10.51	9.95	18.83	17.66	16.87	22.21	21.55	20.97
0.5/0.5	3.62	3.38	3.30	7.25	6.88	6.64	9.79	9.52	9.29
0.5/0.9	0.48	0.46	0.46	1.10	1.05	1.02	1.63	1.59	1.55
0.9/0.1	9.32	8.29	7.88	15.16	14.29	13.70	18.10	17.65	17.25
0.9/0.5	3.13	2.93	2.87	6.37	6.07	5.87	8.63	8.44	8.26
0.9/0.9	0.44	0.42	0.42	1.02	0.98	0.95	1.52	1.48	1.46

*Matrix values represent the reflected radiation, in w/sr, corresponding to the emissivity combinations shown.

SECRET RESTRICTED DATA

TABLE XIII. (S) REFLECTED RADIATION MATRIX FOR THE 3-5 μ BAND AT 30 DEGREES ASPECT ANGLE (U)

Visible Surface Emissivities (Inner Wall/Outer Wall)	Nonvisible Surface Emissivities (Inner Wall/Outer Wall)								
	0.1/0.1	0.1/0.5	0.1/0.9	0.5/0.1	0.5/0.5	0.5/0.9	0.9/0.1	0.9/0.5	0.9/0.9
0.1/0.1	*43.50	41.35	40.66	66.71	63.77	61.82	77.40	75.54	73.94
0.1/0.5	11.28	11.47	11.68	22.47	21.80	21.36	30.21	29.59	29.05
0.1/0.9	1.43	1.49	1.55	3.20	3.13	3.08	4.71	4.62	4.55
0.5/0.1	31.66	30.40	30.64	50.48	48.46	47.12	59.60	58.37	57.30
0.5/0.5	9.65	9.81	10.00	19.46	18.88	18.52	26.26	25.78	25.40
0.5/0.9	1.32	1.37	1.42	2.98	2.91	2.88	4.40	4.33	4.27
0.9/0.1	24.79	23.95	23.74	40.64	39.16	38.18	48.60	47.75	47.01
0.9/0.5	8.36	8.50	8.66	17.10	16.65	16.36	23.20	22.84	22.53
0.9/0.9	0.90	0.94	0.97	2.76	2.71	2.68	4.10	4.05	4.00

*Matrix values represent the reflected radiation, in w/sr, corresponding to the emissivity combinations shown.

SECRET
SECRET
SECRET
SECRET
Page 101 of 120 Pages

Page 102 of 120 Pages

SECRET UNCLASSIFIED

TABLE XIV. (S) REFLECTED RADIATION MATRIX FOR THE 2-3 μ BAND AT 45 DEGREES ASPECT ANGLE (U)

Visible Surface Emissivities (Inner Wall/Outer Wall)	Nonvisible Surface Emissivities (Inner Wall/Outer Wall)								
	0.1/0.1	0.1/0.5	0.1/0.9	0.5/0.1	0.5/0.5	0.5/0.9	0.9/0.1	0.9/0.5	0.9/0.9
0.1/0.1	*12.99	11.31	10.65	19.65	18.24	17.30	22.74	21.85	21.09
0.1/0.5	3.14	2.93	2.86	6.11	5.75	5.50	8.17	7.87	7.60
0.1/0.9	0.37	0.35	0.35	0.80	0.75	0.73	1.16	1.12	1.09
0.5/0.1	9.59	8.44	7.99	15.04	14.01	13.33	17.69	17.05	16.49
0.5/0.5	2.75	2.57	2.50	5.39	5.09	4.87	7.23	6.98	6.76
0.5/0.9	0.35	0.33	0.33	0.76	0.72	0.69	1.11	1.07	1.04
0.9/0.1	7.59	6.73	6.38	12.17	11.40	10.88	14.51	14.02	13.60
0.9/0.5	2.44	2.28	2.23	4.82	4.56	4.38	6.49	6.28	6.09
0.9/0.9	0.33	0.31	0.31	0.72	0.69	0.66	1.06	1.03	1.00

*Matrix values represent the reflected radiation, in w/sr, corresponding to the emissivity combinations shown.

SECRET UNCLASSIFIED

SECRET RESTRICTED
83
0103 of 120 Pages

TABLE XV. (S) REFLECTED RADIATION MATRIX FOR THE 3-5μ BAND AT 45 DEGREES ASPECT ANGLE (U)

Visible Surface Emissivities (Inner Wall/Outer Wall)	Nonvisible Surface Emissivities (Inner Wall/Outer Wall)								
	0.1/0.1	0.1/0.5	0.1/0.9	0.5/0.1	0.5/0.5	0.5/0.9	0.9/0.1	0.9/0.5	0.9/0.9
0.1/0.1	*34.52	32.80	32.24	52.66	50.20	48.57	61.01	59.34	57.91
0.1/0.5	8.37	8.52	8.69	16.40	15.86	15.50	21.93	21.39	20.92
0.1/0.9	1.00	1.05	1.09	2.16	2.10	2.07	3.15	3.07	3.01
0.5/0.1	25.50	24.47	24.18	40.31	38.55	37.38	47.48	46.28	45.24
0.5/0.5	7.34	7.47	7.62	14.48	13.99	13.69	19.41	18.95	18.58
0.5/0.9	0.95	0.99	1.03	2.06	2.01	1.98	3.01	2.94	2.89
0.9/0.1	20.19	19.49	19.32	32.69	31.35	30.46	38.96	38.05	37.26
0.9/0.5	6.51	6.63	6.77	12.95	12.56	12.30	17.44	17.06	16.73
0.9/0.9	0.90	0.94	0.97	1.97	1.92	1.89	2.88	2.82	2.77

*Matrix values represent the reflected radiation, in w/sr, corresponding to the emissivity combinations shown.

UNCLASSIFIED

Page 104 of 120 Pages

SECRET

TABLE XVI. (S) REFLECTED RADIATION MATRIX FOR THE 2-3μ BAND AT 60 DEGREES ASPECT ANGLE (U)

Visible Surface Emissivities (Inner Wall/Outer Wall)	Nonvisible Surface Emissivities (Inner Wall/Outer Wall)								
	0.1/0.1	0.1/0.5	0.1/0.9	0.5/0.1	0.5/0.5	0.5/0.9	0.9/0.1	0.9/0.5	0.9/0.9
0.1/0.1	*10.80	9.39	8.83	16.27	15.03	14.20	18.81	17.96	17.24
0.1/0.5	2.37	2.20	2.15	4.52	4.22	4.01	6.02	5.73	5.49
0.1/0.9	0.25	0.24	0.23	0.51	0.48	0.46	0.74	0.70	0.67
0.5/0.1	7.38	6.92	6.54	12.27	11.36	10.74	14.41	13.77	13.22
0.5/0.5	2.08	1.94	1.89	3.99	3.71	3.54	5.31	5.06	4.85
0.5/0.9	0.24	0.23	0.23	0.50	0.46	0.44	0.72	0.68	0.65
0.9/0.1	6.13	5.42	5.13	9.75	9.03	8.55	11.57	11.06	10.62
0.9/0.5	1.85	1.72	1.68	3.55	3.32	3.16	4.74	4.52	4.33
0.9/0.9	0.23	0.22	0.22	0.48	0.45	0.43	0.70	0.66	0.63

*Matrix values represent the reflected radiation, in w/sr, corresponding to the emissivity combinations shown.

UNCLASSIFIED

TABLE XVII. (S) REFLECTED RADIATION MATRIX FOR THE 3-5μ BAND AT 60 DEGREES ASPECT ANGLE (U)

Visible Surface Emissivities (Inner Wall/Outer Wall)	Nonvisible Surface Emissivities (Inner Wall/Outer Wall)								
	0.1/0.1	0.1/0.5	0.1/0.9	0.5/0.1	0.5/0.5	0.5/0.9	0.9/0.1	0.9/0.5	0.9/0.9
0.1/0.1	*28.71	27.26	26.80	43.61	41.43	39.99	50.47	48.88	47.51
0.1/0.5	6.31	6.43	6.57	12.14	11.68	11.39	16.16	15.65	15.21
0.1/0.9	0.68	0.71	0.74	1.39	1.35	1.32	2.01	1.94	1.88
0.5/0.1	20.97	20.10	19.86	32.90	31.32	30.28	38.68	37.48	36.45
0.5/0.5	5.55	5.66	5.79	10.71	10.29	10.03	14.26	13.82	13.45
0.5/0.9	0.66	0.69	0.72	1.35	1.31	1.29	1.95	1.88	1.83
0.9/0.1	16.31	15.74	15.60	26.13	24.92	24.11	31.05	30.10	29.28
0.9/0.5	4.94	5.04	5.15	9.54	9.19	8.96	12.75	12.35	12.01
0.9/0.9	0.64	0.67	0.70	1.31	1.27	1.25	1.89	1.83	1.78

*Matrix values represent the reflected radiation, in w/sr, corresponding to the emissivity combinations shown.

SECRET

Page 99 of 126 pages

SECRET

UNCLASSIFIED

TABLE XVIII. (S) DIRECT RADIATION MATRIX FOR THE 2-3 μ BAND AT 0 DEGREES ASPECT ANGLE (U)

Visible Surface Emissivities (Inner Wall / Outer Wall)	Percent Coolant Flow Distribution (Inner Wall/Outer Wall/Base)											
	10/80/10	10/85/5	10/90/0	20/70/10	20/75/5	20/80/0	30/60/10	30/65/5	30/70/0	40/50/10	40/55/5	40/60/0
0.1/0.1	**2.80	2.74	6.79	1.45	1.35	5.37	1.42	1.26	5.24	1.81	1.56	5.44
0.1/0.5	2.78	2.65	6.53	2.14	1.93	5.78	2.54	2.20	5.96	3.46	2.98	6.50
0.1/0.9	2.44	2.68	6.50	2.43	2.18	5.96	2.98	2.57	6.24	4.08	3.54	6.91
0.5 0.1	8.08	8.06	6.53	2.42	2.37	6.36	1.41	1.33	5.30	1.28	1.17	5.09
0.5 0.5	6.98	6.91	10.87	2.5	2.41	6.41	1.97	1.78	5.65	2.20	1.99	5.70
0.5 0.9	6.59	6.50	10.38	2.62	2.45	6.73	2.21	1.91	5.79	2.69	2.37	5.98
0.9/0.1	11.26	11.25	15.22	2.92	2.91	6.87	1.35	1.33	5.29	0.96	0.92	4.80
0.9/0.5	10.50	10.48	14.43	2.84	2.80	6.74	1.49	1.43	5.34	1.26	1.17	5.04
0.9/0.9	10.24	10.21	14.15	2.81	2.77	6.69	1.53	1.46	5.36	1.35	1.24	5.09

*The visible base area emissivity is 0.1 for all combinations.
**Matrix values represent the direct and inner-reflected radiation, in w sr, from all visible surfaces of the suppressor.

TABLE XIX. (S) DIRECT RADIATION MATRIX FOR THE 3-5μ BAND AT 0 DEGREES ASPECT ANGLE (U)

Visible Surface Emissivities	Percent Coolant Flow Distribution (Inner Wall/Outer Wall/Base)											
Inner Wall / Outer Wall	10/80/10	10/85/5	10/90/0	20/70/10	20/75/5	20/80/0	30/60/10	30/65/5	30/70/0	40/50/10	40/55/5	40/60/0
0.1/0.1	**17.30	16.95	27.55	12.26	11.73	22.23	11.99	11.16	21.44	13.65	12.52	22.32
0.1/0.5	20.35	19.54	29.46	18.51	17.34	27.08	20.58	18.80	28.11	24.90	22.71	30.93
0.1/0.9	21.78	20.81	30.47	21.00	19.59	29.06	23.85	21.74	30.69	29.06	26.61	34.19
0.5/0.1	42.06	41.94	29.46	19.59	19.38	29.93	13.37	13.03	23.47	11.81	11.32	21.53
0.5/0.5	38.65	38.23	48.44	21.25	20.62	30.73	17.55	16.58	26.44	18.18	16.96	26.21
0.5/0.9	37.60	37.06	47.08	22.23	21.43	31.34	19.54	18.30	27.91	21.04	19.58	28.37
0.9/0.1	56.94	56.95	67.53	23.64	23.62	34.18	13.92	13.84	24.36	10.57	10.43	20.87
0.9/0.5	54.01	53.90	64.35	23.49	23.31	33.70	15.00	14.69	25.00	12.63	12.19	22.28
0.9/0.9	52.97	52.83	63.23	23.43	23.20	33.55	15.35	14.97	25.22	13.26	12.77	22.73

*The visible base area emissivity is 0.1 for all combinations.
**Matrix values represent the direct and inner-reflected radiation, in w/sr, from all visible surfaces of the suppressor.

SECRET
Page 107 of 120 Pages

SECRET

Page 107 of 126

SECRET

SECRET

TABLE XX. (S) DIRECT RADIATION MATRIX FOR THE 2-3 μ BAND AT 15 DEGREES ASPECT ANGLE (U)

Visible Surface Emissivities (Inner Wall/Outer Wall)	Percent Coolant Flow Distribution (Inner Wall/Outer Wall/Base)											
	10/80/10	10/85/5	10/90/0	20/70/10	20/75/5	20/80/0	30/60/10	30/65/5	30/70/0	40/50/10	40/55/5	40/60/0
0.1/0.1	**2.63	2.56	6.45	1.43	1.32	5.20	1.47	1.29	5.12	1.92	1.64	5.35
0.1/0.5	2.51	2.37	6.11	2.05	1.84	5.53	2.51	2.16	5.76	3.47	2.97	6.33
0.1/0.9	2.50	2.34	6.03	2.24	1.99	5.63	2.81	2.41	5.95	3.92	3.36	6.61
0.5/0.1	7.39	7.35	6.11	2.25	2.19	6.03	1.43	1.23	5.14	1.43	1.28	5.02
0.5/0.5	5.92	5.83	9.59	2.30	2.16	5.89	2.02	1.79	5.46	2.52	2.17	5.69
0.5/0.9	5.46	5.36	9.08	2.32	2.16	5.85	2.22	1.94	5.56	2.87	2.47	5.90
0.9/0.1	10.30	11.25	14.11	2.67	2.64	6.45	1.35	1.29	5.09	1.13	1.04	4.80
0.9/0.5	10.50	8.75	12.53	2.49	2.40	6.16	1.61	1.47	5.19	1.74	1.51	5.15
0.9/0.9	8.34	8.29	12.05	2.40	2.31	6.05	1.64	1.48	5.18	1.35	1.60	5.20

The visible base area emissivity is 0.1 for all combinations.
Matrix values represent the direct and one-reflected radiation, in watts, from all visible surfaces of the suppressor.

SECRET

TABLE XXI. (S) DIRECT RADIATION MATRIX FOR THE 3-5μ BAND AT 15 DEGREES ASPECT ANGLE (U)

Visible Surface Emissivities (Inner Wall/Outer Wall)	Percent Coolant Flow Distribution (Inner Wall/Outer Wall/Base)											
	10/80/10	10/85/5	10/90/0	20/70/10	20/75/5	20/80/0	30/60/10	30/65/5	30/70/0	40/50/10	40/55/5	40/60/0
0.1/0.1	**16.68	16.29	26.46	12.34	11.75	21.80	12.43	11.51	21.33	14.42	13.15	22.45
0.1/0.5	19.27	18.44	27.95	18.22	17.00	26.29	20.66	18.80	27.66	25.36	22.96	30.73
0.1/0.9	20.19	19.23	28.54	20.06	18.65	27.70	23.16	21.02	29.59	28.60	25.98	33.21
0.5/0.1	39.02	38.83	27.95	18.71	18.41	28.49	13.48	12.98	22.93	12.67	11.94	21.61
0.5/0.5	34.21	33.66	43.39	20.20	19.39	28.95	18.07	16.82	26.09	19.98	18.30	26.86
0.5/0.9	32.76	32.11	41.69	20.80	19.84	29.20	19.67	18.17	27.21	22.44	20.51	28.64
0.9/0.1	52.66	52.60	62.74	22.23	22.08	32.18	13.82	13.55	23.57	11.46	11.03	20.88
0.9/0.5	46.84	46.53	56.43	21.80	21.33	31.10	15.86	15.11	24.71	15.52	14.41	23.61
0.9/0.9	45.00	44.65	54.49	21.52	20.97	30.65	16.27	15.39	24.89	16.46	15.19	24.20

*The visible base area emissivity is 0.1 for all combinations.
**Matrix values represent the direct and inner-reflected radiation, in w/sr, from all visible surfaces of the suppressor.

SECRET
SECRET
SECRET

Page 116 of 166 Pages

TABLE XXII. (S) DIRECT RADIATION MATRIX FOR THE 2-3μ BAND AT 30 DEGREES ASPECT ANGLE (U)

Visible Surface Emissivities (Inner Wall/Outer Wall)	Percent Coolant Flow Distribution (Inner Wall/Outer Wall/Base)											
	10/80/10	10/85/5	10/90/0	20/70/10	20/75/5	20/80/0	30/60/10	30/65/5	30/70/0	40/50/10	40/55/5	40/60/0
0.1/0.1	**2.19	2.13	5.60	1.22	1.12	4.57	1.27	1.11	4.52	1.66	1.42	4.73
0.1/0.5	2.13	2.01	5.33	1.81	1.61	4.90	2.24	1.93	5.13	3.12	2.66	5.65
0.1/0.9	2.15	2.01	5.28	2.02	1.79	5.03	2.57	2.20	5.34	3.59	3.08	5.96
0.5/0.1	6.27	6.24	5.33	1.94	1.88	5.30	1.27	1.17	4.57	1.32	1.16	4.50
0.5/0.5	4.91	4.81	8.15	2.06	1.91	5.22	1.94	1.70	4.95	2.51	2.15	5.24
0.5/0.9	4.45	4.34	7.64	2.15	1.97	5.23	2.24	1.94	5.13	3.00	2.57	5.55
0.9/0.1	8.96	8.93	12.34	2.36	2.32	5.72	1.25	1.18	4.57	1.11	1.00	4.34
0.9/0.5	7.33	7.26	10.61	2.27	2.16	5.48	1.59	1.52	4.79	2.01	1.72	4.89
0.9/0.9	6.71	6.62	9.94	2.27	2.13	5.42	1.92	1.69	4.92	2.42	2.07	5.15

*The visible base area emissivity is 0.1 for all combinations.
**Matrix values represent the direct and inner-reflected radiation, in w/sr, from all visible surfaces of the suppressor.

SECRET

SECRET

TABLE XXIII. (S) DIRECT RADIATION MATRIX FOR THE 3-5μ BAND AT 30 DEGREES ASPECT ANGLE (U)

Visible Surface Emissivities (Inner Wall/Outer Wall)	Percent Coolant Flow Distribution (Inner Wall/Outer Wall/Base)											
	10/80/10	10/85/5	10/90/0	20/70/10	20/75/5	20/80/0	30/60/10	30/65/5	30/70/0	40/50/10	40/55/5	40/60/0
0.1/0.1	**13.94	13.60	22.65	10.46	9.95	18.96	10.63	9.84	18.59	12.41	11.30	19.61
0.1/0.5	16.46	15.71	24.17	15.90	14.81	23.08	18.19	16.54	24.42	22.41	20.28	27.20
0.1/0.9	17.49	16.62	24.88	17.60	16.53	24.57	20.75	18.32	26.41	25.72	23.34	29.75
0.5/0.1	32.86	32.67	24.17	15.97	15.68	24.65	11.74	11.27	20.11	11.26	10.57	19.15
0.5/0.5	28.56	28.00	36.60	17.86	17.04	25.49	16.73	15.48	23.62	19.02	17.34	24.78
0.5/0.9	27.31	26.61	35.03	18.88	17.85	26.08	18.91	17.34	25.20	22.23	20.21	27.16
0.9/0.1	45.22	45.11	54.14	19.33	19.16	28.14	12.31	12.01	20.91	10.53	10.07	18.78
0.9/0.5	39.14	38.74	47.45	19.58	18.98	27.56	15.53	14.60	22.96	16.22	14.90	22.76
0.9/0.9	36.93	36.40	44.96	19.94	19.15	27.56	17.12	15.91	24.03	18.85	17.18	24.65

*The visible base area emissivity is 0.1 for all combinations.
**Matrix values represent the direct and inner-reflected radiation, in w/sr, from all visible surfaces of the suppressor.

SECRET
101
Page 111 of 120 Pages
SECRET

Page 112 of 120 Pages

SECRET

102

CONFIDENTIAL

TABLE XXIV. (S) DIRECT RADIATION MATRIX FOR THE 2-3μ BAND AT 45 DEGREES ASPECT ANGLE (U)

Visible Surface Emissivities (Inner Wall/Outer Wall)	Percent Coolant Flow Distribution (Inner Wall/Outer Wall/Base)											
	10/80/10	10/85/5	10/90/0	20/70/10	20/75/5	20/80/0	30/60/10	30/65/5	30/70/0	40/50/10	40/55/5	40/60/0
0.1/0.1	**1.70	1.65	4.45	1.02	0.93	3.72	1.08	0.95	3.70	1.43	1.22	3.88
0.1/0.5	1.70	1.59	4.26	1.60	1.43	4.06	2.03	1.74	4.30	2.82	2.41	4.78
0.1/0.9	1.77	1.68	4.25	1.86	1.64	4.23	2.41	2.07	4.56	3.37	2.90	5.15
0.5/0.1	4.68	4.65	4.26	1.58	1.53	4.30	1.11	1.02	3.76	1.18	1.04	3.73
0.5/0.5	3.46	3.36	6.04	1.78	1.64	4.29	1.86	1.62	4.21	2.45	2.11	4.54
0.5/0.9	3.01	2.89	5.52	1.94	1.75	4.35	2.27	1.96	4.47	3.10	2.67	4.96
0.9/0.1	6.62	6.60	9.36	1.92	1.88	4.64	1.12	1.05	3.79	1.04	0.94	3.63
0.9/0.5	5.00	4.92	7.61	1.94	1.82	4.48	1.72	1.52	4.13	2.15	1.86	4.33
0.9/0.9	4.24	4.13	6.77	2.03	1.86	4.47	2.13	1.85	4.38	2.85	2.44	4.79

*The visible base area emissivity is 0.1 for all combinations.
**Matrix values represent the direct and inner-reflected radiation, in w/sr, from all visible surfaces of the suppressor.

TABLE XXV. (S) DIRECT RADIATION MATRIX FOR THE 3-5μ BAND AT 45 DEGREES ASPECT ANGLE (U)

Visible Surface Emissivities	Percent Coolant Flow Distribution (Inner Wall/Outer Wall/Base)											
Inner Wall/Outer Wall	10/80/10	10/85/5	10/90/0	20/70/10	20/75/5	20/80/0	30/60/10	30/65/5	30/70/0	40/50/10	40/55/5	40/60/0
0.1/0.1	**11.05	10.75	18.06	8.66	8.21	15.44	8.96	8.28	15.33	10.52	9.58	16.25
0.1/0.5	13.63	12.95	19.72	13.85	12.87	19.48	16.09	14.61	20.86	19.87	18.01	23.40
0.1/0.9	14.89	14.07	20.62	15.98	14.80	21.18	18.90	17.13	23.08	23.48	21.34	26.21
0.5/0.1	24.87	24.69	19.72	12.87	12.59	19.84	9.93	9.49	16.62	9.77	9.16	16.03
0.5/0.5	21.25	20.69	27.54	15.20	14.39	21.11	15.30	14.07	20.48	17.86	16.29	21.99
0.5/0.9	20.21	19.47	26.09	16.71	15.64	22.11	18.14	16.54	22.61	21.92	19.95	25.06
0.9/0.1	33.77	33.66	40.96	15.44	15.26	22.51	10.48	10.17	17.34	9.32	8.88	15.87
0.9/0.5	27.95	27.49	34.40	16.40	15.73	22.53	14.66	13.64	20.18	16.21	14.87	20.83
0.9/0.9	25.44	24.77	31.46	17.43	16.47	23.01	17.41	15.97	22.15	20.42	18.60	23.95

*The visible base area emissivity is 0.1 for all combinations.
**Matrix values represent the direct and inner-reflected radiation, in watts, from all visible surfaces of the suppressor.

SECRET
103
Page 113 of 120 Pages
SECRET

Page 114 of 120 Pages

SECRET

UNCLASSIFIED

TABLE XXVI. (S) DIRECT RADIATION MATRIX FOR THE 2-3μ BAND AT 60 DEGREES ASPECT ANGLE (U)

Visible Surface Emissivities	Percent Coolant Flow Distribution (Inner Wall/Outer Wall/Base)											
Inner Wall/Outer Wall	10/80/10	10/85/5	10/90/0	20/70/10	20/75/5	20/80/0	30/60/10	30/65/5	30/70/0	40/50/10	40/55/5	40/60/0
0.1/0.1	**1.38	1.33	3.29	0.90	0.83	2.78	0.99	0.86	2.78	1.31	1.12	2.96
0.1/0.5	1.43	1.32	3.16	1.51	1.34	3.15	1.95	1.67	3.41	2.71	2.33	3.87
0.1/0.9	1.53	1.39	3.17	1.81	1.60	3.35	2.39	2.05	3.70	3.35	2.89	4.30
0.5/0.1	3.51	3.48	3.16	1.36	1.30	3.24	1.02	0.94	2.85	1.11	0.98	2.84
0.5/0.5	2.36	2.27	4.11	1.62	1.47	3.29	1.85	1.60	3.35	2.47	2.13	3.72
0.5/0.9	1.91	1.77	3.55	1.84	1.64	3.39	2.35	2.02	3.68	3.26	2.81	4.24
0.9/0.1	4.78	4.76	6.69	1.61	1.57	3.50	1.04	0.97	2.88	1.00	0.90	2.77
0.9/0.5	3.16	3.07	4.92	1.71	1.58	3.41	1.76	1.54	3.31	2.27	1.97	3.59
0.9/0.9	2.28	2.15	3.93	1.88	1.66	3.43	2.31	1.99	3.65	3.17	2.74	4.18

*The visible base area emissivity is 0.1 for all combinations.
**Matrix values represent the direct and inner-reflected radiation, in w/sr, from all visible surfaces of the suppressor.

TABLE XXVII. (S) DIRECT RADIATION MATRIX FOR THE 3-5μ BAND AT 60 DEGREES ASPECT ANGLE (U)

Visible Surface Emissivities	Percent Coolant Flow Distribution (Inner Wall/Outer Wall/Base)											
(Inner Wall/Outer Wall)	10/80/10	10/85/5	10/90/0	20/70/10	20/75/5	20/80/0	30/60/10	30/65/5	30/70/0	40/50/10	40/55/5	40/60/0
0.1/0.1	**9.23	8.35	14.03	7.63	7.21	12.23	8.06	7.42	12.28	9.51	8.66	13.16
0.1/0.5	12.01	11.34	15.89	12.89	11.94	16.36	15.19	13.78	17.85	18.82	17.08	20.31
0.1/0.9	13.51	12.69	17.00	15.32	14.14	18.32	18.36	16.62	20.36	22.84	20.81	23.47
0.5/0.1	19.21	19.02	15.89	10.86	10.58	15.62	8.87	8.43	13.36	8.94	8.36	13.04
0.5/0.5	16.05	15.46	20.07	13.61	12.78	17.27	14.67	13.43	17.61	17.49	15.97	19.41
0.5/0.9	15.12	14.33	18.66	15.55	14.41	18.61	18.12	16.44	20.22	22.33	20.36	23.10
0.9/0.1	25.11	24.97	30.07	12.71	12.51	17.56	9.31	8.99	13.96	8.60	8.18	12.95
0.9/0.5	19.48	18.97	23.62	14.23	13.49	18.05	14.25	13.14	17.42	16.41	15.05	18.67
0.9/0.9	16.71	15.93	20.30	15.71	14.68	18.91	17.89	16.26	20.08	21.84	19.92	22.74

*The visible base area emissivity is 0.1 for all combinations.
**Matrix values represent the direct and inner-reflected radiation, in w/sr, from all visible surfaces of the suppressor.

SECRET
Page 115 of 120 Pages

Page 116 of 170 Pages

TABLE XXVIII. (S) MINIMUM IR SIGNATURES FROM COMBINED JR AND JD MATRICES, 2-3 μ (U)

Aspect Angle (deg)	*Visible Surface Emissivities (Inner Wall/Outer Wall)	Nonvisible Surface Emissivities (Inner Wall/Outer Wall)	Coolant Distribution Inner/Outer Base (percent)	Minimum Total Radiation (w/sr)
0	0.9/0.9	0.1/0.9	30/65/5	1.53
15	0.9/0.9	0.1/0.9	40/55/5	2.10
30	0.9/0.9	0.1/0.9	30/65/5	2.11
45	0.1/0.9	0.1/0.9	20/75/5	1.99
60	0.1/0.9	0.1/0.9	10/85/5	1.62

*Base emissivity was 0.1 for all optimization studies.

SECRET

UNCLASSIFIED

TABLE XXIX. (S) MINIMUM IR SIGNATURES FROM COMBINED JR AND JD MATRICES, 3-5 μ (U)

A A .e g)	.sible Surface Emissivities (Inner Wall/Outer Wall)	Nonvisible Surface Emissivities (Inner Wall/Outer Wall)	Coolant Distribution Inner/Outer/Base (percent)	Minimum Total Radiation (w/sr)
0	0.9/0.9	0.1/0.1	40/55/5	13.63
15	0.9/0.9	0.1/0.1	40/55/5	16.64
30	0.9/0.9	0.1/0.1	30/65/5	16.81
45	0.1/0.9	0.1/0.1	10/85/5	15.07
60	0.1/0.9	0.1/0.1	10/85/5	13.32

*Base emissivity was 0.1 for all optimization studies.

SECRET
Page 117 of 126 Pages

SECRET

UNCLASSIFIED
SECRET
(This Page is Unclassified)

DISTRIBUTION

Director of Defense Research & Engineering	1
Assistant Secretary of the Army (R&D)	1
Chief of Research & Development, DA	1
Army Materiel Command	1
USAMC IRCM Product Manager	5
Hq, Army Air Mobility R&D Laboratory	1
Systems Research Integration Officer, USAAMRDL	1
Ames Directorate, Army Air Mobility R&D Laboratory	1
Eustis Directorate, Army Air Mobility R&D Laboratory	6
Langley Directorate, Army Air Mobility R&D Laboratory	1
Lewis Directorate, Army Air Mobility R&D Laboratory	2
Army Advanced Materiel Concepts Agency	1
Army Materiel Systems Analysis Agency	1
Army Electronics Command	1
Air Force Materials Laboratory	2
Naval Air Systems Command	1
Chief of Naval Research	1
Defense Documentation Center	2

Page 115 of 120 Pages

SECRET
(This Page is Unclassified)
UNCLASSIFIED

UNCLASSIFIED

Chief, Doc, USAAMRDL
3
Declassify on: 31 Dec 1987

Unclassified
Security Classification

DOCUMENT CONTROL DATA - R & D

(Security classification of title, body of abstract and indexing annotation must be entered when the overall report is classified)

1. ORIGINATING ACTIVITY (Corporate author)	2a. REPORT SECURITY CLASSIFICATION
Pratt & Whitney Aircraft Division United Aircraft Corporation Florida Research and Development Center West Palm Beach, Florida	Secret

3. REPORT TITLE

RESEARCH PROGRAM TO OPTIMIZE THE ST9 DEMONSTRATOR ENGINE IR SUPPRESSOR (U)

4. DESCRIPTIVE NOTES (Type of report and inclusive dates)

Final Technical Report

5. AUTHOR(S) (First name, middle initial, last name)

Daniel E. Booz, Jr.
Edward B. Thayer
C. Michael Willard

6. REPORT DATE	7a. TOTAL NO. OF PAGES	7b. NO. OF REFS
November 1972	124	5

8a. CONTRACT OR GRANT NO.	9a. ORIGINATOR'S REPORT NUMBER(S)
DAAJ02-71-C-0043	USAAMRDL Technical Report 72-50
b. PROJECT NO. Task 1F162205AA5203	
c.	9b. OTHER REPORT NO(S) (Any other numbers that may be assigned this report)
d.	PWA-FR-4833

10. DISTRIBUTION STATEMENT

Distribution limited to U.S. Government agencies only; test and evaluation, November 1972. Other requests for this document must be referred to the Eustis Directorate, U.S. Army Air Mobility Research and Development Laboratory, Fort Eustis, Virginia 23604.

11. SUPPLEMENTARY NOTES	12. SPONSORING MILITARY ACTIVITY
	Eustis Directorate U.S. Army Air Mobility R&D Laboratory Fort Eustis, Virginia

13. ABSTRACT

(U) The purpose of this program was to optimize the surface temperature/emissivity of the ST9 Demonstrator Engine infrared (IR) suppressor to yield the lowest IR signature possible without additional cooling flow requirements. New IR-signature analysis computer programs developed by General Dynamics - Pomona under U.S. Army Air Mobility Research and Development Laboratory (USAAMRDL) Contract DAAJ02-69-C-0077 were used to conduct an analytical optimization study. A parametric variation of the temperature and emissivity of the suppressor wall surfaces, divided into many segments, permitted the optimum combination to be chosen. Emissivity-control coatings were then applied to the suppressor surfaces, and the coated suppressor was tested under simulated engine operating conditions. The test results showed that a 22% reduction in the IR signature was achieved and that the measured signature compared favorably with that predicted by the computer programs.

DD FORM 1473 REPLACES DD FORM 1473, 1 JAN 68, WHICH IS OBSOLETE FOR ARMY USE.

Unclassified
Security Classification

UNCLASSIFIED

UNCLASSIFIED
SECRET

(This page is unclassified)

Unclassified
Security Classification

14 KEY WORDS	LINK A		LINK B		LINK C	
	ROLE	WT	ROLE	WT	ROLE	WT
Infrared						
Suppressor						
Emissivity						
Coatings						
Infrared Signature						
Film Cooling						

Unclassified
Security Classification

UNCLASSIFIED
SECRET

(This page is unclassified)